Design of nanoparticle systems with antimicrobial properties

DISSERTATION

ZUR ERLANGUNG DES GRADES

DOKTOR DER NATURWISSENSCHAFTEN

IM FACHBEREICH CHEMIE, PHARMAZIE UND GEOWISSENSCHAFTEN

DER JOHANNES GUTENBERG-UNIVERSITÄT MAINZ

VORGELEGT VON

VÉRONIQUE BERNADETTE SCHWARTZ,

GEBOREN IN BERNKASTEL-KUES,

MAINZ, 2011

Dekan:

1. Berichterstatter:

2. Berichterstatter:

Tag der mündlichen Prüfung: 30.01.2012

Table of Contents

Abbreviations/glossary

AFU	Arbitrary fluorescence units
AMP	Antimicrobial peptide
ANOVA	Analysis of variance - statistical method for data evaluation, often used in biological experiments
Bactericidal	Refers to a substance or condition capable of killing bacteria
Bacteriophage	Virus that infect bacteria
Bacteriostatic	Refers to a substance of condition arresting the growth or multiplication of bacteria
CFU	Colony forming unit
CMC	Critical micelle concentration
CTAC	Cetyltrimethylammonium chloride, hexadecyltrimethylammonium chloride
D_H	Hydrodynamic diameter (as obtained from DLS measurements)
DLS	Dynamic light scattering
DMAEMA	(N,N'-dimethylamino)ethyl methacrylate
EDS	Energy-dispersive X-ray spectroscopy
FACS	Fluorescence-activated cell sorting
FDA	US Food and Drug Administration
HAI	Hospital acquired infections
ICP-OES	Inductively-coupled plasma optical emission spectroscopy
IESL-FORTH	Institute for Electronic Structure and Laser/Foundation for Research and Technology
IESL-FORTH	Institute of Electronic Structure and Laser-Foundation of Research and Technology-Hellas, Greece
LB	Lysogeny broth - a nutritionally rich medium used for the growth of bacteria.
Lutensol AT 50	Non-ionic surfactant based on a poly(ethylene oxide)-hexadecyl ether with and EO block length of 50 units
mPEGMA	Methoxy-poly(ethyleneglycol methylmethacrylate)
MPIP	Max Planck Institute for Polymer Reserach
NC	Nanocrystal
NMR	Nuclear magnetic resonance
NP	Nanoparticle
OD	Optical density
PCL	Poly-ε-caprolacton
PDI	Polydispersity index
PEG	Poly(ethylene glycol), poly(ethylene oxide)
PEGMA	Poly(ethyleneglycol methylmethacrylate)
PEI	Poly(ethyleneimine)

PLA	Poly(lactide)
PLGA	Poly(lactic-co-glycolic acid)
PLLA	Poly(L-lactide)
PNIPAAm	Poly(*N*-isopropylacrylamide)
PP	Poly(propylene)
PqDMAEMA	Poly-(2-methacryloyloxyethyl)dodecyldimethylammonium methacrylate)
PVP	Poly(4-vinylpyridine)
QAC	Quaternary ammonium compound
qDMAEMA	(2-Methacryloyloxyethyl)dodecyldimethylammonium methacrylate)
QS	Quorum sensing: bacterial communication
ROS	Reactive oxygen species
SAM	Self-assembled monolayer
SDS	Sodium dodecylsulfate
SEC	Size exclusion chromatography
SEM	Scanning electron microscopy
Surfmer	Surfactant monomer: Surfactant molecule, which contains a polymerizable group
Systemic antibiotics	Antibiotic treatments which affects the whole body
TEM	Transmission electron microscopy
UKK	University Clinic of Cologne
UMC	University Medical Centre of Mainz
V59	2,2'-azobis(2-methylbutyronitrile) – oil-soluble initiator

1. Introduction

1.1 Motivation

Nosocomial infection, or hospital-acquired infection (HAI) is a general term, summarizing various infections, which develop in hospital environments, particularly amongst immunocompromised patients, but also hospital staff. In many cases, such infections are caused by multiresistant bacteria, entailing major medical and economical sequelae. According to European Centre for Disease Prevention and Control, about 4 100 000 patients are affected by healthcare-associated infections in the EU every year, including approximately 37 000 lethal cases. The most frequent infections are related to urinary tract infections (28%), followed by respiratory tract infections (25%) and bloodstream infections (10%) [1]. A significant number of infections is most commonly associated with implantable devices such as catheters (urinary, vascular), surgical implants (e.g. vascular grafts, cardiac pacemakers), and mechanical ventilation apparatuses [2, 3].

A notable proportion of HAIs are man-made. Although the development of advanced technologies has greatly revolutionized modern medicine within the past 100 years, the overconsumption of antibiotics outside of hospital use, combined with deficiencies in intensive hygiene control programs have contributed to the development of antimicrobial resistance of microorganisms. The most prominent pathogens include methicillin-resistant and methicillin-sensitive *Staphylococcus aureus* (MRSA, MSSA) as one of the main causes of pneumonia, surgical wound and bloodstream infections [4], followed by *Escherichia coli*, a remarkable food-borne pathogen. Additionally, both *Klebsiella pneumonia* and *Pseudomonas aeruginosa* are particular opportunistic pathogens of pronounced multidrug resistance in individuals with impaired immune system. Other important candidates include penicillin non-susceptible *Streptococcus pneumonia* (PNSP), *Enterocossus faecalis* and vancomycin-resistant *Enterococcus faecium* (VRE)[5].

The origin of implant-associated infections can be tracked back to the implantation site, where bacterial colonization and subsequent biofilm formation generate a highly inert surface layer to current medical treatment. Consequently, in many cases implant removal and/or amputation represent the only alternative [6]. Upon implantation into the body, a “race for the surface” is initiated between tissue cell integration and microbial colonization, which is

generally decided within several hours. Since most of the patients are immunocompromised, host defense usually fails to prevent colonization prior to tissue integration [7]. The implant surface is generally coated by a conditioning layer of surface-adsorbed proteins and other organic substances. Most of the pathogens are found ubiquitously on the patient's skin or in the patient's body and thus can freely access the implantation site. In the first 2 h after implantation, bacterial colonization is governed by reversible physical adsorption. After 2-3 h, chemical bridging reactions ensure a much stronger adhesion between bacteria and substrate. Subsequently, within a period of 24 h or longer, the excretion of extracellular substances ensures both microbial multiplication and resistance to mechanical, immunological and medical attempts of removal [8]. This biofilm formation is highly dependent on the bacterial species and some colonized devices may not become clinically infected at all, or the infection can emerge only after several months after implantation [2].

In conclusion, the prevalence of HAIs gives rise to significant clinical and economical damage, which is predominantly related to implant-associated infections. Therefore, the prevention of bacterial attachment and colonization of medical implants is of critical interest to significantly reduce morbidity, mortality and health care costs.

1.2 Antimicrobial agents - state of the art

Apart from local antimicrobial prophylaxis - via careful hygiene of surgical intstruments etc - strategies to prevent implant-associated infections are based on the development of adequate coatings such as (*i*) anti-adhesive coatings to impede initial attachment, (*ii*) contact-active, non-leaching coatings, aiming at killing the pathogens upon surface-contact and (*iii*) active release coatings to disable the pathogen via the release of suitable antimicrobials [9].

Anti-adhesive coatings (*i*) are most commonly derived from surfaces functionalized with poly(ethylene glycol) (PEG) or oligo(ethylene glycol) derivatives. Although PEG-based surfaces are more successful at repelling proteins due to complex interactions of the hydrated polymer chains, significant repulsion has also been observed for some microorganisms [10]. Yet, those approaches are temporary and cannot eliminate the source of infection, although the combination with other strategies might prove beneficial [11].

Contact-active, non-leaching coatings (*ii*) describe any surface coating with covalently immobilized, antimicrobial functionalities on the surface. Synthetic as well as natural cationic polymers, based on quaternary ammonium compounds (QACs) have demonstrated remarkable bactericidal properties *in vitro*, in particular against gram-positive species [9]. Self-assembly, grafting from via free radical polymerization and controlled polymerization methods have been employed to functionalize various surfaces (glass, paper, hard polymers) with alkylated polyvinylpyridines (PVP), alkylated polyethylenimines (PEI) and alkylated (dimethylamino)ethyl methacrylates (DMAEMA) [12-14]. As a result of the balanced charge density and hydrophobicity of the alkylchain, those polyelectrolytes have proven to be detrimental for microbial cell membranes [15]. Furthermore, such materials provide an easy-accessible and cheap platform for the design of more complex polymeric networks based on amphipathic macromonomers [16] and polylelectrolyte multilayers [17]. As a natural alternative, the biodegradable chitosan has been widely used to impart antibacterial properties to wound dressings and orthopedic devices, though its antibacterial performance is highly pH-dependent [18, 19].

Another class of antimicrobials is presented by the so-called antimicrobial peptides (AMPs). The term refers to naturally abundant host-defense components of the innate immune system of many species, which are active against a broad spectrum of microorganisms, as a result of evolution in their specific ecological niche. AMPs are relatively short (10-50 amino acids) and mainly composed of spatially organized sectors of hydrophobic and cationic amino acids. Similar to cationic polymers, their antibacterial mechanism of action is based on membrane disruption [20, 21]. Different systems of surface-tethered AMPs indicate that they are still active upon immobilization, although the role of 2D/3D configuration on the antibacterial mechanism is not clear [22-24]. Also, compared to synthetic polymers, their development is relatively expensive. As a result, alternative synthetic approaches were developed to imitate the essential features of AMPs, notably the combination of cationic and hydrophobic segments, similar to QACs. In this context, contact-active polymer compounds, referred to as “SMAMPs” (synthetic mimics of antimicrobial peptides) have been synthesized via ring-opening metathesis polymerization of amphipathic monomers [25].

Although a great variety of highly efficient contact-killing surfaces have been created, the main disadvantage of those surfaces lies in the possibility of dead bacterial layers piling up on

the surface. With antimicrobial functionalities blocked by the dead bacteria, new attachment sites for viable species could be again possible. Simple washing procedures have been used to restore the activity of blocked surface coatings [13], although ideally a more sophisticated design of self-cleaning surfaces could solve this problem.

Eventually, active-release coatings (*iii*) cover a great variety of composite systems, where the antimicrobial agent is gradually released from a biocompatible polymeric reservoir (e.g. thin films, networks, latex particles). The polymeric matrixes are usually composed of various PEG networks, hydrogels, polyelectrolyte multilayers, biodegradable polymers (polylactide (PLA), poly(lactic-co-glycolic acid) (PLGA)), hydroxyapatites, and polyurethanes [26-28]. For instance, several systems of antibiotics incorporated into polyurethane catheters have demonstrated clinical efficacy [29, 30]. Compared to systemic treatments, which require a relatively high dosage of antibiotics, antibiotic coatings are much more advantageous because the antibiotic is concentrated at the infection site. Thus, due to local concentrations of antibiotics, toxic side effects are minimized [3]. However, most of the nosocomial pathogens have shown increased resistance towards antibiotics. Therefore, more and more research activities have been focused towards replacing antibiotics with other antimicrobial agents.

Silver-based coatings have been successfully used as topical agents, for example in silver sulfadiazine creams and wound dressings, especially for burn patients, but also in various models of catheters. Their high activity is generally believed to be derived from the affinity of silver ions toward thiol groups of various proteins, and their consecutive denaturation. Only few microorganisms are known to have developed resistance towards silver [31]. However, cytotoxicity towards mammalian cells has become a notable concern of silver-based coatings [32]. More recently, advances in nanotechnology have spurred the exploration of silver nanoparticles (NPs) [33] and other inorganic NPs for biomedical applications. For instance, copper and copper oxide NPs [34] have shown biocidal activity. Photosensitive semiconductor nanomaterials, especially titania but also zinc oxide NPs, have been discovered to be effective antimicrobials against a broad range of microorganisms [28, 35, 36]. Upon activation by light or other surface reactions, those nanomaterials are believed to produce highly bio-detrimental reactive oxygen species (ROS) like hydroxyl radicals [31, 37].

Another class of radical-generating antimicrobial agents is presented by nitric oxide (NO). NO is produced in small quantities within the body to regulate several biological actions,

which include innate immune responses towards pathogens. As a strong oxidizer, NO is able to target bacterial cell membranes, DNA and proteins. Therefore, various polymer composite coatings have been developed to release NO upon decomposition of suitable precursor functions (e.g. diazeniumdiolates) in contact with aqueous media [6].

Finally, several antimicrobial agents based on biological active compounds, should be mentioned. For instance, immunotherapy with locally transferred IgG antibodies from a hydrogel matrix have shown promising results to reduce implant infections *in vivo* [38]. Recently, bacteriophages have attracted significant interest due to their specific targeting of individual species of bacteria [39, 40]. Bacteriophages ("phages") are viruses that infect prokaryotic cells by injecting their DNA and replicating it inside of the host until the host expires. Although the *in vivo* susceptibility of bacterial pathogens to phages it still poorly understood, promising results have been obtained with physically tethered phage surfaces against a number of food-borne pathogens [41]. Conversely, a very different approach aims at intervening into bacterial communication, also known as quorum sensing (QS) [42]. QS represents an important tool for bacteria to regulate different activities involved in biofilm formation, swarming, excretion of extracellular substances etc. It is characterized by the release of specific molecules, so-called auto-inducers (AI), which are then housed by specific receptor proteins. This process can be inhibited by developing a release system based on synthetic mimics of these AI molecules (e.g. furanones), which are able to target the AI receptor proteins and consecutively block them [43].

In view of the wide-range of existing antimicrobial agents, the development of active release coatings is particularly challenging in terms of dose-properties relations. High concentrations of antimicrobials can easily become cytotoxic or induce other side effects, in particular when dealing with broad-range antimicrobials such as inorganic NPs and radical formers (NO). On the other hand, low concentrations of antimicrobials increase the risk of microbes to develop resistance. Therefore, the window between sufficient antimicrobial activity and cytotoxicity should be carefully monitored by simultaneous experiments on both, microorganisms and mammalian cells. Although implant-associated infections represent quite a common reality, the variety of the above-described approaches and the ongoing research on developing novel antimicrobial systems provide powerful tools to encounter the ever-ongoing bacterial evolution.

1.3 Aim and outline

The aim of this work has been to combine traditional and colloidal polymer chemistry approaches with materials chemistry to develop novel, versatile, functional (composite) systems, capable of reducing microbial attachment or kill adhering microbes for potential applications as implant-coatings.

The presented work was an integral part of the European FP7 project EMBEK1, having the aim to develop and fully characterize novel nano-structured and nanocomposite polymer thin films with antimicrobial properties. In addition to the synthesis of materials, EMBEK1 comprised multidisciplinary studies in close collaborations with various international institutes to investigate the attachment and growth of colonizing wild type and mutant bacteria, as well as the cytotoxicity to non-prokaryotes. The European project was supported by complementary theoretical modeling of bacteria-substratum surface interactions [44].

The development and characterization of antimicrobial, functional (composite) systems requires a fundamental understanding of various colloidal polymer and materials chemistry techniques (e.g. emulsion polymerization, dispersion techniques, thin film processing), suitable nanomaterial characterization techniques, and the exploration of their interactions with microorganisms and cells. Different projects have been developed as part of this work, based on the classification of antimicrobial coating strategies as (*i*) anti-adhesive, (*ii*) contact-active and (*iii*) active release strategies given in section 1.2. The projects are structured into generations of materials from I to V. Though each generation of materials has its individual attributes, each system is build on the experience of the previous one and the complexity of the systems increases from generation I to V. The mostly colloidal systems were chosen to maximize the amount of functional surface groups, following the high surface-to-volume ratio, typical of nanoscale colloidal systems.

The 1st generation of materials was based on an anti-adhesive approach. PEGylated systems have demonstrated anti-adhesive properties towards proteins and some microorganisms, and thus represented a desirable system to start with. Therefore, PEG-functionalized polymeric NPs were prepared by miniemulsion copolymerization of styrene and various PEG-macromonomers. The influence of different PEG concentrations and chain lengths on the colloidal stability of the particles was studied as well as their interactions with *P. aeruginosa.*

The 2nd generation and 3rd generations of materials were based on contact-active QACs of alkylated DMAEMA in a novel colloidal approach. The quaternization of DMAEMA with a long hydrophobic alkyl chain imparts antimicrobial functionalities to the monomer as well as surface-active properties. Therefore, the miniemulsion copolymerization of styrene and quaternized DMAEMA (qDMAEMA) should give access to stable, surfactant-free colloidal dispersions of functional NPs (2nd generation). Additionally, the formulation of pure, surfactant-free PqDMAEMA NPs by miniemulsification and subsequent solvent evaporation of dispersed PqDMAEMA polyelectrolyte chains aimed at further increasing the surface functionalities with respect to its antibacterial performance (3rd generation). In addition to the material characterization, the antimicrobial activity and interaction with mammalian cells were investigated and evaluated.

The 4th and 5th generations of materials were based on leaching systems. ZnO NPs were chosen as an antimicrobial agent because they represent a very versatile material (e.g. photocatalyst), whose biocidal properties have only recently been discovered and remain to be explored systematically [45]. Furthermore, well-defined NPs are easily accessible by solvothermal synthetic methods. The incorporation of ZnO NPs into poly(L-lactide) (PLLA) colloids (4th generation) provides a multifunctional platform to use the photocatalytic properties of ZnO to trigger their release from the biodegradable PLLA matrix and thus exploit their antibacterial properties. On the other hand, the incorporation of ZnO NPs into a biocompatible, photocrosslinkable poly(*N*-isopropylacrylamide)-based hydrogel gives access to antimicrobial thin films, where the amount of ZnO and its release rate can be tuned by simply varying the film thickness. Bacterial and cell growth were simultaneously investigated in collaboration within the group and the University Medical Centre Mainz.

In light of the multidisciplinary character of this project, the interactions of the different materials generations with various microorganisms and cells have been carried out in close collaboration with the University of Bath, the University Clinic of Cologne, including microbiological training sessions on different assays, and the University Medical Centre Mainz. The antimicrobial studies were focused on nosocomial-active strains of *S. aureus* (MSSA476), *P. aeruginosa* (PAO1) and *E. coli*. The development of nanocomposite ZnO-hydrogel thin films is the result from a close collaboration with the Institute for Electronic

Structure and Laser/Foundation for Research and Technology – Hellas, Greece (IESL-FORTH).

2. Theoretical Background

2.1 Preparation techniques for polymeric nanoparticles

The number of applications related to polymeric nanoparticles (NPs) has tremendously increased within the last years ranging from numerous technological applications in electronics, sensing devices, and waste water treatment to the biomedical sector of drug delivery/targeting systems and cosmetics [46-48]. The preparation technique is governed by general considerations on the type of polymeric system, the area of application, the size requirements and the surface functionalization. For biomedical applications for example, factors related to the biocompatibility of the polymeric system and the toxicity of additives/organic solvents, represent critical parameters. Polymeric NPs are accessible by either polymerization of suitable monomers via classical polymerization methods (mini-, micro-, macroemulsion, interfacial and controlled/living radical polymerization) or by dispersion of preformed polymers (solvent evaporation, nanoprecipitation, salting-out, dialysis and supercritical fluid technology) as illustrated in Fig. 1 [49].

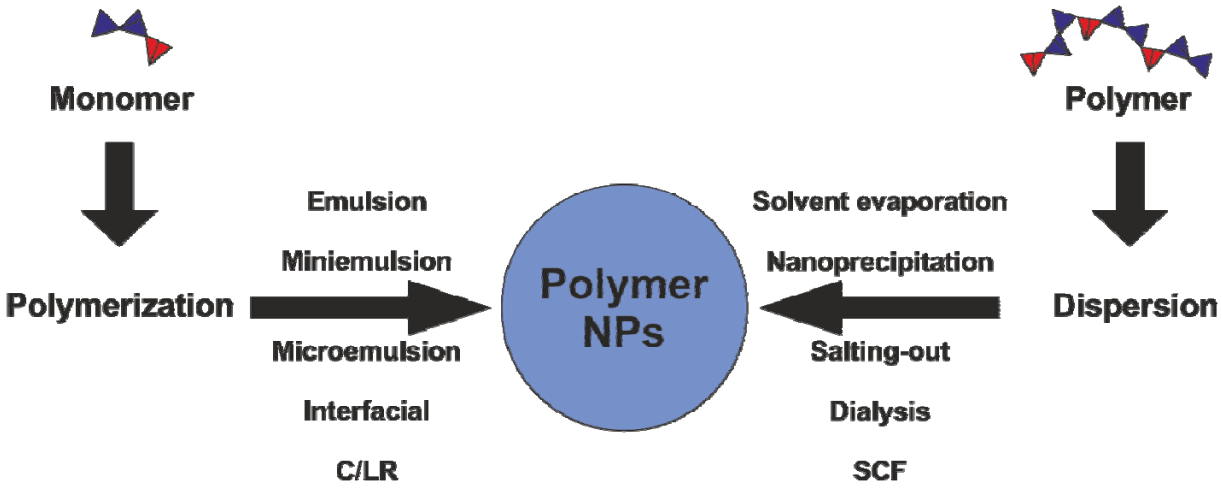

Fig. 1. Schematic presentation of different methodological routes for the fabrication of polymer NPs (C/LR: controlled/living radical, SCF: supercritical fluid technology).

In the following, different techniques of polymer NP fabrication will be discussed with a main focus on miniemulsion polymerization and solvent evaporation used in this work.

2.1.1 Polymerization techniques

The polymerization of monomers offers different routes to design functional polymeric latexes. The method of choice determines the nucleation mechanism, the presence of additives, size, size distribution and morphology, which are key determinants of the properties and applications [50].

2.1.1.1 Emulsion polymerization

Conventional emulsion ("macroemulsion") polymerization is a heterophase polymerization technique, which involves the emulsification of monomers in an aqueous phase and consecutive stabilization of the droplets by surfactant molecules. The main ingredients of a conventional protocol include a vinyl or acryl monomer of low water solubility, a dispersing medium (water), surfactant and a water-soluble initiator. The surfactant concentration is generally higher than its critical micelle concentration (CMC). Therefore, surfactant-micelles are formed upon solubilization of the surfactant into the dispersing medium. After addition of the surfactant, the monomer is dispersed into the aqueous phase by stirring. Consequently, the emulsion contains monomer droplets, small amounts of solubilized monomer in the water phase and monomer swollen surfactant-micelles. Since the number of micelles is much higher than the number of monomer droplets, the polymerization is located within the surfactant micelles. The radical formation is initiated in the water phase, followed by diffusion of the radical seeds into the surfactant micelles where the polymerization proceeds. Continuous monomer diffusion through the water phase from the monomer droplets into the micelles ensures adequate propagation. The polymerization kinetics can be classified into three intervals: During the nucleation stage (I), oligomeric radical seeds are generated in the water phase, where they grow until after a few additions, surface-active species with a polymerization degree z are formed ("z-mer"), which then predominantly enter monomer swollen micelles, thus forming the particles. The particle number is limited by the surfactant concentration. Once, it drops below its CMC, the particle formation is finished. Subsequently, the polymerization proceeds within the monomer swollen micelles (interval II) until the monomer droplets are consumed, as characterized by a gradual decrease of the monomer concentration in the particles and water phase (interval III). Preformed latex particles may be added prior to polymerization to form monomer-swollen latex particles, in which case one obtains a seeded polymerization.

The colloidal stabilizers in emulsion polymerization include ionic and non-ionic molecular or (block co-) polymeric surfactants. Several commonly used surfactants are listed in Fig. 2. The resulting latex particle sizes range between 50 and 500 nm. Typical applications of latexes produced by conventional emulsion polymerization include paints, coatings, adhesives, and carpet backings. The use of water as dispersing medium ensures excellent heat dissipation in an environmentally friendly process. Compared to solution polymerization, higher rates of polymerization and higher molar masses are obtained. Applications in biomedicine are restricted depending on the nature of physically adsorbed surfactants and other additives [50, 51].

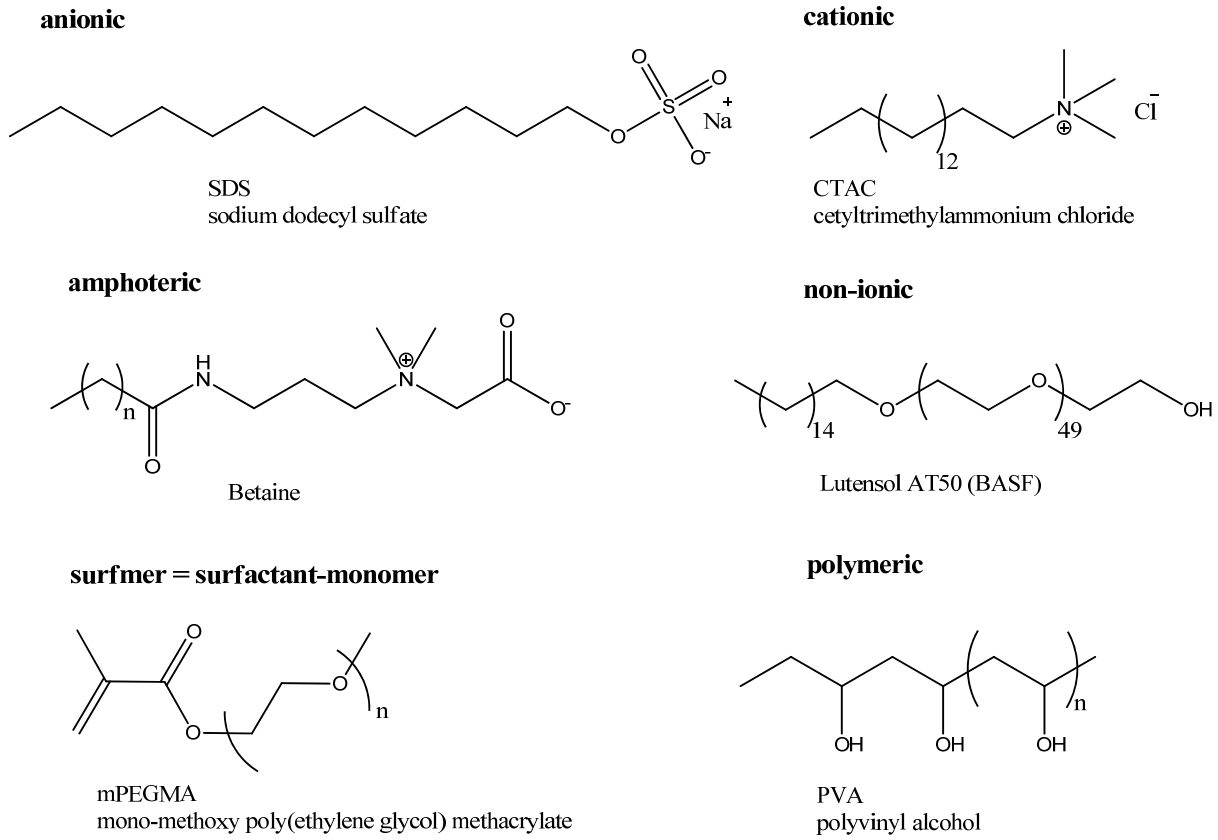

Fig. 2. Different types of common stabilizers used in emulsion polymerization.

As an alternative to surfactant-stabilized systems, surfactant-free emulsion polymerization can be of interest for the fabrication of "clean" latexes. A typical protocol for an emulsifier-free system comprises, water, a water-soluble initiator (e.g. potassium persulfate) and vinyl or acryl monomers. To ensure colloidal stability, either an initiator bearing charged end groups for electrostatic stabilization or an ionic comonomer has to be selected. In the absence of

surfactants, micellar nucleation still dominates for slightly water-soluble monomers via micellization of the z-mers, which now bear charged end groups. However in case of more water-soluble monomers, micellar nucleation is replaced by a homogeneous nucleation mechanism: particle formation occurs by collapse (coil-to-globule transition) of oligomeric radical seeds when reaching a critical degree of polymerization greater than z. Since the collapsed chain is hydrophobic, it will be swollen by consecutive monomer diffusion, which ensures propagation and subsequent particle formation. During propagation, particle nucleation decreases at the expense of growing monomer-swollen latexes, which progressively consume any newly formed z-mers before the latter reach the critical degree of polymerization for homogeneous nucleation. Therefore, the number of particles is much smaller compared to conventional emulsion polymerization and the particle sizes achieved by emulsifier-free techniques are slightly larger than in the presence of surfactants, with narrow size distributions [52, 53].

Other emulsifier-free techniques are available where the surfactant is completely replaced by a surface active monomer. Surfactant-monomers, also known as surfmers, are characterized by an amphipathic structure, in addition to a polymerizable entity. These polymerizable surfactants serve as comonomer and simultaneously form micelles in aqueous solutions above their CMC. Similar to the emulsifier-free emulsion polymerization, the emulsifier will be intrinsically immobilized on the latex particle by copolymerization. Therefore, the stability of the latexes is much improved when submitted to high shear, freeze-drying or film formation, where physically adsorbed surfactants usually tend to migrate. For instance, Cochin and Laschewsky demonstrated enhanced colloidal stability of PS latexes synthesized in emulsion polymerization in the presence of polymerizable surfactants and cationic polysoaps, as compared to the same latexes, stabilized by a conventional surfactant [54]. Naturally, the process requires an adequate compatibility of the key monomer component and the surfmer. On the other hand, the reactivity of the surfmer should be slightly slower than for the main monomer to secure time for sufficient stabilization. A combination of both techniques, notably emulsifier-free emulsion copolymerization with a surface-active, hydrophilic comonomer generally leads to polymer particles with relatively narrow size distribution due to the rapid nucleation rate of the additionally stabilized oligomer radical seeds [55, 56].

In general, suitable latexes can be obtained by emulsion polymerization of monomers with moderate water solubility. In case of water-soluble monomers, aqueous phase polymerization competes with emulsion polymerization. This problem can be eluded by moving towards inverse (water in oil) emulsion polymerization, whereby monomer-swollen water droplets are polymerized in an oil phase. On the other hand, water-insoluble monomers cannot be polymerized by conventional emulsion polymerization neither because the monomer diffusion into the micelles requires a minimum of water solubility. Therefore, the polymerization locus has to be moved towards the monomer droplets, which is realized in micro- and miniemulsion polymerization [50].

2.1.1.2 Miniemulsion polymerization

A typical system for miniemulsion polymerization contains water, monomer, co-stabilizer, surfactant and initiator (oil or water-soluble). In contrast to conventional emulsion polymerization, the monomer droplets are created by high shear devices (e.g. ultrasound, high-pressure homogenizer). The locus of polymerization is within the monomer droplets (droplet nucleation), which in direct miniemulsion (oil-in-water, o/w) are internally stabilized by an ultrahydrophic molecule (costabilizer). In a typical process, high shear homogenization of preemulsified monomer droplets leads to the formation of small, stable droplets in the size range of 50 to 500 nm by consecutive fusion and fission. The monomer droplets serve as so-called “nanoreactors” for the generation of almost identical polymeric copies [57].

Small droplets generally tend to grow from coalescence and Ostwald ripening due to multiple collision and diffusion processes [58]. In miniemulsion, coalescence is suppressed by ionic or steric repulsion of the surfactant-stabilized nanodroplets. However, the amount of surfactant is much lower than their CMC, which results in incomplete surface coverage and relatively high surface tension of the final latexes. Despite of these thermodynamically unfavorable conditions, the droplets are additionally restrained from fusing by the addition of the hydrophobic co-stabilizer, which generates an osmotic pressure within the droplets. This agent is confined to the inside of the particle due to its hydrophobicity and therefore effectively counterbalances the pressure related to the unfavorable surface-to-volume ratio of the smaller droplets, which otherwise would initiate Ostwald ripening. The latter stress factor is diminished by polymerization and subsequent phase separation of the hydrophobic polymeric NPs [59, 60].

The miniemulsion polymerization method is a highly versatile technique for the preparation of functional polymeric nanoparticles. Owing to the concept of the individually acting nanoreactors, various reactions can be conducted in or at the interface of the droplets, i.e. organic reactions, enzymatic reactions, crystallization processes and sol-gel reactions [61-64]. The method can be applied in direct (oil-in-water, o/w) or indirect (water-in-oil, w/o) mode of operation to a number of different monomers or monomer mixtures. Furthermore, the process allows for the efficient encapsulation of different inorganic and organic entities, which has been used for instance for the encapsulation of dyes, hydrophobic metal complexes or DNA [65-67]. In contrast to conventional emulsion techniques, miniemulsion polymerization is not restricted to free radical polymerization. Multiple examples can be found in the literature of controlled radical polymerization, anionic and cationic polymerization, enzymatic polymerization and polyaddition, -condensation processes [68-71].

2.1.1.3 Microemulsion polymerization

The main ingredients in a typical microemulsion polymerization do not differ from conventional emulsion protocols. In contrast to the other emulsion types, thermodynamically stable monomer-swollen micelles are formed upon addition of large amounts of surfactant. Therefore, the surface-coverage of the very small nanodroplets is complete and the interfacial tension at the oil/water interface is close to zero. Polymerization takes place within the monomer-swollen micelles. However, owing to the small droplet size, initiation does not occur simultaneously in all nanodroplets. Therefore, very small latexes of 5-50 nm in size are formulated, in parallel to empty micelles and secondary nucleation products. Typical polymer formulations require large amounts of surfactant in relation to the monomer and are therefore very dilute to ensure full solubilization of the surfactant [72, 73].

The size ranges of latex particles obtained via different heterophase polymerization techniques are schematically presented in Fig. 3. Nanoscale latexes below 500 nm are accessible via emulsifier free, conventional and miniemulsion. The microemulsion technique applies for latexes much smaller than 100 nm.

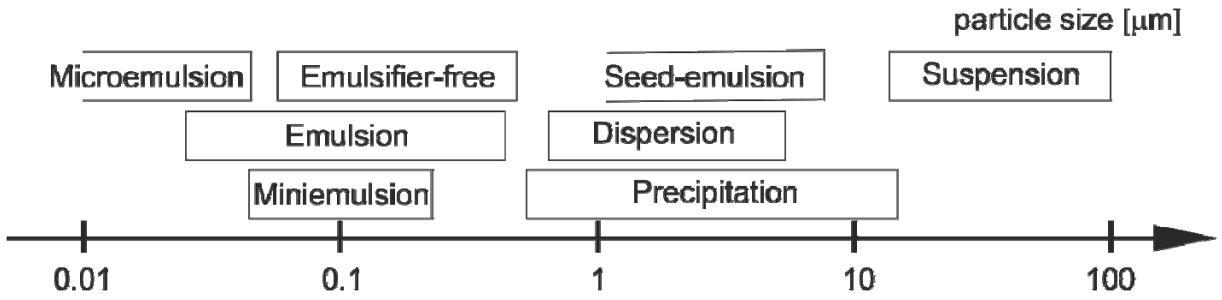

Fig. 3. Schematic presentation of polymerization techniques and the resulting size distribution for the synthesis of polymeric NPs [74].

2.1.1.4 Interfacial polymerization

Interfacial polymerization is a heterophase step polymerization process of two reagents which are dissolved in two different phases. After emulsification, interfacial crosslinking reactions such as polyaddition and polycondensation take place at the interface of the two liquids (water, organic solvent). Technically speaking, interfacial polymerization can be performed in micro- [75] and in particular miniemulsion systems [73]. Polymeric NPs as well as nanocapsules (e.g. polyurethane capsules) are obtained, the latter by using aprotic solvents as monomer reservoir. Though the technique offers various possibilities for the encapsulation of pharmaceutical products, is affords a relatively limited control on particle size and distribution. Membrane reactors, which allow for the controlled addition of reactants to the continuous phase, have demonstrated a more precise control on the average NP size. However, large-scale applications are limited due to the high costs of suitable membranes [76].

2.1.1.5 Controlled/living radical polymerization (C/LRP)

The motivation to replace free radical polymerization by C/LRP methods is driven by the need to synthesize better defined polymers in terms of molar mass, polydispersity and end-functionalities for biomedical applications. Three approaches, based on nitroxide-mediated polymerization (NMP), atom transfer radical polymerization (ATRP) and reversible addition and fragmentation chain transfer polymerization (RAFT) in heterophase have been successfully applied to generate well defined latexes [77-79]. The particle size of the final product is critically influenced by the nature and concentration of the radical mediator, but also by the monomer, initiator and the emulsification technique used. The disadvantages of

the method are the complexity and cost of the process and residual amounts of the radical mediator [49].

2.1.2 Dispersion techniques

2.1.2.1 Solvent Evaporation

Solvent evaporation is a widely employed dispersion technique to prepare polymer NPs from mostly biodegradable polymers (poly(lactide) (PLA), poly(lactic-co-glycolic acid) (PLGA), poly-ε-caprolacton (PCL)) in pharmaceutical industry because it allows for an easy encapsulation of hydrophobic and hydrophilic components. Many drug delivery systems, based on the encapsulation of for example antibiotics [80], minerals [81] or genetic material (RNA) [82] have been fabricated by this technique. In addition, the method is not restricted to synthetic polymers, but can be also used for natural polymers such as chitosan, polysaccharides, alginates or gelatin. Depending on the nature of the encapsulated drug, single (o/w) or double emulsions (w/o/w) are utilized [49]. In single emulsions, the polymer is dissolved into a good (organic) solvent and emulsified into an aqueous surfactant-enriched solution via high speed homogenization or ultrasound. Subsequent evaporation of the solvent leads to the precipitation of the polymer in the aqueous suspension. As a basic requirement, the good solvent should be volatile and exhibit a lower boiling point than water. Single emulsions are very well suited to encapsulate hydrophobic compounds. Conversely, hydrophilic substances can be encapsulated via double emulsions. Thereby, the hydrophilic drug is dissolved in water and emulsified in the organic phase, which contains the polymer under stabilization of a lipophilic surfactant. The resulting w/o emulsion is then emulsified a second time with an aqueous phase under additional stabilization of a hydrophilic surfactant (w/o/w), followed by the evaporation of the solvent. Multiple studies in the literature have identified the crucial determinants for particle size and size distribution to be related to (*i*) the concentration of emulsifier, (*ii*) the polymer concentration and (*iii*) the type of solvent [79, 83, 84]. Homogenizer and evaporation speed proved to be less influential in single emulsions. In contrast, in double emulsions, the mixing technique for the second emulsification step was found to play a significant role [85].

A special case of a solvent-free process was presented by Quaglia and coworkers [86]. Based on a melting/sonication technique, a liquid, water-immiscible copolymer was emulsified in

water at a temperature higher than the melting temperature of the polymer. Subsequent cooling of the liquid/liquid phase-system induced the solidification and consecutive precipitation of the copolymer.

2.1.2.2 Nanoprecipitation

In contrast to the high-energy emulsification processes of miniemulsion and solvent evaporation, the nanoprecipiation method, also known as solvent displacement or interfacial deposition, relies on intrinsic physicochemical properties of the system [87]. The main components include a polymer, a partially water-miscible polymer solvent (e.g. ethanol, acetone, binary solvent blends) and a non-solvent for the polymer (water). In a typical formulation process, the organic phase including the dissolved polymer is added to the aqueous phase under moderate stirring. The solvent displacement under rapid diffusion into the water phase leads to the precipitation of the polymer NPs. The diffusion process of the organic solvent is thermodynamically oriented towards the phase where it has greater solubility [88]. Thus, the solubility depends on the individual concentrations of each component in the three-phase system. Remarkably well defined particle sizes of narrow size distribution are obtained if the ratio of organic phase to water and the mixing conditions are well adjusted [89]. Generally, biodegradable polyesters for biomedical applications are commonly formulated by this technique because it does not require additional stabilization by surfactants although stabilizers are occasionally added to improve the colloidal stability [90].

Other related methods, such as the emulsion-diffusion method [91] or the ouzo effect [92] similarly exploit the spontaneous mixing or phase separation phenomena depending on the composition of a multiphase system (polymer, water-miscible solvent, non-solvent and other additives) for the formulation of biodegradable polyester nanocapsules.

2.1.2.3 Salting-Out

The salting-out procedure is very similar to the nanoprecipitation method. Basically, the oil-in-water emulsion is formulated from a dissolved polymer in a water-miscible solvent with an aqueous solution of salt. The addition of salt alters the solvent miscibility with water, therefore inducing the spontaneous emulsification. A reverse salting-out effect is achieved after diluting the mixture with larger quantities of water, which results in the precipitation of the polymer NPs via solvent-displacement [93].

2.1.2.4 Dialysis

As opposed to the nanoprecipitation method, in the dialysis process, the polymer is dissolved in organic, water –miscible solvent (e.g. DMF, DMSO), placed into a dialysis tube of defined molecular weight cut-off and dialyzed against a non-solvent for the polymer (water). Various NPs of preformed well-defined copolymers have been prepared this way. The morphology and particle size distribution is mainly affected by the type of solvent [49].

2.1.2.5 Supercritical fluid technology

The supercritical fluid technology (SCF) offers the possibility to fabricate polymeric NPs of high purity in the absence of organic solvents [94]. In the rapid expansion of supercritical solution (RESS) mode, the polymer/solute is dissolved into supercritical fluid (e.g. CO_2, CO, NH_3), followed by spraying into an ambient air reservoir. Particle precipitation is induced via the rapid pressure reduction and consecutive phase transition of the fluid. Thereby, the solubility limit of the supersaturated solute is exceeded. The size and size distribution of the polymer particles is determined by the polymer saturation in the supercritical fluid, material and processing conditions. However, the RESS technique merely allows for the generation of micronsized products. In a modified variant, the rapid expansion of supercritical solution into liquid solvent (RESOLV) technique, the supercritical fluid is expanded into a polymer non-solvent (water), which leads to the formation of nanoscale precipitates [95]. The typical setup for a SCF system includes a pressurized syringe pump, a heating unit to reach the supercritical state, an expansion nozzle and the final reservoir (air, water). Despite the cleanliness of the technique, the main drawback lies in the poor solubility of suitable polymers in supercritical fluids.

2.2 Preparation techniques for monodisperse inorganic nanocrystals

Owing to their unique electrical, optical and magnetic properties, the exponential growth of nanotechnological applications based on inorganic nanocrystals (NCs) in the last two decades has spurred the ongoing research on the synthesis of well-defined nanomaterials [96-98]. The synthesis of inorganic NCs can be achieved by physical approaches (top-down), for example metal evaporation and ball milling or solution phase colloidal chemistry routes (bottom-up). Physical methods are generally suited for large scale production but only provide limited

control on the particle characteristics (size, shape, size distribution). On the other hand, chemical methods give access to the controlled synthesis of monodisperse nanomaterials [99]. In general, homogeneous nucleation of inorganic NCs happens in one shot ("burst nucleation"), i.e. many nuclei are formed at the same time when the degree of supersaturation of the "monomeric species" exceeds the energy barrier for nucleation. In this case, the monomeric species corresponds to the minimum subunit of bulk crystal. Since the consumption of the monomeric species is much faster than its production, nucleation ceases in favor of NC growth as long as the monomeric species is supplied [100-102]. Therefore, the key strategy towards controlled size distributions is to initially induce a single nucleation event and then separate nucleation and growth. This can be accomplished by various methods, such as reduction, thermal decomposition and hydrolytic and non-hydrolytic sol-gel reactions. In the following, those techniques will be briefly characterized [103].

2.2.1 Reduction methods

The reduction of metal precursors is a general procedure to access metal NPs. One of the most prominent reactions is the Turkevitsch and Frens method for the synthesis of Au NPs using sodium citrate to reduce $HAuCl_4$ and stabilize the resulting NPs [104, 105]. The polyol process relies on the reduction of metal salts in high boiling point alcohols to create NCs within the Pt group [106].

2.2.2 Thermal decomposition

Various nanomaterials based on metals, semiconductors and metal oxides can be synthesized by the thermal decomposition of organometallic and inorganic precursors in the presence of surfactants. The nucleation of the NCs can be either initialized by hot-injection of the precursor material into the surfactant solution or by rapidly heating the full mixture to a specific temperature. The process generally allows for the generation of monodisperse, highly crystalline products such as CdSe [107] or ZnO [108].

2.2.3 Sol-gel methods

Sol-gel reactions involve the hydrolysis and condensation of metal alkoxydes in acidic or basic aqueous alcohol media. The method is widely employed for the synthesis of nanoscale metal oxides in aqueous media [103].

2.2.4 Non-hydrolytic sol-gel methods

In analogy to the classical sol-gel methods, the thermal decomposition of metal alkoxydes or carboxylates is carried out at high temperatures (200-300 °C) in organic media via alkyl halide or ester elimination reactions to produce metal oxide bridges. It is well suited for the formation of electron-deficient NCs from Ti^{4+}, Zr^{4+}, Hf^{4+} and Sn^{4+} [99].

2.3 Preparation of inorganic/polymeric composite materials

The hybridization of inorganic nanoparticles and polymeric materials is of significant technological interest to enhance mechanical strength and thermal resistance, or introduce optical, magnetic and biomedical properties to the polymer [51]. The basic motivation of blending inorganic/polymeric materials is to protect the inorganic material from the environment and vice versa and to exploit the synergistic properties of both materials. In the following, a brief review on some current synthetic strategies for the fabrication of nanocomposite materials will be given, including selected examples.

2.3.1 Colloid-based hybrid latexes

The key strategy to successfully combine inorganic and polymeric materials relies on the surface modification of the inorganic entities to make them compatible with organic monomers/polymers. The resulting morphologies, e.g. core-shell, multinuclear, raspberry-like, or multipod-like, are governed by the surface interactions between both materials via the adsorption of surfactants, organosilanes, titanates, macromonomers, surfmers, ionic initiators or ionic monomers [109]. Three methodologies can be differentiated, including (*i*) the dispersion of preformed inorganic NPs into monomer solution, (*ii*) the *in situ* formation of inorganic NPs in combination with preformed latexes, and (*iii*) the combined *in situ* formation of both materials. Route (*i*) generally leads to the formation of inorganic@polymer type composites, whereas (*ii*) and (*iii*) can be used to additionally fabricate polymer@inorganic type composites.

2.3.1.1 Inorganic@polymer type composites

These types of nanomaterials are usually synthesized by various emulsification and dispersion techniques. For example, CdSe quantum dots were hydrophobized by the stabilization with

copolymer units of acrylic acid and butyl acrylate, followed by dispersion into styrene and subsequent emulsion polymerization [110]. Various anisotropic structures of core-shell spheres, ellipsoids and doublets were synthesized by the seeded emulsion polymerization of vinyl-functionalized silica-coated Fe_3O_4 and styrene [111]. The *in situ* formation of Ag NPs, encapsulated into a nanoreactor of poly(vinylpyrrolidone) has been demonstrated in an inverse miniemulsion system [112].

2.3.1.2 Polymer@inoganic type composites

Many state-of-the-art NP preparations afford well-defined core-shell structures by decomposition of organometallic precursors in a solution environment of ready-made latexes [113]. For instance, PS@Ag core-shell nanocomposites have been fabricated by the precipitation of silver precursor material on preformed PS latexes using poly(ethyleneimine) as reducing agent [114]. On the other hand, Caruso and coworkers initially demonstrated an electrostatic self-assembly process of SiO_2 on PS NPs coated with polyelectrolyte multilayers [115]. Another, very common process makes use of the stability of so-called pickering emulsions, where a monomer is emulsified through stabilization of inorganic NPs, followed by polymerization to generate stable, inorganic NP-coated latexes [116, 117].

2.3.2 Other inorganic/polymeric nanocomposite architectures

The field of inorganic/polymer nanocomposites is immensively vast. Industrial applications of inorganic/polymeric nancomposite coatings have been used for decades for instance in automotive industry, e.g. for the enhancement of mechanical stability or for corrosion protection [118]. As part of the evolution of synthetic strategies which allow for the design of ever increasing well-defined nanostructures, the research on complex material engineering has been boosted. The greatest challenge of blending inorganic and polymeric materials is to control the dispersion of the filler particles within the polymer matrix, i.e. to avoid agglomeration [119]. As mentioned above, those factors can be influenced by mediating NP polymer interactions with adequately functionalized ligands. The agglomeration of inorganic NPs can be controlled by several strategies. For instance, performing the NP synthesis directly in the polymer matrix slows down coalescence, owing to the viscous nature of the polymer [120]. The main drawback of this technique lies in the restricted control of NP characteristics. A great deal of work has been dedicated to the compatibilization of inorganic

NPs with monomeric solutions via intricately functionalized linker molecules (for examples, see 2.3.1). Yet, this process is costly for large scale productions. Another strategy involves the solution mixing of both preformed components, followed by subsequent dropcasting or spin-coating. Although this technique is very simple, it requires a common solvent for both materials [119]. In the following, a few examples of smart nanocomposite materials for biomedical applications are presented that are accessible through the techniques described above.

Smart materials are materials that can change significantly their mechanical, thermal, optical, or electromagnetic properties in a controlled fashion by external stimuli [121]. Nanocomposite polymer hydrogels can be classified as such due to the reversible swelling properties of the polymer network in combination with intrinsic properties of inorganic structures [122]. For example, gels made of PEG and Laponite (silicate nanoplatelets of ~30 nm) demonstrated reversible crosslinking with tuneable viscoelastic properties that could be potentially applied for self-healing materials [123]. Another system of Au NP hydrogel (PVP) composites demonstrated significant pH sensing behavior, which could be monitored via small changes in the surface-plasmon resonance [124]. The authors used the Turkevich method to reduce the Au NPs within chemically crosslinked PVP membrane coatings. Antibacterial composite materials were generated by the *in situ* production of Ag NPs in crosslinked poly(*N*-isopropylacrylamide)-co-poly(sodium acrylate). Surface coupling with carboxylated hydrogel groups assured a uniform NP distribution within the polymer matrix [125]. On the other hand, numerous studies have been reported on the combination of magnetic materials with thermoresponsive polymers, so-called ferrogels [126]. For example, recently, Zao and coworkers presented an alginate-based ferrogel with magnetoresponsive visco-elastic properties as release system for various drugs, DNA and cells. The ferrogel was prepared by solution mixing of functionalized alginate and Pluronic F127-modified magnetite NPs, followed by crosslinking via carbodiimide chemistry [127].

In conclusion, selected examples have highlighted the synthetic versatility and potential of inorganic/polymer nanocomposites for important biomedical applications such as sensing, drug delivery, antimicrobial reservoirs, hyperthermia and tissue engineering.

2.4 Microbiological background

This chapter aims at summarizing a few microbiological principles, which contribute to the understanding of the major factors involved in bacterial colonization of surfaces.

Bacteria are categorized as single-cell prokaryote microorganisms, which can adopt a wide range of shapes, notably spheres, rods, and spirals. Their typical dimensions vary between less than 1 µm to a few micrometers in length. The main representatives used in this work are strains of *Staphylococcus aureus*, *Pseudomonas aeruginosa* and *Escherichia coli*. *S. aureus* is a gram-positive coccal (spherical) bacterium that can be found on the body surface (skin, nose). It typically infects skin and wounds, ranging from minor skin irritations to life-threatening diseases such as pneumonia, meningitis, and sepsis. The most prominent strain associated to antibiotic resistance and healthcare infections worldwide is the methicillin-resistant *S. aureus* (MRSA). *P. aeruginosa* is a gram-negative rod-like soil and water germ that is also part of the skin flora. It can cause inflammation and sepsis, which can be critical when attaining major organs (lungs, kidney) and urinary tracts in combination with common combined resistance towards antibiotic treatment. Both species are prominent pathogenic candidates in nosocomial infections with a high affinity to colonize on catheters and ventilators. On the other hand, *E. coli* is a gram-negative rod-like bacterium, typically found in the gut flora of living organisms. Though the majority of strains are inoffensive, some strains are responsible for serious food poisoning (e.g. enterohemorrhagic *E. coli* (EHEC)), hospital-acquired urinary tract infections, blood stream infections, or respiratory illnesses [128, 129]. According to the annual epidemiological reports of the European Union [1], the resistance of *E. coli* to common antibiotics such as aminopenicillins or fluoroquinolones tends to increase over several years .

Gram-positive and gram-negative bacteria significantly differ in their cell wall structure. Both cell walls are composed of a rigid layer of peptidoglycan, which is a polysaccharide composed of two sugar derivatives and a few amino acids. As illustrated in Fig. 4, gram-positive bacteria have relatively simple wall architectures, based on a single layer of peptidoglycan with embedded negatively charged teichoic acid. These are capsular polymers of polyalcohols connected via phosphate esters and sugar units that are directly attached to the peptidoglycan layer or membrane lipids (lipoteichoic acids). In contrast, the cell wall of gram-negative bacteria is much more complex. An additional outer membrane layer with linked

lipid and polysaccharide units, called the lipopolysaccharide layer (LPS), can be found on top of a relatively thin peptidoglycan layer (periplasm). Protein channels (porins) regulate the exchange of hydrophilic low-molecular-weight substances. The toxic properties of pathogenic gram-negative bacteria are associated with the LPS layer, in particular lipid A [128, 129].

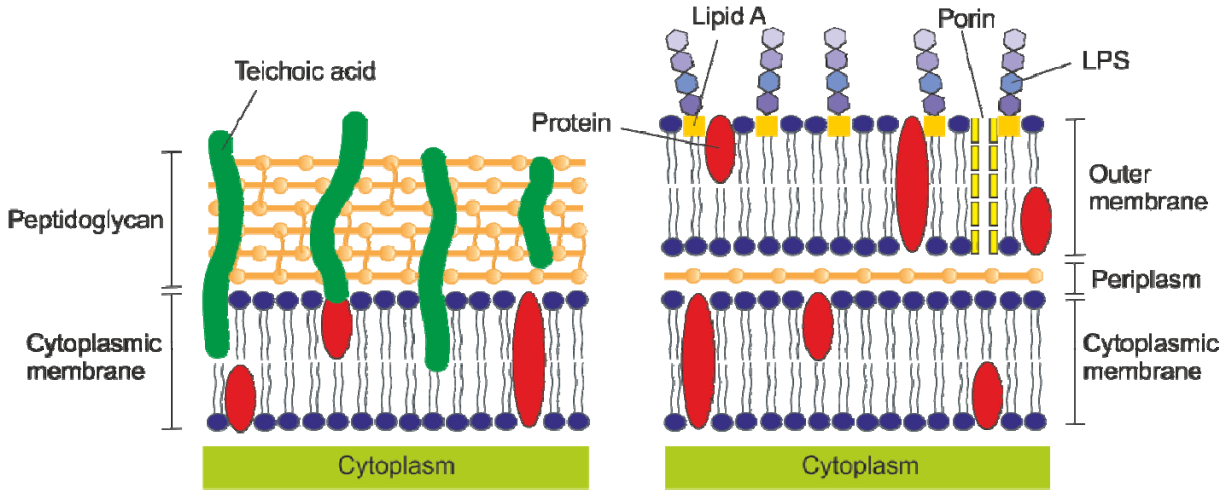

Fig. 4. Schematic presentation of the gram-positive (left) and gram-negative (right) cell wall.

The natural proceedings of sessile bacterial species involve the colonization and multiplication in biofilms. Biofilms are surface-attached bacterial assemblies in a polysaccharide matrix. The biofilm formation proceeds as a regulated developmental sequence, which is schematically represented in Fig. 5. The initial stage is governed by reversible physical adsorption. Second, the irreversible attachment is directed as a result of a series of genetic and environmental responses. The next stage of the biofilm development is characterized by the aggregation of cells into colonies, the production of slimy polysaccharide matrix, and subsequent crosslinking. Intercellular communication via the excretion of signaling molecules, so-called quorum sensing, ensures further maturation and reproduction. The final biofilm is a multicellular dynamic complex of more than one bacterial species, which offers a prominent host for microbial survival and self-defense for several reasons. First, the hydrogel-like, viscoelastic properties of the polysaccharide layer ensure adequate shear stability from environmental stress sources (e.g. weather or current). Second, biofilms are highly resistant to phagocytosis, toxic molecules (e.g. antibiotics, antimicrobial agents), UV light, and acid exposure. Third, the close association facilitates nutrient exchange and communication. Furthermore, internal regulation mechanisms can direct an eventual detachment to colonize new niches. The high degree of inertness of bacterial biofilms has

significant detrimental implementations in medicine and industrial applications (food industry, marine fouling, fuel pipelines, drinking water processing). In particular, the implication of biofilms on medical implants entails serious medical sequelae. The complex interaction between the biofilm pathogen and the host inflammatory response triggers a series of uncontrollable modifications and alterations on both sides. Therefore, the focus of medical treatments concentrates on preventing the initial stages of biofilm formation, notably physical and chemical adhesion [6, 8].

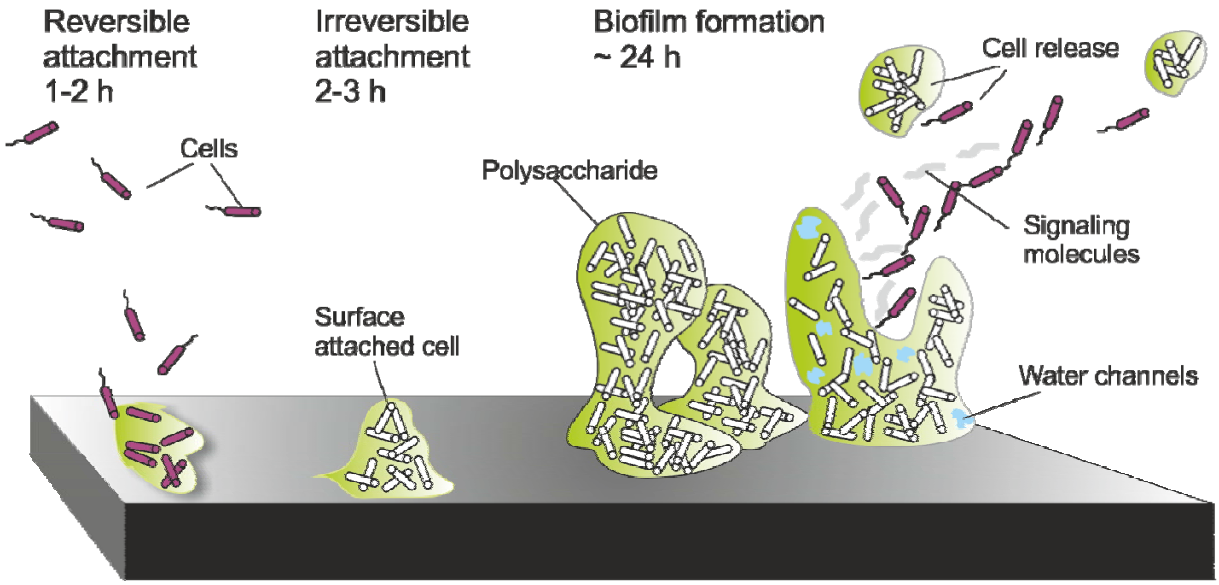

Fig. 5. Schematic presentation of a typical mushroom-shaped biofilm formation observed for *P. aeruginosa*.

Several noteworthy studies based on thermodynamic approaches and combined modeling have been performed to elucidate the complex physico-chemical interactions between pathogen and substrate surface [130-134]. Bacterial adhesion is generally influenced by factors related to hydrophobicity, motility, intrinsic charges and the release of extracellular substances. When immersed in an aqueous environment, conditioning layers of proteins or organic molecules determine the surface texture of the substratum surfaces. Other factors depending on the type (pH, ionic strength) and hydrodynamic condition of the medium etc further complicate precise predictions. The initial reversible physical interactions are generally described by an extended DLVO-theory (Derjaguin, Landau, Verwey, Overbeek) based on surface thermodynamic analysis of bacterial cells and substratum via contact angle

measurements, zeta potentials and adhesion forces by atomic force microscopy. According to those studies, physical adsorption of bacteria is dominated by short-range, attractive acid-base interactions, which are strain-specific and cannot be generalized, in combination with non-specific long-range Lifshitz-van-der-Waals forces [130, 134]. The additional consideration of chemical interactions via excretion of extracelluar substances such as polysaccharides, esters, carboxylic acids, and carboxylates further complicates modeling approaches and the overall adhesion phenomenon is not completely understood yet [135].

In brief, we have seen that the combat against bacterial colonization requires multi-faceted solutions. Understanding the fundamentals of microbial adhesion is therefore crucial for designing adequate surfaces that can meet the aforementioned challenges.

3. Methods

3.1 Electron microscopy

Electron microscopy has evolved to be one of the most important imaging tools to study the morphology and composition of materials at the nanoscale. The image acquisition in electron microscopy is based on interactions of the sample material with a high-energy electron beam.

The general resolution limit for any microscope is given by the following equation:

$$d = \frac{0.61\,\lambda}{NA} \qquad (1)$$

where λ is the wavelength of the illuminated medium between the sample object and the objective lens and *NA*, the numerical aperture of the lens. The latter is determined by the angular aperture $\sin\alpha$ and the refractive index n of the medium between sample and objective:

$$NA = n \cdot \sin\alpha \qquad (2)$$

Owing to the small de Broglie wavelength of the accelerated electrons in the electric field, electron microscopy images can be observed up to atomic-level magnifications.

Upon contact with the specimen, different kinds of interactions between the incident electron beam and the sample material can be recorded, which are schematically illustrated in Fig. 6 and will be discussed in the following.

3.1.1 Transmission electron microscopy

In transmission electron microscopy (TEM) the electrons are emitted from an electron gun and accelerated by an anode at high voltages (40-400 keV). Subsequent convergence/divergence by electromagnetic lenses (illumination system) focuses the beam through the specimen. The emerging electron beam is then magnified by the imaging system (objective lens, projector lens) and visualized on a fluorescent screen or via a CCD camera. A cross-sectional image of a microscope column is shown in Fig. 7.

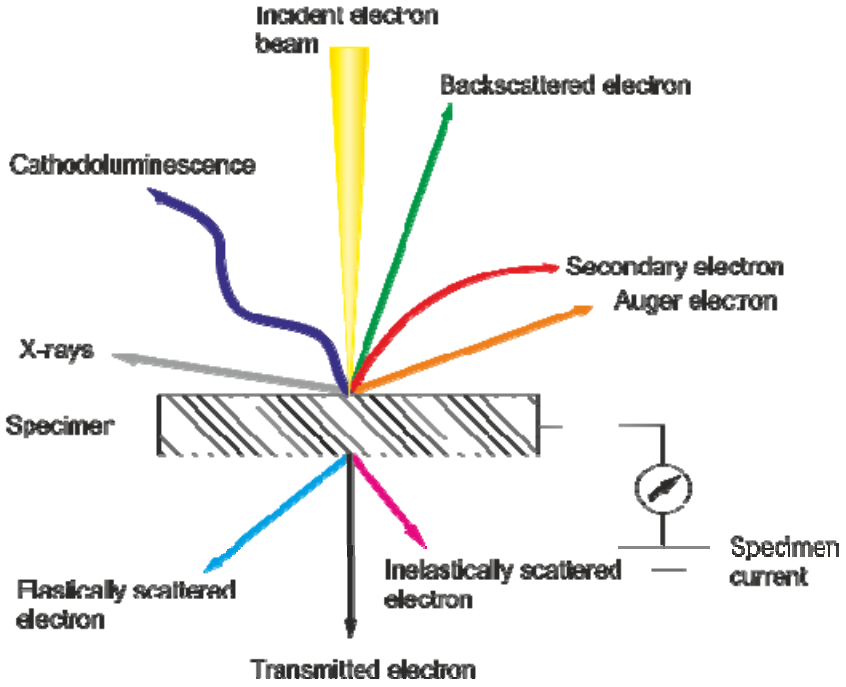

Fig. 6. Schematic presentation of the various signal sources in electron microscopy through interaction of the electron beam with the specimen.

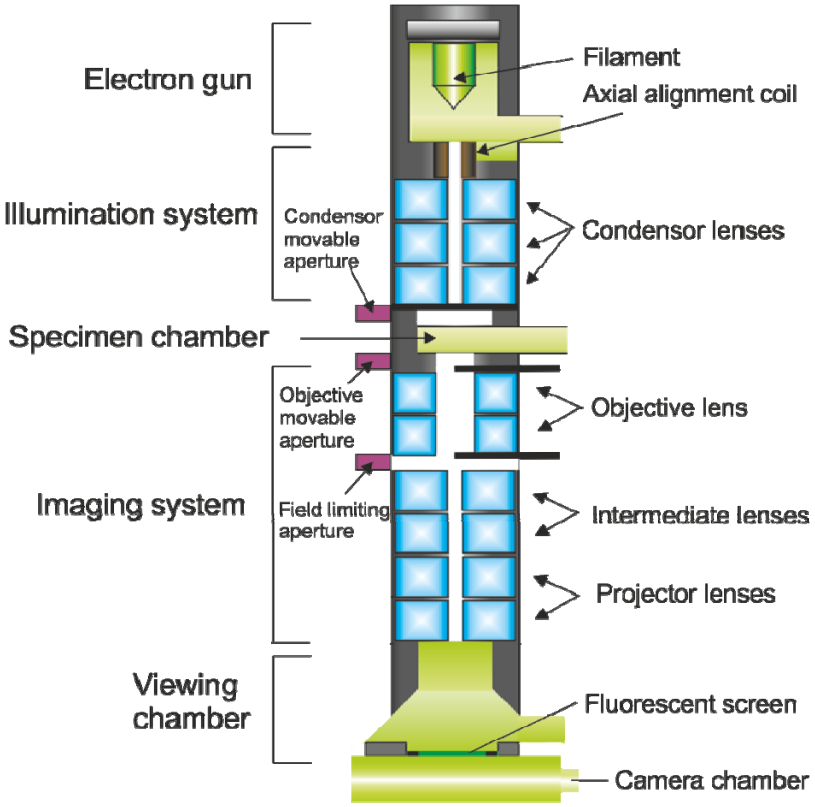

Fig. 7. Cross-sectional image of a transmission electron microscope column.

Electromagnetic lenses are comprised of an excitation coil, which is enclosed within a magnetic yoke. Therefore the electron beam brightness and direction is controlled by the magnetic field that is generated from the current flow in the coil. Similar to optical lenses, electromagnetic lenses are subjected to different aberration phenomena such as astigmatism, spherical and chromic aberration, which can be corrected by different methods as discussed elsewhere [136]. The instrument is operated in high vacuum to avoid interferences between the electron beam and any gas molecules.

In TEM, structural information is mainly provided by the transmitted and elastically scattered electrons. The primary contrast is given by those scattering processes which depend on the mass/atomic number and thickness of the sample. Additional Bragg diffraction of crystalline samples enhances the contrast when eliminated by the objective aperture in the so-called "bright-field image". Conversely, a "dark-field image" is obtained by moving the objective aperture away from the transmitted beam to capture only the diffracted electrons [137]. In high-resolution transmission electron microscopy (HRTEM), the objective aperture is very large or even removed to capture the entire bandwidth of transmitted and diffracted electrons. The resulting phase contrast relies on differences in the phase between transmitted and scattered electrons leaving the sample and allows visualizing lattice fringes of crystalline nanomaterials at the sub-angstrom level. The successful interpretation of complex diffraction patterns requires very low lens aberrations.

In the present work, TEM has been the main tool for morphological characterization and analysis of the particle size distribution of different (hybrid) latex particles. The contrast of soft polymer NPs (e.g. PLLA) was enhanced by shadowing the samples with a thin carbon coating, which additionally protects them from beam damage to a certain degree.

3.1.2 Scanning electron microscopy

In scanning electron microscopy (SEM), conversely to TEM, the illumination system and objective lens are both placed on top of the specimen to converge the high-energy electrons into a fine beam and focus it onto the specimen. Subsequently, the electron beam is scanned in x and y-direction via a deflection coil, which allows to adjust the magnification. Therefore, the magnification does not depend on the lens system and is solely determined by the dimensions of the image display area (L) in relation to the electron beam scan width (W) on

the sample, which can be controlled by the current and voltage supplied to the deflection coil. The image is formed by collecting the different types of signals (see Fig. 6) by signal-specific detectors.

Upon penetration of the incident electron beam, a large number of low-energy secondary electrons (SE) are projected from the outer shell of the surface-bound specimen atoms via inelastic scattering. The SE are essentially used to obtain structural and topographical information of the sample at resolutions in the sub-nanometer range. The compositional distribution can be detected via back-scattered electrons (BSE). In this case, the incident electrons interact with one or more nuclei within the probing depth of the specimen and are then elastically scattered out into the vacuum and captured by a BSE detector. Similar to TEM, the contrast formation of BSE is related to the atomic mass of the specimen.

Additional analytical information can be retrieved via X-ray and Auger electron emission, which are characteristic for a specific element. X-rays are generated through electron relaxation to the ground state to fill up vacancies of electrons in the inner shell, which have been ejected by the incident electron bombardment of the specimen [138]. Alternatively, when the energy of the incident beam is transferred to other electrons, Auger emission takes place.

Because of the variety of information which can be retrieved from the different signals, SEM is a very versatile tool of imaging a large selection of materials. In the present work, SEM was employed to obtain compositional and structural information on inorganic/polymer hybrid latexes and thin films. Energy-dispersive X-ray spectroscopy (EDS) has also been performed on selected samples to check the crystalline structure of the inorganic material.

3.2 Dynamic light scattering

Dynamic light scattering (DLS), also known as photon correlation spectroscopy (PCS), is a widely-used technique to determine size distributions of (polymer) particles as well as various conformational characteristics of macromolecular systems in solution/suspension [139]. In a typical experiment, the scattering intensity of laser light, when passing a specific probe volume at a fixed angle, is recorded as a function of time.

Colloidal particle dispersions generally undergo thermal Brownian motion, which leads to random concentration fluctuations with size-dependent velocities. Since the particles are constantly in motion the speckle pattern of scattered light on the fixed detector will not be stationary. Therefore, the scattering intensity contains a whole spectrum of shifted frequencies in analogy to the Doppler effect. The quantitative analysis of the time-dependent intensity fluctuations is analyzed by a digital correlator, which calculates the time correlation function of the scattering intensity. This is achieved by comparing the scattered intensity with a delayed version of itself. For a given scattering angle θ and corresponding scattering vector q, the time autocorrelation function of the scattered intensity $g^2(q,\tau)$ is defined as:

$$g^2(q,\tau) = \frac{\langle I(q,0)I(q,\tau)\rangle}{\langle I(q)\rangle^2} \qquad (3)$$

$I(q,t)$ and $I(q,t+\tau)$ represent the scattering intensities at time t and $t+\tau$, respectively, q is the magnitude of the scattering vector and the angle brackets indicate averaging over time. For the sake of simplicity, a change of variable can be performed, and $g^2(q,\tau)$ is often rewritten as $g^2(q,\mathrm{t})$.

The scattering vector q is defined as the difference between the incident wave vector k_0 and the scattered wave vector k_s as illustrated in Fig. 8. As a result of the geometrical considerations in Fig. 8, the scattering vector elegantly combines the experimental parameters of the scattering angle θ, wavelength λ and refractive index n of the medium:

$$q = \frac{4\pi\, n}{\lambda} sin\left(\frac{\theta}{2}\right) \qquad (4)$$

In order to obtain some information on the size distribution of a colloidal system, the time autocorrelation function of the scattered intensity $g^2(q,t)$ is converted into the autocorrelation function $g^1(q,t)$ of the electric field by the so-called Siegert relation $g^1(q,\tau) = B\sqrt{g^2(q,\tau)-1}$, with B representing the degree of spatial coherence of the scattered light with respect to the detector area. $g^1(q,t)$ is the correlation function of the electric field amplitudes $E(q,t)$ and generally defined as:

$$g^1(q,t) = \frac{\langle E(q,0)E^*(q,\tau)\rangle}{\langle E(q)^2\rangle} \qquad (5)$$

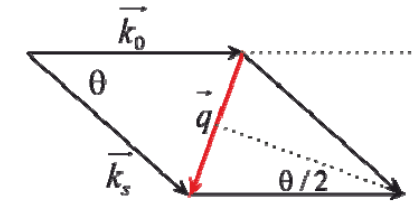

$$\vec{q} = \vec{k_s} - \vec{k_0} \quad \text{and} \quad k_s = k_0 = \frac{2\pi}{\lambda}$$

$$\Rightarrow \sin\left(\frac{0}{2}\right) = \frac{q/2}{k} = \frac{q\lambda}{\pi 4}$$

Fig. 8. Geometrical considerations for the definition of the scattering vector *q*.

Assuming the simplest case of monodisperse colloidal particles dispersed into a dilute medium, then the electric field autocorrelation function decays exponentially with the diffusion coefficient *D* of the particles:

$$g^1(q,\tau) = e^{-q^2 D\tau} \qquad (6)$$

Consequently, the relationship between particle diffusion and particle size is given by the Stokes-Einstein equation, which relates the hydrodynamic radius r_H of spherical particles in a solution to their diffusion coefficient:

$$D = \frac{k_B T}{6\pi\eta r_H} \qquad (7)$$

where r_H is the radius of the sphere, η the viscosity of the solvent, k_B the Boltzmann's constant and T the absolute temperature. Though the relationship strictly holds for spherical particles only, it is generally used for any sample, representing the hydrodynamic radius of an equivalent sphere. To avoid multiple scattering processes, ideally, the colloidal dispersion should be diluted to ~10^{-4} g cm^{-3} and not show any sedimentation or flocculation.

3.3 Zeta potential measurements

The zeta potential (ζ-potential) is defined as the electric potential in the interfacial double layer of colloidal systems. The presence of charged colloids generally affects the distribution of ions in the surrounding medium, which leads to the adsorption of a more or less fixed electrical double layer of oppositely-charged ions. The double layer is composed of a strongly

bound, dense coverage of counterions, the so-called *Stern layer*, and a more *diffuse layer* of less densely-packed ions, as outlined in Fig. 9. Particle motion in the solution then takes place as a counterion-particle entity of the particle itself including the Stern layer and some parts of the diffuse layer of counterions, known as the *slippling plane* or *surface of hydrodynamic shear*. The ζ-potential gives the difference between the electrical potential of the dispersion medium and the stationary counterion-particle entity [140].

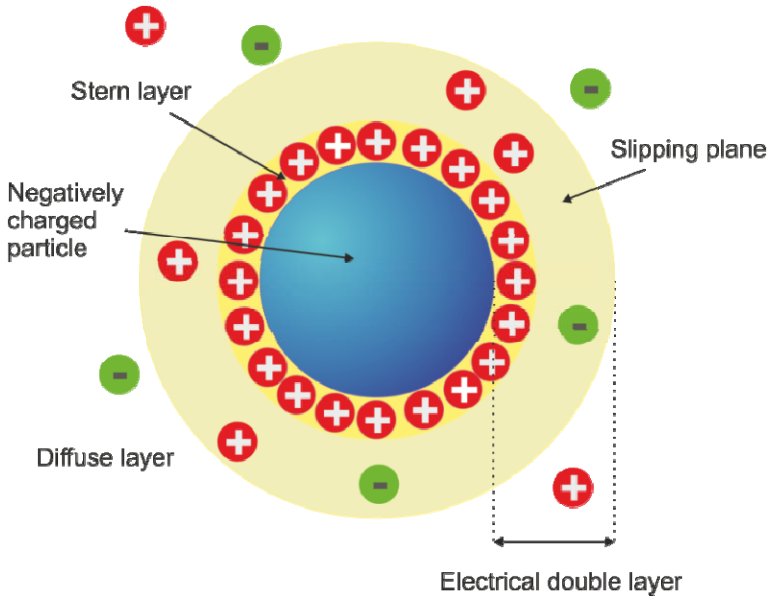

Fig. 9. Schematic representation of the electrical double layer of a charged colloid in solution.

The magnitude of the ζ-potential is characteristic of the stability of colloidal dispersions because it indicates the degree of repulsion between adjacent, similarly charged particles in solution. In case of a low value, attraction can overcome repulsion and entail flocculation. The threshold for breaking up the dispersion typically ranges from ±11 to ±25 mV, depending on the ionic strength and pH of the surrounding medium. Alternatively, the ζ-potential indirectly represents a means to estimate the electrical charge of the particle, since it is difficult to directly measure the electric surface potential of a colloidal system.

In this work, the ζ-potential was determined by electrophoretic light scattering. Therefore, the scattering intensity of a laser beam is recorded as a function of time. In electrophoretic light scattering, as opposed to DLS in which the particles are required to be under random Brownian motion conditions, the colloidal particles are simultaneously subjected to an electric field. Therefore directed electrophoretic motion competes against random Brownian motion.

The detector will record a speckle pattern of shifted frequencies due to electrophoretic motion, which is proportional to the velocity of the particle in an electric field, the so-called electrophoretic mobility. On the other hand, the ζ-potential is related to the electrophoretic mobility μ via Henry's law:

$$\mu = \frac{2\,\varepsilon\,\zeta\,f(ka)}{3\eta} \qquad (8)$$

including the viscosity of the medium η and the dielectric contstant ε. Henry's function *f(ka)* is equal to 1.0 in case of small particle systems in low dielectric constant media as determined by the Hückel-approximation. For larger particle systems (> 0.2 μm), *f(ka)* is given by the Smoluchosky theory [141].

3.4 Inductively coupled plasma optical emission spectroscopy

Inductively coupled plasma optical emission spectroscopy (ICP-OES) is a versatile, highly sensitive trace elemental analysis technique (~ppb), widely used for the quality control in food industry and environmental analysis. The principle relies on the combination of an inductively coupled plasma as source of ionization and optical emission spectroscopy to quantify the amount of analyte based on its characteristic atomic spectral lines. In a typical experiment, the sample passes a nebulizer and the resulting aerosol is directed through a radio-frequency generated plasma of partially ionized argon gas. Due to the high temperatures of the plasma (5000 - 9000 K), the analyte is vaporized, dissociated into atoms and ionized to a high extend. Therefore, many intense emission lines are generated at the same time, which can be rapidly assigned to a specific element and quantified via an standard calibration curve [142].

Generally, ICP analysis is employed for the detection of predominantly metal ions in aqueous solutions. Recently, a detailed study within our group has shown that it can be expanded to quantify the amount of metal-complexes in polymeric colloidal dispersions [143]. Reliable metal contents were obtained by standard addition of additional surfactant to both sample and calibration solutions. In the present work, ICP-OES was employed to quantify both metal oxide contents in polymeric colloidal systems and polymer thin films.

3.5 UV-Vis absorption spectroscopy

Absorption spectroscopy is a versatile optical technique to analyze and quantify the amount of a specific substance based on its interaction with light. The sample of interest is placed into the pathway of the exciting beam, whose transmitted intensity is detected accordingly and compared to the intensity of the incident beam. Upon excitation with a specific wavelength, the analyte will be subjected to an electron transition from a HOMO to a LUMO state, which will then significantly reduce the intensity signal. In case of a dilute solution of a single analyte, the signal intensity of the absorbance is given by the Beer-Lambert law as follows:

$$A = log\frac{I_0}{I} = \varepsilon_i \, c \, d \qquad (9)$$

with A representing the absorbance, I_0 the intensity of the incident light at a fixed wavelength, I the transmitted intensity after passing the sample solution, ε_i the molar extinction coefficient of the analyte, c the concentration of the analyte, and d the path length of the light when passing the probe volume. The molar extinction coefficient is characteristic for each substance and its magnitude depends on the wavelength of the incident light, the nature of the solvent, temperature, and pressure [144].

Depending on the frequency range and purpose of the experiment, the instrumental arrangements may vary significantly. In this work, absorption spectroscopy was employed to analyze inorganic/polymer nanocomposite thin films in air and in aqueous solution. The samples were coated on quarz glass and mounted on a specially built sample holder, which could be set as a flow cell, as illustrated in Fig. 10. Potential scattering effects from the polymer were minimized by the small film thickness of 60-300 nm and by recording control spectra from the native polymer.

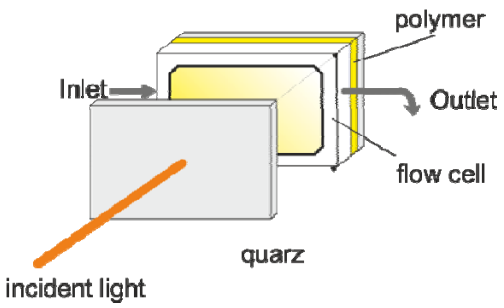

Fig. 10. Experimental arrangement used in this work to measure the absorption on composite polymeric thin films in air or aqueous solution.

4. Experimental

In analogy to the results section, the experimental part is divided into different generations of materials, which are fully described in terms of materials, synthesis and characterization methods.

4.1 Synthesis of various PEGylated NPs (1st generation of materials)

Synthesis of poly(styrene)-co-poly(ethylene glycol) methacrylate (PS-co-PEGMA) NPs by miniemulsion copolymerization

Materials: Styrene (Merck) and various (methoxy-)poly(ethylene glycol) methacrylates ((m)PEGMA, M_n~326, 526, 2000 g mol^{-1}, Aldrich) were purified by column chromatography to remove the stabilizer. All other reagents were used without further purification: hexadecane (Aldrich, 99%), the hydrophobic initiator 2,2'-azobis(2-methylbutyronitrile) (V59) from Wako Chemicals, Japan, and the surfactant Lutensol AT50 from BASF. All experiments were performed in demineralized water.
Synthesis: For the preparation of PS-co-PEGMA latexes, a given amount of styrene (6 g) and (m)PEGMA (3, 5, 10, 15%, w/w styrene) with various molecular weights (Mn~326, 526, 2000 g mol-1), 250 mg of hexadecane (ultrahydrophobe) and 100 mg of the initiator V59 were added to a solution of 200 mg of Lutensol AT50 in 24 g of water. The mixture was stirred for 1 h for pre-emulsification and submitted to sonication for 120 s at 90% (Branson sonifier W450 Digital, 1/2" tip) at 0 °C for miniemulsification. The polymerization was carried out at 72 °C for 12 h. The latex particles were purified by repetitive centrifugation/redispersion in demineralized water.
Characterization: The total solid content and monomer conversion was measured gravimetrically using a Kern RH 120-3 gravimeter. The particle sizes were measured by means of dynamic light scattering using a NICOMP360 zetasizer. Morphological characterizations were carried out with a ZeissEM902 operating at 80 kV (for instrumental details and general sample preparation, see list of instruments). The molecular weight of lyophilized samples was determined by GPC (THF, PS standard).
Antimicrobial activity: The antimicrobial properties of the PS-co-PEGMA NPs against *Pseudomonas aeruginosa* (PAO1) were determined at the University of Bath by different methods. For this purpose, NP samples with varying PEGMA contents and chain lengths and surfactant stabilization were lyophilized and resuspended in sterile lysogeny broth (LB) at ~ 1000 mg mL^{-1}. Serial dilutions from 10^0 to 10^{-9} mg mL^{-1} were prepared accordingly. The sample description is summarized in Table 1.

Table 1. Summary of the different samples used for the antibacterial assays.

Sample name	Type	M_n [g mol^{-1}]	Comonomer content (w/w styrene) [%]
VS12.0	PS		0
VS12.4	PS-co-mPEGMA	2000	15
VS13.0	PS-co-mPEGMA, no surfactant	2000	15
VS15.3	PS-co-PEGMA	526	10

P. aeruginosa was grown in 10 mL LB overnight at 37 °C with shaking at 200 rpm until it reached a cell density of 10^9 CFU mL^{-1}. The latter was extrapolated from a standard curve for optical density (λ_{600nm}). The bacterial suspension was centrifuged at 13 200 rpm for 3 min and the pellet was washed and resuspended in LB. Then, for each sample, 2 sets of 500 µL sample dispersion and serial dilutions were inoculated with 500 µL of the bacterial suspension. NP-free LB served as control. The first sample series was incubated for 48 h at 37 °C and bacterial growth was determined by measuring the optical density (λ_{600nm}). For the second sample series, sterile filter pads were plunged into the PAO1-inoculated NP dispersions and placed onto Agar plates. After incubation at 37 °C for 24 h, the agar plates were examined for inhibition zones. NP-free filter pads served as control.

A fluorometric assay was carried out with non-woven polypropylene (PP) nappies that were plunged into the undiluted NP suspensions. After drying, the non-wovens were inoculated with PAO1-enriched LB medium (10^6 CFU mL^{-1}) and incubated at 37 °C for 24 h. NP-free sterile and non-sterile non-wovens served as controls. Subsequently, the infected non-wovens were stained with a commercially available dye mixture (LIVE/DEAD BacLight™, Invitrogen) and examined under the confocal microscope. The staining process involves two fluorescent dyes which allow for a reliable distinction between viable and dead species: SYTO9 emits in the green following enzymatic deesterification within the viable cells; Propidium iodide emits in the red by interaction with the DNA of necrotic cells.

4.2 Synthesis of different NPs functionalized with quaternary ammonium groups (2nd and 3rd generation of materials)

Synthesis of (2-methacryloyloxyethyl)dodecyldimethylammonium methacrylate (qDMAEMA)

Materials: 2-(Dimethylamino) ethyl methacrylate (DMAEMA) and 1-dodecyl bromide were obtained from Sigma-Aldrich and used without further purification as well as the solvents, which were of analytical grade.

Synthesis: qDMAEMA was synthesized according to Hamid and Sherrington [145]. DMAEMA (1eq) and 1-dodecyl bromide (0.5 eq) were stirred at 50 °C for 24 h. The

generated precipitate was washed with diethyl ether and recrystallized from acetone to give a white crystalline powder. Yield: 50%.

Characterization: FD-MS (Field Desorption Mass Spectrometry, 8 kV): *m/z* [u*e_0^{-1}] = 324.2 (100 %) $[M]^+$, 728.5(15 %) $[2M+Br]^+$ for $C_{20}H_{40}BrNO_2$

^{1}H-NMR ($CDCl_3$): δ (ppm) = 0.82 (t, 3 H, J = 6.25 Hz $N^+(CH_3)_2(CH_2)_{11}CH_3$), 1.19 (m, 18 H, $N^+(CH_3)_2CH_2CH_2(CH_2)_9CH_3$), 1.70 (m, 2 H, $N^+(CH_3)_2CH_2CH_2(CH_2)_9CH_3$), 1.89 (s, 3 H, $CH_2=C(CH_3)$), 3.47 (s, 6 H, $N^+(CH_3)_2(CH_2)_{11}CH_3$), 3.58 (m, 2 H, $N^+(CH_3)_2CH_2(CH_2)_{10}CH_3$), 4.12 (m, 2 H, $OCH_2CH_2N^+(CH_3)_2(CH_2)_{11}CH_3$), 4.61 (m, 2 H, $OCH_2CH_2N^+(CH_3)_2(CH_2)_{11}CH_3$), 5.62 and 6.08 (s, 2 H, $CH_2=C(CH_3)$

^{13}C-NMR ($CDCl_3$): δ (ppm) = 13.76 ($N^+(CH_3)_2(CH_2)_{11}CH_3$), 17.99 ($CH_2=C(CH)_3$), 22.18 ($N^+(CH_3)_2(CH_2)_{10}CH_2CH_3$), 25.99 ($N^+(CH_3)_2CH_2CH_2(CH_2)_9CH_3$), 29.38 ($N^+(CH_3)_2(CH_2)_2(CH_2)_7(CH_2)_2CH_3$), 31.60 ($N^+(CH_3)_2(CH_2)_9CH_2CH_2CH_3$), 51.59 ($N^+(CH_3)_2(CH_2)_{11}CH_3$), 57.73 ($OCH_2CH_2N^+(CH_3)_2(CH_2)_{11}CH_3$), 61.74 ($N^+(CH_3)_2CH_2(CH_2)_{10}CH_3$), 65.51 ($OCH_2CH_2N^+(CH_3)_2(CH_2)_{11}CH_3$), 127.19 ($CH_2=C(CH_3)$), 134.63 (-COO), 166.04 ($CH_2=C(CH_3)$

TGA (40 – 800 °C, 10 K min^{-1}): T_d ~200 °C

DSC (-20 – 100 °C, 10 K min^{-1}): T_m = 71.6 °C

4.2.1 Synthesis of poly(styrene)-co-(2-methacryloyloxyethyl)dodecyldimethylammonium methacrylate) (PS-co-PqDMAEMA) NPs by miniemulsion copolymerization (2nd generation of materials)

Materials: see 4.1; qDMAEMA: see above. Cetyltrimethylammonium chloride (CTAC) was purchased from Sigma Aldrich (99.9%) and used without further purification.

For the preparation of PS-co-PqDMAEMA latexes, a given amount of styrene (6 g) and qDMAEMA (3, 5, 8, 10 % w/w styrene), 250 mg of hexadecane (ultrahydrophobe) and 100 mg of the initiator V59 were added to 24 g of water containing (*i*) 125 mg of CTAC, (*ii*) 200 mg of Lutensol AT50 or (*iii*) no surfactant at all. The mixture was stirred for 1 h for pre-emulsification and submitted to sonication for 120 s at 90% (Branson sonifier W450 Digital, 1/2" tip) at 0 °C for miniemulsification. The polymerization was carried out at 72 °C for 12 h. CTAC-stabilized and surfactant-free samples were purified by dialysis (Dialysis Tubing Visking, Carl Roth, Cut-off: 14 000 Da) whereas the Lutensol-stabilized samples were submitted to repetitive centrifugation/redispersion in demineralized water.

Characterization: The total solid content and monomer conversion was measured gravimetrically using a Kern RH 120-3 gravimeter. The particle sizes (as well as the zeta potentials) were measured by means of (electrophoretic) dynamic light scattering using a NICOMP360 zetasizer. Morphological characterizations were carried out with a Zeiss EM902 operating at 80 kV (for instrumental details and general sample preparation, see list of instruments). The molecular weight of lyophilized samples was determined by GPC (THF, PS standard).

Antimicrobial activity: The antimicrobial properties of the PS-co-PqDMAEMA NPs were assessed by optical density measurements in collaboration with the University Clinic of

Cologne (UKK). To this end, surfactant-free copolymer NPs, copolymer NPs stabilized with various surfactants (CTAC, Lutensol AT50) with 5 % qDMAEMA (w/w styrene) content, as well as native CTAC-stabilized PS NPs were lyophilized and resuspended in sterile PBS buffer at a final concentration of 10 mg mL^{-1}. NP-free medium served as control.
20 mL of Tryptic Soy Broth (TSB) were inoculated with 150 µl of *S.. aureus* (MSSA476) overnight culture, which was kindly provided by Geraldine Mulley from the University of Bath and incubated in baffled Erlenmeyer flasks at 37 °C/170 rpm for 24 h. The bacterial growth was monitored by optical density (OD) measurements (λ_{600nm})(Genesys 10UV, Thermo Scientific, Madison, WI, USA). After 90 min of incubation, the NP suspensions were combined with the bacterial suspensions and diluted to a final concentration of 0.5 mg mL^{-1}. The OD was measured in regular intervals in a total period of 24 h.

Synthesis of poly(2-methacryloyloxyethyl)dodecyldimethylammonium meth-acrylate) (PqDMAEMA) by radical polymerization

Materials: qDMAEMA: see before. 2,2'-azobis(isobutyronitrile) (AIBN, Aldrich) was recrystallized from methanol. Ethanol (Aldrich, analytical grade) was distilled over Na. All other reagents were of analytical grade and used as received.
Synthesis: qDMAEMA (7 mmol, 1 eq) and 0.036 mmol AIBN (0.005 eq) were dissolved in dried ethanol in a Schlenk tube under argon atmosphere. The mixture was degassed by three freeze-pump-thaw-cycles. Following the degassing procedure, the mixture was purged in argon and heated up to 70 °C for 24 h. The monomer conversion was monitored by TLC (chloroform: methanol 5:2, qDMAEMA: R_f = 0.39; PqDMAEMA: R_f = 0.21). After removal of the excess solvent, the polymer was purified by recrystallization from acetone. The final product was dried in vacuo to give a white powder. Yield: 2.6 g (87 %).
Characterization:
^{1}H-NMR ($CDCl_3$): δ (ppm) = 0.84 (t, 3 H, J = 6.25 Hz $N^+(CH_3)_2(CH_2)_{11}CH_3$), 1.15 (broad s, 3 H, $[CH_2C(CH)_3COOR]_n$), 1.22 (broad m, 18 H, $N^+(CH_3)_2CH_2CH_2(CH_2)_9CH_3$), 1.76 (broad m, 2 H, $N^+(CH_3)_2CH_2CH_2(CH_2)_9CH_3$), 2.16 (broad s, 2H, $[CH_2C(CH)_3COOR]_n$), 3.44 (broad s, 6 H, $N^+(CH_3)_2(CH_2)_{11}CH_3$), 3.69 (broad m, 2 H, $N^+(CH_3)_2CH_2(CH_2)_{10}CH_3$), 3.99 (sept, 2 H, $OCH_2CH_2N^+(CH_3)_2(CH_2)_{11}CH_3$), 4.51 (broad m, 2 H, $OCH_2CH_2N^+(CH_3)_2(CH_2)_{11}CH_3$)
Molecular weight (g mol^{-1}): M_w = 210 997, M_n = 108 387, PDI = 1.95 (GPC, DMF, PS standard, 50 mM LiBr)
TGA (40 – 800 °C, 10 K min^{-1}): T_d ~200 °C
DSC (-20 – 100 °C, 10 K min^{-1}): T_g = 100-160 °C
Antimicrobial activity:
Sample preparation for the PqDMAEMA homopolymer: PqDMAEMA was dissolved in ethanol in various concentrations (1.5, 3, 5, 10%, w/v) and spin-coated on PS culture dishes (Nunc, Ø = 60 mm) which were previously activated by oxygen plasma treatment ($p(O_2)$ = 0.2 mbar, t = 10 min, 50 W). The samples were dried at 40 °C for 2 h.

The antibacterial activity of the NPs was determined against *Staphylococcus aureus* (MSSA476) and *Pseudomonas aeruginosa* (PAO1). Both strains were kindly provided from the University of Bath. Strains were cultivated in LB (Luria/Miller) (Carl-Roth, Karlsruhe Germany) and stored at -80 °C in 20% (v/v) glycerol (GE-Gealthcare, Munich, Germany).
Antibacterial assays were conducted according to a modified form of the EN ISO 22196-2007 standard. In brief, both bacterial strains were grown in 6 mL of LB for 18 h at 37° C with shaking at 170 rpm (3032 GFL, Burgwedel, Germany). The bacterial suspensions were centrifuged at 5000 x g for 5 min and 23 °C (Biofuge Primo R, Thermo Scientific, Thermo Scientific, Madison, WI USA) and the pellets washed and resuspended in 1:10 diluted LB (LB diluted in sterile ultra pure water). Then the viable cell number was adjusted to 10^5 CFU mL^{-1} as monitored by optical density measurements (λ_{600nm}) and 200 µL of the bacterial suspension were added onto the polymer-coated culture dish. The bacterial suspensions were covered by a 20±4 mm^2 sterilized polypropylene cover film (VWR international, Darmstadt, Germany) and incubated in a box with moistened paper towels at 37 °C for 24 h. After incubation, the surfaces were thoroughly rinsed by adding 2 mL of LB medium to the culture dishes and pooling the washings. In the next step, serial dilutions of the washing solution were prepared in 0.9% (v/v) NaCl and spread onto LB agar. After incubation at 37 °C for at least 24 h, colonies were counted and used to calculate the mean CFU. Uncoated petri dishes served as control. Additionally, serial dilutions of the initial bacterial suspensions were plated and incubated as well, to assure the initial plate count of ~10^5 CFU mL^{-1}. The PqDMAEMA NP assays were carried out with three replicates of each test sample. The results are reported as the mean ± standard deviation (SD). The antimicrobial tests were conducted in collaboration with the University Clinic of Cologne (UKK).
***In vitro* cytotoxicity assay:** The *in vitro*-toxicity of the polymer NPs was assessed by fluorimetric viability tests as well as microscopic documentation of the cell morphology based on NIH/3T3 Swiss mouse fibroblasts. The samples were prepared in analogy to the antibacterial assay. 10^4 cells were seeded onto the coated culture dishes (Ø 35 mm, Nunc, tissue engineering) and incubated with 5% CO_2 at 37 °C for 24 h or 5 d, respectively. After incubation in cell growth medium (DMEM, FBS, Pen/Strep), cells were stained with alamarBlue© (Invitrogen) following the manufacturer's protocol. The main component of the staining is resazurin, a non-fluorescent dye. In metabolic active cell, resazurin will be reduced to its fluorescent form resofurin. Hence the amount of the fluorescence is proportional to the number of viable cells. Non-coated culture dishes served as controls. For the long-term study, the culture medium was replaced after 3 d. The fluorescence was measured with a Typhoon Scanner (GE). Microscopic documentation was performed on an Axio Observer.A1 (Zeiss). The cytotoxicity assays were carried with four replicates of each test sample. The results are reported as the mean ± standard deviation (SD). The cytotoxicity assays were conducted in collaboration with the UKK.

4.2.2 Preparation of PqDMAMEA (PS) NPs by miniemulsion and solvent evaporation (3rd generation of materials)

Materials: PqDMAEMA: see above. Cetyltrimethylammonium chloride (CTAC), purchased from Sigma Aldrich (99.9%) and chloroform (Fisher Scientific, 99.98%) were used as received.

Synthesis: Polymer NPs were obtained by a combination of miniemulsification of PqDMAEMA (PS) homopolymer and solvent evaporation of chloroform. A commercially available PS standard (M_w = 85 000 g mol^{-1}, PDI = 1.06, Alfa Aesar) was employed for all PS NP syntheses. A given amount of PqDMAEMA (PS) (80 mg) was dissolved in 2 g of chloroform. The macroemulsion was prepared by adding 4.8 g of water to the organic phase and subsequent magnetic stirring for 1 h at 1500 rpm. Small polymer/chloroform droplets were prepared by ultrasonication of the sample under ice cooling for 180 s at 70 % amplitude in a pulsed modus (20 s on, 10 s off) using a Branson 450W sonifier and a ¼" tip. The resulting miniemulsion was heated to 40 °C for 6 h under magnetic stirring (500 rpm) to evaporate the organic solvent. PS and CTAC-stabilized PqDMAEMA NPs were prepared accordingly, using a PS standard or the PqDMAEMA monomer and adding 25 mg or 10 mg of CTAC to the aqueous phase.

Characterization: The particle sizes (as well as the zeta potentials) were measured by means of (electrophoretic) dynamic light scattering using a NICOMP360 zetasizer. Morphological characterizations were carried out with a Zeiss EM902 operating at 80 kV (for instrumental details and general sample preparation, see list of instruments).

Antimicrobial activity:

Sample preparation for the PqDMAEMA NPs: The aqueous suspensions of the PqDMAEMA NPs were adjusted to 3% w/w and dropcasted on plasma-activated PS culture dishes (Nunc, Ø = 30 mm). The samples were dried at room temperature overnight and transported to the UKK for antibacterial assessment.

The antibacterial activity of the NPs was determined against *Staphylococcus aureus* MSSA476 and *Pseudomonas aeruginosa* PAO1. Both strains were kindly provided by Geraldine Mulley from the University of Bath. Strains were cultivated in LB (Luria/Miller) (Carl-Roth, Karlsruhe Germany) and stored at -80 °C in 20% (v/v) glycerol (GE-Gealthcare, Munich, Germany).

Short term (24 h) antibacterial assays were conducted according to a modified form of the EN ISO 22196-2007 standard. In brief, both bacterial strains were grown in 6 mL of lysogeny broth (LB) for 18 h at 37 °C with shaking at 170 rpm (3032 GFL, Burgwedel, Germany). The bacterial suspensions were centrifuged at 5000 x g for 5 min and 23 °C (Biofuge Primo R, Thermo Scientific, Thermo Scientific, Madison, WI USA) and the pellets washed and resuspended in 1:10 diluted LB (LB diluted in sterile ultra pure water). Then the viable cell number was adjusted to 10^5 CFU mL^{-1} as monitored by optical density measurements (λ_{600nm}) and 200 µL of the bacterial suspension were added onto the polymer-coated culture dish. The bacterial suspensions were covered by a 20±4 mm^2 sterilized polypropylene cover film (VWR international, Darmstadt, Germany) and incubated in a box with moistened paper towels at

37 °C for 24 h. After incubation, the surfaces were thoroughly rinsed by adding 2 mL of LB medium to the culture dishes and pooling the washings. In the next step, serial dilutions of the washing solution were prepared in 0.9% (v/v) NaCl and spread onto LB agar. After incubation at 37 °C for at least 24 h, colonies were counted and used to calculate the mean CFU. Uncoated petri dishes served as control. Additionally, serial dilutions of the initial bacterial suspensions were plated and incubated as well, to assure the initial plate count of ~10^5 CFU mL^{-1}. The PqDMAEMA NP assays were carried out on at least three different days with three replicates of each test sample. The results are reported as the mean ± standard deviation (SD).

The long term stability of the coatings was determined in analogy to the previous assay.The coatings were inoculated with bacteria in diluted LB, covered by a polypropylene film and incubated at 37 °C for 24 h. After adding 2 mL of 0.9% (w/v) NaCl and pooling of the washings, the viable cell counts were performed according to the above-mentioned surface spread-plate method. In the meanwhile, the 0.9% (v/v) NaCl solution was removed from the sample surface and the surfaces were inoculated for a second (third – fifth) time with 200 µL of 10^5 CFU mL^{-1} bacteria and consecutively covered by a polypropylene cover film. This procedure was repeated for the same sample over a total period of five days with three replicates of each test sample. The results are reported as the mean ± standard deviation (SD). The antimicrobial tests were conducted in collaboration with the UKK.

***In vitro* cytotoxicity assay:** The *in vitro*-toxicity of the polymer NPs was assessed by fluorimetric viability tests as well as microscopic documentation of the cell morphology based on NIH/3T3 Swiss mouse fibroblasts. The samples were prepared in analogy to the antibacterial assays. 10^4 cells were seeded onto the coated culture dishes (Ø 35 mm, Nunc, tissue engineering) and incubated with 5% CO_2 at 37 °C for 24 h or 5 d, respectively. After incubation in cell growth medium (DMEM, FBS, Pen/Strep), cells were stained with alamarBlue© (Invitrogen) following the manufacturer's protocol. The main component of the staining is resazurin, a non-fluorescent dye. In metabolic active cell, resazurin will be reduced to its fluorescent form resofurin. Hence the amount of the fluorescence is proportional to the number of viable cells. Non-coated culture dishes served as controls. For the long-term study, the culture medium was replaced after 3 d. The fluorescence was measured with the Typhoon Scanner (GE). Microscopic documentation was performed on an Axio Observer.A1 (Zeiss). The cytotoxicity assays were carried with four replicates of each test sample. The results are reported as the mean ± standard deviation (SD). The cytotoxicity assays were conducted in collaboration with the UKK.

4.3 Preparation of various inorganic/polymer nanocomposite materials (4th and 5th generation of materials)

4.3.1 Synthesis of ZnO NPs via thermal decomposition

Materials: Zinc acetylacetonate monohydrate ($Zn(acac)_2 \cdot H_2O$), oleic acid (OLAC, 90%) and oleylamine (OLAM, 70%), were purchased from Aldrich and used without further purification. All solvents used were of analytical grade and purchased from Aldrich and Riedel.

Synthesis: ZnO NPs were synthesized using zinc acetylacetonate monohydrate (5 mmol) as metal precursor in the presence of two distinct surfactants, namely oleylamine (15 mmol) and oleic acid (3 mmol). The resulting mixture was initially submitted to a degassing process, and then heated under argon flux. The synthesis was carried out at 240 °C for 20 min under argon flow, to allow for the growth of the ZnO NPs. After cooling, the resulting nanocrystalline product was extracted from the reaction mixture by precipitation upon addition of absolute ethanol. The product was separated by centrifugation and thoroughly purified by repeated cycles of dispersion in chloroform and reprecipitation with absolute ethanol to remove precursor and surfactant residuals. The final NPs were dispersed in chloroform and stored under dark conditions.

Characterization: After air drying, a white powder was obtained for X-ray diffraction and UV-Vis absorption measurements. X-ray diffraction studies were obtained from a θθ-Diffractometer (Bruker D8 Advance2). The ZnO concentration was determined by measuring the mass content upon solvent evaporation. The morphology of the NPs was characterized by transmission electron microscopy (TEM) using a Zeiss EM902 microscope working at an accelerating voltage of 80 kV. The samples were prepared by casting highly-diluted NP dispersions from chloroform onto carbon-coated grids. High-resolution transmission electron microscope (HRTEM) images were recorded with a FEI Tecnai F20 with an accelerating voltage of 200 kV. A NICOMP zetasizer, measuring at a fixed scattering angle of 90° was utilized to determine the particle size distributions by dynamic light scattering. The measurements were carried out at 23 °C on diluted dispersions in chloroform.

4.3.2 Preparation of ZnO/Poly(L-lactide) hybrid NPs by miniemulsion and solvent evaporation (4th generation of materials)

Materials: ZnO NPs: see above. Poly(L-lactide) (M_w = 85-160 000 g mol^{-1}, Sigma-Aldrich), sodium n-dodecyl sulfate (SDS) (Alfa Aesar, 99%) and chloroform (Fisher Scientific, 99.98%) were used as received. All experiments were performed in demineralized water.

Synthesis: Hybrid ZnO/PLLA NPs were obtained by a combination of miniemulsification of ZnO/PLLA and solvent evaporation of chloroform. Prior to mixing with PLLA, the ZnO/chloroform dispersion was subjected to ultrasoniation of 5 min. Then, a given amount of PLLA (60 mg) was dissolved into 2 g of a ZnO/chloroform dispersion (14%, w/w

chloroform) and homogenized by orbital shaking at 400 rpm/18 °C in darkended containers. After dissolution of the PLLA pieces, the mixture was subjected to 10 s of ultrasonication at 10% amplitude (inverse sonifier, Branson, USA) for intensified homogenization. The macroemulsion was prepared by adding an aqueous solution of SDS (15 mg in 4.8 g water) to the organic phase and subsequent magnetic stirring for 1 h at 1500 rpm. Small hybrid/chloroform droplets were prepared by ultrasonication of the sample under ice cooling for 180 s at 70% amplitude in a pulsed modus (20 s on, 10 s off) using a Branson 450W sonifier and a ¼" tip. The resulting miniemulsion was heated to 40 °C for 6 h under magnetic stirring (500 rpm) to evaporate the organic solvent. Pure PLLA NPs were prepared accordingly. The samples were stored at 4 °C under dark conditions.

Characterization: The particle sizes (as well as the zeta potentials) were measured by means of (electrophoretic) dynamic light scattering using a NICOMP360 zetasizer. Morphological characterizations were carried out with a Zeiss EM902, operating at 80 kV. The surface of native ZnO, hybrid ZnO/PLLA and PLLA was characterized by atomic force microscopy (Dimension 3100 NanoScope 3a controller) and SEM (Leo Gemini 1530, Zeiss) (for instrumental details, see list of instruments). The samples were prepared by dropcasting diluted NP dispersions on Si wafer and dried at ambient conditions.

UV-degradation studies of selected ZnO/PLLA hybrid and native PLLA NP samples were performed on a UV lamp (Till Photonics) at 356 nm. The aqueous NP dispersions were irradiated in a quarz cuvette for 15 min every 48 h (3 times a week) in a total period of 45 d. The molecular weight of the lyophilized samples was monitored by GPC (chloroform, PS standard) before, after 2 weeks and at the end of the total irradiation experiment.

The encapsulation efficiency was analyzed by thermogravimetric analysis (TGA) (40 – 900 °C, 10 K min^{-1}) and ICP-OES (for instrumental details, see list of instruments). The nanocomposite colloidal dispersions were diluted with demineralized water to a solid content of 0.1% (w/w) and measured at λ = 481.053 nm.

Antimicrobial activity: The antimicrobial activity of the ZnO/PLLA nanocomposite particles was determined by using an agar dilution method as follows: *S. aureus* (MSSA476, St. Georges University London, UK) and *P. aeruginosa* (PAO1, Harvard Medical School, USA) were grown on Agar plates (CASO-Agar, TSA) overnight at 37 °C. After incubation, 3 mL of an aqueous bacterial suspension (NaCl, 0.85 %) were adjusted to an approximate cell density of ~10^8 CFU mL^{-1}, as monitored by a 0.5 McFarland turbidity standard, and spread on fresh Agar plates (CASO-Agar, TSA). Subsequently, circular holes were cut out from the agar surface with a sterile pipette and filled with 30 µL aqueous sample dispersions of 0.1% (w/w) ZnO/PLLA nanocomposite particles and pure PLLA NPs which were purified by dialysis, as well as non-dialysed nanocomposite particles. Ultrapure water and SDS solution (3.1 mg mL^{-1}) were used as control samples. After 20 h of incubation at 37 °C, the agar plates were examined for inhibition zones close to the sample holes. The antibacterial assays were carried out in collaboration with the University Medical Center of Mainz.

4.3.3 Preparation of ZnO/Poly(*N*-isopropylacrylamide) nano-composite thin films (5th generation of materials)

Synthesis of the poly(N-isopropylacrylamide) terpolymer (PNIPAAm)

The PNIPAAm terpolymer consisting of NIPAAm, methacrylic acid (MAA) and 4-benzophenone methacrylate (MABP) in a molar ratio of 90:5:1 was obtained by free radical polymerization as described in previous work [146].

Characterization:

^{1}H-NMR (methanol-d_4): δ (ppm) = 1.03-1.30 (m,-CH_3), 1.30-1.84 (m,-CH_2-), 1.84-2.40 (m, NIPAAm backbone CH), 3.97 (s, CH_3-CH-CH_3), 7.10-8.20 (m, C-H_{arom})

Molecular weight (g mol^{-1}): M_w = 151 005, M_n = 65 154, PDI = 2.32 (GPC, DMF, PMMA standard)

Synthesis of 4-(3-triethoxysilyl)propoxybenzophenone (BP-silane)

Materials: 4-Allyloxybenzophenone (Fluka), allyl bromide (Aldrich), triethoxysilane (Alrich) and catalyst (10% Pt on activated charcoal, puriss., Fluka) were used without further purification.

Synthesis: 4-Allyloxybenzophenone was obtained by alkylation of 4-hydroxybenzophenone with allyl bromide as described in previous work [146]. The product (9.9 g, 50 mmol) was dissolved in triethoxysilane (4.8 ml, 550 mmol) at room temperature under argon flow. After the addition of the catalyst, (Pt on activated charcoal) the solution was stirred at room temperature until full conversion was proved by TLC (heptane: acetone 5:1.5: 4-allyloxybenzophenone R_f = 0.48; BP-silane: R_f = 0.22) after 2 d. After filtering off the catalyst, the excess of triethoxysilane was removed in high vacuum and the yellowish product oil was stored in an ethanolic solution under argon and used without further purification.

Characterization: FD-MS (Field Desorption Mass Spectrometry): *m/z* = 402.0 $[M]^+$, 804.8 $[2M]^+$, 1206.8 $[3M]^+$

^{1}H-NMR ($CDCl_3$): δ (ppm) = 0.77 (t, 2H, 3-propoxy), 1.23 (t, 9H, CH_3 ethoxy), 1.93 (td, 2H, 2-propoxy), 3.85 (q, 6H, CH_2 ethoxy), 4.02 (t, 2H, 1-propoxy), 6.95 (d, 2H, 3,5-phenone), 7.47 (t, 2H, 3,5-benzyl), 7.56 (t, 1H, 4-benzyl), 7.72 (d, 2H, 2,6-benzyl), 7.79 (d, 2H, 2,6-phenone)

Silanization of glass substrates

Glass coverslips (Thermo Scientific, Menzel Gläser) or quartz glass (PGO) were cut into 2.5x2.5 cm^2 pieces or 1.2x2.4 cm^2 pieces, respectively, cleaned by immersion and sonication in Hellmanex solution (Hellma optic), followed by repeated rinsing with ultrapure water and

ethanol. The substrates were treated with a 5 mg ml^{-1} ethanolic solution of 4-(3-triethoxysilyl) propoxybenzophenone (BP-silane) for 24 h, dried for 1 h at 50 °C, thoroughly rinsed with ethanol and stored in dark containers under argon before use.

Preparation of the ZnO/PNIPAAm nanocomposite films

Materials: ZnO, PNIPAAm: see before. All solvents were of analytical degree and used as received (ethanol, Aldrich; chloroform, Fisher Scientific, 99.98%).

Preparation: ZnO/PNIPAAm nanocomposite films were prepared by mixing both components in 2 or 5 wt-% solutions of PNIPAAm in chloroform with varying NP/polymer ratios of 1, 5, 10, 15, 25 and 35 wt-% ZnO. The chloroform was evaporated at room temperature and the components were redispersed in the equivalent amount of ethanol and homogenized by sonication and orbital shaking at 600 rpm. The sample solutions were spin-coated on silanized glass coverslips (2.5x2.5 cm^2), dried at 40 °C for 3 h and crosslinked by UV irradiation (365 nm) in a Stratalinker 2400 (Stratagene) for 60 min, which corresponds to a total photocrosslinking energy dose of 6.28 J cm^{-2}. All samples were stored in dark containers before further use.

Characterization: Morphological characterization was performed using a Zeiss 1530 Gemini field emission scanning electron microscope (SEM) (700V@2mm WD; InLens detector). The samples were prepared by spin-coating the sample solutions on plasma-activated ($p(Ar:O_2)$: 0.9:0.1 mbar, 300 W, 10 min) Si-wafer with subsequent drying and crosslinking. EDS was performed on selected samples at 2.5 kV using a Hitachi SU8000 coupled with a Bruker XFlash 5010. The film thickness was determined by a surface profiler (Tencor P10, alpha-stepper). For this purpose, composite films, spin-coated on plasma-activated Si-wafers, were scratched with a needle and subsequently scanned by the profiler to probe the depth of the film.

UV-Vis absorbance spectra were recorded on a Lambda 900 spectrometer (Perkin Elmer), using coated quartz substrates. For the kinetic measurements in buffer solution (PBS, 0.01 M), a teflon flow cell (d = 5 mm, V = 1 mL) with two quartz (PGO) windows was employed, one of them coated with ZnO/PNIPAAm nanocomposite films of varying NP content. A peristaltic pump (Ismatec, Reglo Digital) controlled the flow while the sample cell was rinsed for 24 h at 0.1 ml min^{-1}. The concentration of Zn^{2+}-ions within the hydrogel layers was measured by elemental analysis with an inductively-coupled plasma (ICP) emission spectrometer (Horiba Jobin Yvon, Bernsheim, Germany) at λ = 328.233, 334.502 and 481.053 nm respectively. To this end, different sample series of thin and thick films were prepared on glass substrates with varying amounts of ZnO NP. Zinc ions were extracted from the hydrogel matrix by immersing the coated slides into 65% nitric acid for 1 h. Aliquots of 0.5 ml were diluted to 5% nitric acid content and purified through filtration prior to ICP measurements (Millipore Millex-LS, hydrophobic PTFE 0.5 μm). The loading of zinc within the hydrogel film was calculated by normalizing the measured amount of zinc with the total surface area of the coated glass slides multiplied with the film thickness in the dry state.

Statistics: The mean value and standard deviation (SD) were calculated from at least three independent experiments for thickness, UV-Vis and ICP measurements.

Antimicrobial activity:

To determine the antimicrobial activity of the ZnO/PNIPAAm nanocomposite films, coated glass coverslips were covered with a poly(dimethyl)siloxane mask, providing a defined area of 1 cm^2. The composite films were incubated with 300 µl of *E.coli* (TOP 10 with ampicillin resistance, Invitrogen) suspension, which is equivalent to ~ $5x10^5$ CFU ml^{-1}, in minimal LB media at 37 °C in a humidified chamber that prevented drying of the surfaces. After 24 h, the bacterial suspensions were collected and the composite films were washed three times with 150 µl minimal LB media. Bacteria suspensions and washing solutions were combined and 20 µl aliquots of serial dilutions (1:5000 or 1:10000) in 1 ml minimal LB media were plated on LB agar plates for the determination of viable bacteria. The agar plates were incubated for another 24 h at 37 °C to give an estimate of viable cell counts as colony forming units (CFU). Uncoated glass slides and pure hydrogel slides served as control surfaces. The mean value and standard deviation (SD) was calculated from three independent experiments and the results expressed as CFU (%) relative to the pure hydrogel. The antimicrobial activity was carried out in collaboration within the group.

***In vitro* cytotoxicity:**

Toxicity of the ZnO/hydrogel (HG) nanocomposite films to NIH/3T3 Swiss mouse fibroblasts (ATCC/LGC-Standards) was assessed by a fluorimetric viability/proliferation test as well as by determining the fraction of apoptotic and necrotic cells after 24 h exposure to hydrogel layers, doped with different concentrations of ZnO nanoparticles. To this end, $2x10^6$ cells were seeded into 60 mm standard culture dishes, coated with ZnO/HG nanocomposite films and incubated for 24 h at 37 °C and 5% CO_2 in air. As the majority of the cells did not attach to the coatings, direct morphological assessment of the cells could not be performed. For the viability assay, cells were therefore reseeded into non-coated 24-well plates ($2x10^4$ cells per well) and allowed to attach for 24 h. Culture medium was then replaced by a medium containing 10% (v/v) resazurin (PromoKine, Heidelberg), a nontoxic dye that freely diffuses through the cell membrane and is reduced to the highly fluorescent resofurin by metabolically active cells. After 4 h of incubation, the fluorescence of the supernatant medium was measured at excitation/emission wavelengths of 544/590nm. This procedure was repeated every 24 h for 7 d, thus allowing for indirect measurement of cell proliferation since the emission intensity of resofurin is directly proportional to the number of viable cells.

For the detection of apoptosis/necrosis after 24 h exposure of the cells to the ZnO/HG nanocomposite films, cells were dually stained with Annexin V-FITC (AnV) and propidium iodide (PI) and analyzed by flow cytometry (FACSCalibur, BD Heidelberg, CellQuestPro software). Annexin V specifically binds to phosphatidyl serine, which is specifically located on the inner layer of the cell membrane of viable cells. In early apoptosis, membrane asymmetry is lost, exposing phosphatidyl serine to the outside of the cell within the reach of Annexin V. When the cell membrane ruptures in necrotic cells, both Annexin V and propidium iodide (PI), which are normally excluded, are able to enter the cell. PI then intercalates into the nuclear DNA. Thus, the staining pattern is able to differentiate viable

cells (AnV- / PI-) from apoptotic (AnV+ / PI-) and necrotic cells (AnV+ / PI+). Uncoated surfaces served as negative control; hydrogel-coated as well as surfaces coated with a commercially available ultra low attachment surface (ULA, Corning) served as positive control. All experiments were run in technical duplicates or triplicates and repeated on at least three separate occasions. Unless indicated otherwise, results were expressed as mean +/- standard error of the mean (SEM). Statistical analysis was performed using SPSS (v18). For the proliferation assay, Greenhouse-Geisser-corrected repeated measures ANOVA was employed according to Ludbrook [147]. For analysis of flow cytometry results, two-way ANOVA was performed. The separate hydrogels and ZnO concentrations were compared in a Tukey-corrected post-hoc analysis. Statistical significance was assumed at $p<0.05$. The cytotoxicity experiments were performed in collaboration with the University Clinic of Mainz.

4.4 List of characterization methods

1H-NMR (^{13}C-NMR) measurements were carried out on a Bruker 250 (300) MHz Spectrometer Avance with proton (and carbon) routine measurements.

Field-Desorption (FD) mass spectrometric analysis of several samples was measured by a model of Fisons Instruments VG ZAB2 SE FPD Sectorfield MS, which is able to detect molecular masses from 7 – 15 000 g mol^{-1}.

The total solid content and styrene conversion of the all copolymer NPs was measured gravimetrically using a Kern RH 120-3 gravimeter.

Thermogravimetric analysis (TGA) of lyophilized samples was conducted on a Mettler-Toledo TGA851 instrument. If not stated otherwise, the temperature was increased from 40 to 900 °C with a constant heating rate of 10 K min^{-1} under nitrogen atmosphere.

Differential scanning calorimetry (DSC) of lyophilized samples was conducted on a Mettler Toledo DSC823 instrument with a heating rate of 10 K min^{-1}.

The crystal structure of the ZnO NCs was analyzed using a Philips PW1820 X-ray powder diffractometer with Cu-K_α radiation (1.5418 Å).

Inductively-coupled plasma optical emission spectrometry (ICP-OES) was conducted on a ACTIVA M spectrometer (Horiba Jobin Yvon, Bernsheim, Germany) equipped with a Meinhardt-type nebulizer, a cyclone chamber, and controlled by ACTIVAnalyst 5.4 software. The Argon emission line at 404.442 nm was used as reference line. Measurements were performed using at least three different elemental emission lines.

Dynamic light scattering (DLS) and zeta-potentials were measured on a NICOMP zetasizer, measuring at a fixed scattering angle of 90°. The measurements were carried out at 23 °C on diluted NP dispersion in aqueous medium. The NP size distribution were obtained from a multi-modal algorithm (Nicomp), specially provided by the manufacturer for the separation of close bimodals and native populations from aggregate tails. Intensity distributions of various NPs were automatically converted into volume and number distributions using the Mie theory. The results were taken from the number distribution and expressed as mean value ± standard deviation (SD). For the determination of zeta-potentials, the NPs were dispersed into 10^{-3} M KCl solution (pH = 5.3) and subsequently subjected to an electric voltage in a cuvette equipped with electrodes.

Morphological characterizations of all NPs were carried out with a Zeiss EM902, operating at 80 kV. The samples were prepared by casting diluted NP dispersions onto carbon-coated 300 mesh copper grids and dried at ambient temperature. The PqDMAEMA and PLLA-based NP samples were additionally coated with a protective carbon layer. Particle counts of at least 100 particles per transmission electron micrograph were performed via ImageJ. The resulting size distributions were plotted and analyzed using a Gaussian fit. The error was estimated from the half width of the number distribution.

SEM characterization was performed on a Zeiss 1530 Gemini field emission scanning electron microscope (700V@2mm WD; InLens detector). Polymer NP samples were prepared by dropcasting diluted NP dispersions on Si wafer and drying under ambient conditions. For the characterization of the ZnO/PNIPAAm thin films, the samples were prepared by spin-coating the sample solutions on plasma-activated ($p(Ar:O_2)$: 0.9:0.1 mbar, 300 W, 10 min) Si-wafer with subsequent drying and crosslinking. EDS was performed on selected samples at 2.5 kV using a Hitachi SU8000 coupled with a Bruker XFlash 5010.

A surface profiler (Tencor P10, alpha-stepper) was used to determine the ZnO/PNIPAAm film thickness For this purpose, composite films, spin-coated on plasma-activated Si-wafers, were scratched with a needle and subsequently scanned by the profiler to probe the depth of the film.
UV-Vis absorbance spectra of the ZnO/PNIPAAm thin films were recorded on a Lambda 900 spectrometer (Perkin Elmer), using coated quartz substrates. For the kinetic measurements in buffer solution (PBS, 0.01 M), a teflon flow cell (d = 5 mm, V = 1 ml) with two quartz (PGO) windows was employed, one of them coated with ZnO/PNIPAAm nanocomposite films of varying NP content. A peristaltic pump (Ismatec, Reglo Digital) controlled the flow while the sample cell was rinsed for 24 h at 0.1 mL min^{-1}.

5. Results and discussion

The following results section covers the three main areas of antimicrobial strategies, notably anti-adhesive systems, contact-active non-leaching surfaces and biocide release system as described in the introduction. The systems are structured into generations of materials from I-V. Though each generation of materials has its individual attributes, each system is build on the experience of the previous one and the complexity of the systems increases from generation I to V.

5.1 Anti-adhesive nanoparticle design (1st generation of materials)

5.1.1 PEGylated surfaces - state of the art

Biofouling induces significant medical, industrial and economic damage in numerous applications mainly related to medicine, food industry, and marine industry. Current anti-fouling strategies either focus on preventing adhesion or deactivating the biofouling agent. With regard to the first approach, surfaces modified with poly(ethylene glycol) (PEG) or PEG-based variants are generally used to reduce adhesion of proteins, cells, marine organisms, and some other microorganisms [10, 148, 149]. PEG is a synthetic, hydrophilic polymer with low toxicity. It is FDA approved for a number of clinical uses, mainly as excipient in pharmaceutical products [150]. The most studied PEGylated coating strategy includes self-assembled monolayers (SAMs), which have demonstrated prominent resistance to several proteins and body fluids *in vitro* [151, 152]. Several mechanisms of protein rejection have been discussed which are related to steric repulsion and organization of PEG chains within their hydrated environment. Various simulations have shown the magnitude of the repulsive forces to be dependent on the thickness (surface density, chain length) and the flexibility of the polymer chain [153-156]. No difference could be found between hydroxyl or mono-methoxy-terminated oligoethylene chains [157].

Fewer reports can be found on the anti-adhesive effectiveness of PEGylated surfaces towards microorganisms. Tedjo et al. simultaneously investigated protein and bacterial interactions with PEGMA-grafted polypyrrole surfaces *in vitro*. Depending on the type and sequence of

protein exposure, surface adhesion of *S. aureus* was reduced by a factor of 2 to 4 [158]. In contrast, only moderate anti-fouling properties against the foodborne pathogen *Listeria monocytogenes* were observed on plasma-enhanced PEGylated silicon rubber [159]. On the other hand, a strong reduction of adhesion for several bacterial strains with a commercial multi-component crosslinked PEG-based polymer coating (OptiChem®) was reported by Saldarriaga-Fernandez and coworkers [149] in buffer and physiological fluids (urine). However, the anti-adhesive efficiency decreased noticeably in protein-rich media such as blood plasma or saliva. Recently, Khoo et al. [160] have successfully demonstrated the potential of PEGylated peptide coatings with a high affinity to titanium to significantly reduce *S. aureus* attachment and biofilm formation *in vitro* while completely repelling fibronectin.

Although the best anti-fouling results have been observed with SAMs, other coating strategies based on PEGylated brushes, comblike polymers, dendritic architectures, polymer networks, and polymer nanoparticles are widely explored [161-165]. The main disadvantage of SAMs is their lack of robustness [162]. Conversely, the main challenge for other coating strategies is to optimize the surface coverage in terms of surface density, chain length and flexibility [148].

The steric stabilization of latex particles by PEG-based surfactants has been widely employed in emulsion polymerization [166]. Despite of their good colloidal stability in aqueous suspensions, the resulting latex particles are generally unstable in the presence of water-miscible solvents due the mere physically adsorbed surfactants [167, 168]. Surface imparted PEG-moieties have been covalently introduced to latex particles by copolymerization with PEGylated macromonomers by emulsifier-free emulsion polymerization. Several studies on these micro- and nanoparticulate systems have shown excellent anti-adhesive properties against various plasma proteins *in vitro,* and decreased uptake into liver cells due to prolongued circulation times *in vivo* [166, 169-171]. To our knowledge, PEGylated latexes have not yet been characterized with respect to potential anti-adhesive properties towards microorganisms.

The aim of the following study was (*i*) to prepare suitable latexes with maximized PEG surface coverage and colloidal stability and (*ii*) to characterize the surface interaction with different bacteria. Therefore, our model PEG-variant systems are based on copolymer NPs of styrene with different amounts of PEGylated macromonomer (1st generation of materials), which were synthesized by miniemulsion polymerization under additional stabilization of a

PEG-based non-ionic surfactant (Lutensol AT50). Subsequently, the role of PEG-surface modified PS NPs on regulating the extent of bacterial growth in suspension and coated non-wovens has been investigated.

5.1.2 Synthesis and characterization of PS-co-PEGMA nanoparticles

The PEGylated NPs were synthesized by miniemulsion copolymerization of PEG macromonomers with styrene. To this end, styrene and various amounts of poly(ethylene glycol) methacrylate (PEGMA) (3, 5, 10, 15% w/w styrene) of different molecular weights (M_n ~ 326, 526, 2000 g mol^{-1}), an oil-soluble initiator (V59) and hexadecane as ultrahydrophobe were mixed and miniemulsified in an aqueous solution of the non-ionic, PEG-based surfactant Lutensol AT50. The resulting nanodroplets were polymerized at 72 °C for 8 h to generate solid polymeric NPs as illustrated in Fig. 11. Owing to the bulky side chain of the comonomer, steric hindrance and thus consecutive destabilization of the dispersion above a criticial concentration of the comonomer is to be expected. Therefore the amount of comomoner was varied to find the best conditions of colloidal stabililty with the highest degree of PEGylation. Furthermore, comonomers of different molecular weights were introduced to evaluate any anti-adhesive effects of the resulting NPs on bacterial growth which could be related to the chain length of the PEG units.

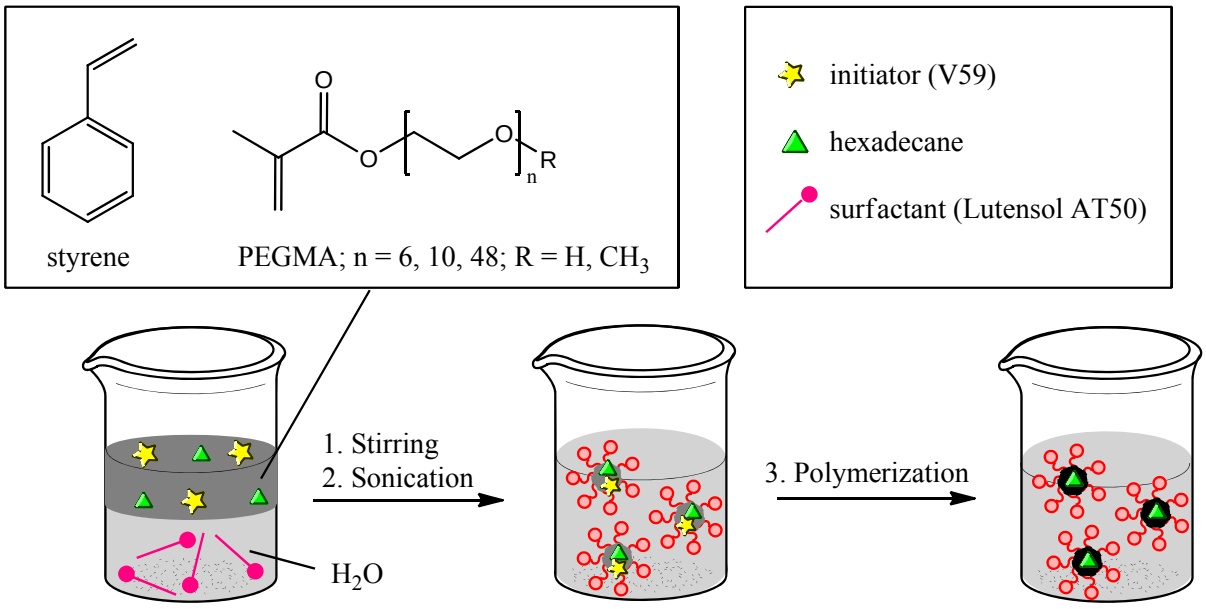

Fig. 11. Schematic presentation of the synthesis of polystyrene-co-poly(ethylene glycol) methacrylate (PS-co-PEGMA) NPs by miniemulsion polymerization.

Stable miniemulsions with spherical NPs in the range of 200-300 nm were obtained for all sample series, independently of the comonomer content and chain length of the PEGylated side chain. However, an increased viscosity of the sample dispersions was observed with increased amounts of comonomer as well as increasing PEG chain. The successful polymerization was proven by the absence of vinylic protons in the NMR spectra. With regard to the large ratio of styrene to PEGMA, the preferential consumption of the latter is rationalized if we assume that the reactivity ratios of styrene and PEGMA are similar to the reported values for styrene and diethylene glycol methylmethacrylate (r_1 = 0.39, r_2 = 0.67) [172]. The glass temperature range of PS and PEG 400 is significantly different, with 80-100°C for PS and -63°C for PEG 400 [172]. DSC measurements of copolymer NPs with 10% of PEGMA 326, revealed the presence of only one glass temperature range of 65-85 °C. The reduced glass temperature range suggests a successful integration of PEGMA units into the PS backbone. However, it could also be due to the presence of the ultrahydrophobe hexadecane, which is entrapped within the NPs.

Size distribution and sample morphology were analyzed by DLS and TEM. Fig. 12 shows the transmission electron micrograph of pure PS (A) and PEG-modified (B) copolymer NPs (10%, $M_n \sim 326$ g mol^{-1}). Close oberservation of the transmission electron micrographs reveals the presence of some distinct ellipsoid species within predominantly spherical NPs for the PEG-modified latexes, in contrast to the exclusively spherical shapes of the pristine PS latexes.

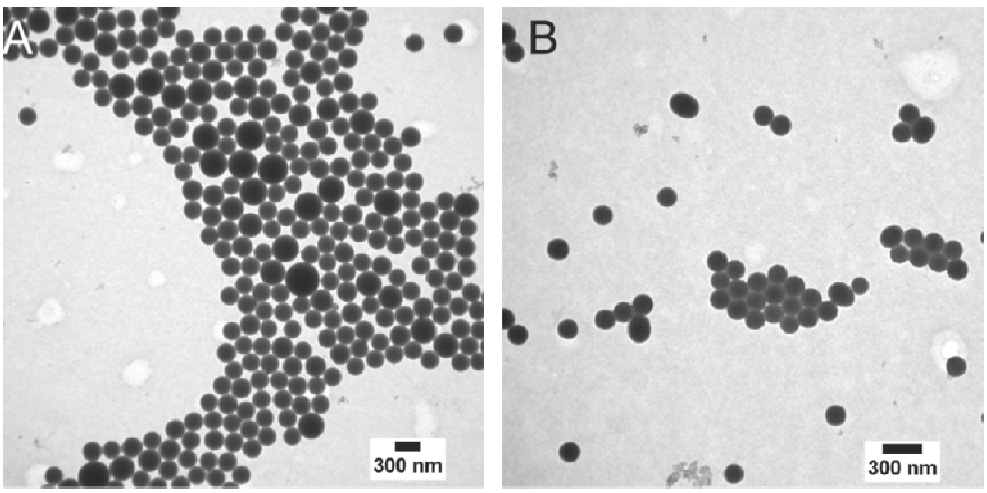

Fig. 12. Transmission electron micrograph of (A) PS NPs and (B) PS-co-PEGMA NPs (10% w/w styrene, M_n = 326 g mol^{-1}), both stabilized by 3.3% Lutensol (w/w styrene).

Table 2. Effect of molecular weight (326, 526, 2000 g mol^{-1}) and amount of PEGMA on the solid content and size distribution of the resulting PS-co-PEGMA latexes as determined by DLS.

Sample name	PEG-type	Solid content [%]	Amount of comonomer [%] (w/w styrene)	Size distribution D_H [nm]
VS5.3	PEGMA 326	21.7	5	294±36
VS15.2	PEGMA 526	19.9	5	251±27
VS12.2	mPEGMA[1] 2000	22.0	5	259±40
VS12.0	/	20.1	0	251±29
VS12.1	mPEGMA 2000	20.3	3	228±25
VS12.2	mPEGMA 2000	22.0	5	259±40
VS12.3	mPEGMA 2000	24.9	10	214±31
VS12.4	mPEGMA 2000	22.0	15	224±26
VS13.0[2]	mPEGMA 2000	23.6	15	293±41

[1]methoxy-PEGMA, [2]surfactant-free sample

Table 2 summarizes the solid content and the size distribution of the final latex particles as determined by DLS with respect to the molecular weight and comonomer content. The solid content of ~20% evidences successful monomer conversion of nearly 100% for all samples. Interestingly, no significant changes in the particle size were detected in relation to the molecular weight and amount of comonomer. In contrast, in a detailed study on the colloidal stability of PEG-modified PS latexes, Dunn et al. described a marked decrease in particle size from 180 to 70 nm with increasing amounts (0.4-6%, w/w styrene) of a similar PEG macromonomer (methoxy-poly(ethylene glycol) acrylate, mPEGA 2000) [171]. Since the particles were synthesized via emulsifier-free emulsion polymerization, the authors attributed the size effect to the surface-active properties of the PEG macromonomer: Similar to surfactant-stabilized systems, increased concentrations of mPEGA were believed to provide sufficient stabilization for smaller particles. In comparison, the absence of size effects with respect to the molecular weight and amount of comonomer in the present copolymer NP system is most likely a consequence of the additional stabilization by the non-ionic, PEG-based surfactant (Lutensol AT50). The narrow, unimodal size distributions (variations in particle size within 15%) indicate a good colloidal stability.

It is known that the colloidal stability of PEGylated PS copolymers does not depend on the presence of any additional surfactant [171]. A proof of concept synthesis of copolymer NPs with 15% of PEGMA 2000 without additional stabilization by Lutensol AT50 evidenced that

this is also valid for the present PS-co-PEGMA miniemulsions. Yet, the comparably enhanced viscosity of both Lutensol-stabilized and "surfactant-free" PS-co-PEGMA dispersions with 15% of PEGMA 2000 suggested an increased intramolecular and intermolecular steric hindrance by the PEG chains. Consequently, stable colloidal miniemulsions by copolymerization with PEGMA macromonomers are accessible to a maximum of PEGMA 2000 content of 15% at the experimental conditions studied. The additional stabilization with Lutensol AT50 offers an alternate possibility to increase the PEG surface coverage to certain extends.

A significant increase of wettability in correlation with higher PEGMA 2000 content was visualized, merely by spreading droplets of latex dispersions on glass surfaces. This observation indicates an increased hydrophilicity and therefore surface coverage with respect to the PEGylated comonomer in good agreement with previously reported studies [169, 171].

The surface concentration of PEGylated latexes has been quantified in different studies by NMR measurements and subsequent calculations based on an independently set PEG calibration curve: For example, Meng et al. obtained PEG surface concentrations of $6 \cdot 10^{-3}$ mol m^{-2} by using carbodiimide chemistry to couple amino-functionalized PEG 3400 to micronsized COOH-terminated latex particles [165]. Conversely, much higher PEG surface concentrations of 2.1 mol m^{-2} were reported by Chern and coworkers for a copolymer latex system [170]. Their composite latex particles of 220-290 nm were obtained via emulsifier-free emulsion copolymerization of styrene with 9% (w/w styrene) PEGA 2000 macromonomer. Judging from these results, the second route via copolymerization of styrene with PEG macromonomers appears much more suitable to achieve high surface concentrations of PEGylated chains, which were primarily targeted in this approach. Subsequent quantification of the PEG surface concentration by NMR did not lead to conclusive results in the present system due to the interference of the additional PEG-based stabilizer with the PEGMA macromonomer signals. Although direct quantification of the PEG surface coverage could not be obtained, the aforementioned results are quite conclusive: Stable colloidal miniemulsions with a marked increase in hydrophilicity at higher comonomer contents were obtained to a maximum of 15% PEGMA 2000. Furthermore, with regard to the monomodal size distribution and uniform DSC thermograph of the PS-co-PEGMA particles, secondary nucleation of isolated PEG or PS species can be excluded. Thus, the results

strongly indicate the generation of uniform copolymer NPs with a high surface coverage of PEGylated chains.

5.1.3 Investigation of the antibacterial properties of the PS-co-PEGMA NPs

Microbiological training was provided at the University of Bath to investigate the antibacterial properties of the PS-co-PEGMA with different techniques based on (*i)* optical density (OD) measurements of NP suspensions, (*ii*) agar-dilution tests of NP-coated filter pads and (*iii*) fluorometric assays of NP-coated polypropylene (PP) non-wovens. All tests were carried out with four different samples, namely PS NPs (negative control), Lutensol-stabilized PS-co-PEGMA 2000 NPs (15%), surfactant-free PS-co-PEGMA 2000 NPs (15%) and Lutensol-stabilized PS-co-PEGMA 526 NPs (10%). To this end, the freeze-dried samples were resuspended in sterile LB-media with a final concentration of ~1000 mg $mL^{-1}$and serial dilution series were prepared for each experiment.

For the first test (*i*), the NP suspensions were inoculated with 10^2 CFU of *P. aeruginosa* PAO1. After incubation at 37 °C for 24 h, the optical density was recorded at 600 nm. Similar values were measured for all NP suspensions, both controls (NP-free medium and native PS NP suspension) included, indicating that the presence of functionalized and non-functionalized NPs does not interfere with the bacterial growth in solution. For the agar dilution test (*ii*), filter pads were plunged into the PAO1-infected NP dispersions and placed on agar culture dishes. After incubation at 37 °C for 24 h, the agar plates were examined for zone of inhibitions. NP-free filter pads served as control. The photograph in Fig. 13 shows an infected agar plate after incubation, including the NP-coated (PS-co-PEGMA 2000, surfactant-free) filter pads. The multiple colony forming units (CFUs) of PAO1 are perceived as a lawn of small white dots. Closer inspection of the photograph does not reveal any zone of inhibition around the filter pads. Similar observations were made for all other samples.

For the fluorometric assays, small pieces of non-woven PP nappies were dipped into the undiluted NP suspensions. After drying, the non-wovens were inoculated with PAO1-enriched LB medium (10^6 CFU mL^{-1}) and incubated at 37 °C for 24 h. NP-free sterile and non-sterile non-wovens were used as controls. Subsequently, the infected non-wovens were stained with a commercially available dye mixture (LIVE/DEAD BacLight™, Invitrogen) and examined under a confocal microscope.

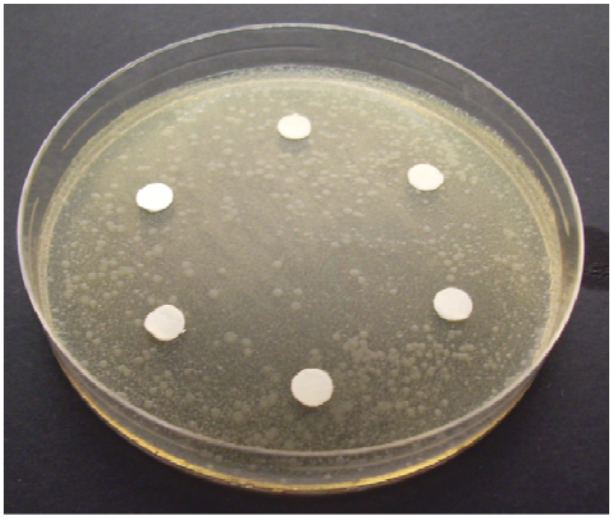

Fig. 13. The effect of Lutensol AT50-stabilized PS-co-PEGMA 526 NPs on the growth of *P. aeruginosa* (PAO1), visualized by a photograph of the inoculated filter pads, incubated on agar plates at 37 °C for 24 h.

The staining process involves two fluorescent dyes which allow for a reliable distinction between viable and dead species: SYTO9 emits in the green, following enzymatic deesterification within the viable cells; propidium iodide emits in the red by interaction with the DNA of necrotic cells. The 3D micrographs of non-coated control and NP-coated non-wovens are presented in Fig. 14. Small green dots of viable bacteria can be perceived within the thin structure of the non-woven control sample (A). The resolution of the NP-coated non-wovens (B) was affected by multiple scattering of the NPs. Despite of that, green-fluorescing structures can be perceived within the non-woven. The image suggests that the bacteria are rather attracted to the NP surface than repelled, since the highest fluorescence intensity appears to be concentrated in NP-rich environment.

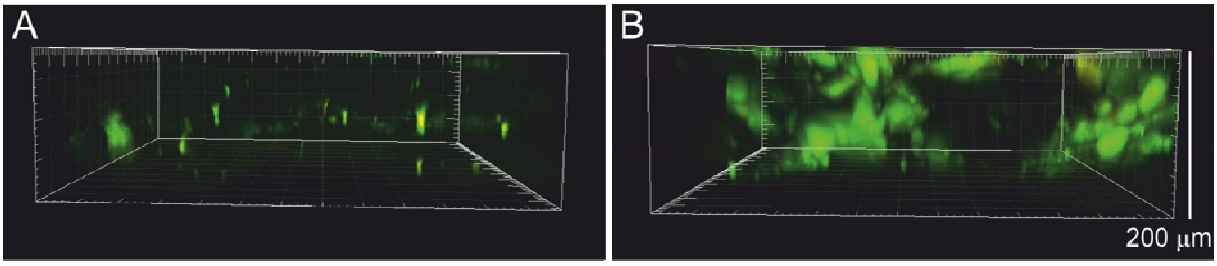

Fig. 14. Confocal micrographs (600x600x200µm) of (A) uncoated and (b) PS-co-PEGMA 500 (5 % w/w styrene) coated PP non-wovens after incubation at 37 °C for 24 h and subsequent staining with Bac Lite™.

In summary, it seems that the bacterial growth of *P. aeruginosa* is not affected by the presence of PS-co-PEGMA NPs, independently of the molecular weight and PEGMA content. Several experimental studies and simulations have shown that the anti-fouling properties of PEGylated surfaces are highly dependent on the conformation of the chains in the PEG-water complex [148]. Hence, the results of the agar dilution test are not necessarily suited to evaluate the anti-fouling properties of the NPs because the highly viscous texture of the agar does not promote NP hydration. On the other hand, sufficient hydration was ensured in both, the OD and fluorometric assays, which are therefore reliable.

A very interesting study was published by Roosjen et al. [173]. The authors investigated the degree of surface-adhesion on PEGylated brushes for six different strains of *P. aeruginosa*. Taking into account the measured motility, zeta potential and surface energy values, three non-adhesive and three adhesive species were identified. Surface adhesion was found to depend on the hydrophobicity of the strain and the release of extracellular substances, which varied between single *P. aeruginosa* species. To our knowledge, no information on the degree of hydrophobicity and secreting properties of the PAO1 strain are available. Yet, the fluorescent images suggest an increased bacterial colonization on the PS-co-PEGMA NP surface. Hence, it seems that PAO1 belongs to the more adhesive species of *P. aeruginosa* mentioned by Roosjen and coworkers [173]. Additional experiments with other bacterial strains might give a more conclusive evaluation of the anti-adhesive potential of the PS-co-PEGMA NPs. Yet, the individual adhesion properties within a single species plainly show that bacterial adhesion is much more complex compared to protein adhesion. Since the bacterial adhesion relies on many factors such as hydrophobicity, motility, the release of extracellular substances, surface texture and charge [130], it appears that PEGylated coatings can only offer a relatively limited protection against a broad range of microorganisms.

5.1.4 Conclusions

Stable, spherical NPs in the range of 200-300 nm with surface-imparted PEGylated chains have been fabricated by the copolymerization of styrene and PEGMA in miniemulsion. DSC measurements demonstrated a reduced glass temperature range of the composite material, suggesting a successful incorporation of the PEG macromonomer into the PS backbone. Furthermore, the effect of different PEGMA contents of various molecular weights (326, 526, 2000 g mol^{-1}) on the colloidal stability and size distribution of the resulting latexes have been

investigated. Stable miniemulsions were obtained to a maximum of 15% (w/w styrene) PEGMA 2000. The surface density of PEG chains was further increased by additionally stabilizing the NPs with the PEG-based non-ionic surfactant Lutensol AT50. Variation in amount and molecular weight of the comonomer did neither affect the size nor size distribution of the final latexes, which was attributed to a compensation effect from the non-ionic stabilizer. Microbiological training was provided at the University of Bath to study the anti-adhesive properties of PEG-surface modified PS NPs on the bacterial colonization of *P. aeruginosa* (PAO1) by different techniques, including OD measurements in growth medium, surface-spread plate method on agar culture dishes and fluorometric assessment of viable species on stained PP non-wovens. The combined results indicated that the *P. aeruginosa* strain (PAO1) used was not sensitive towards the PEGylated NPs. Indeed, due to individual attributes such as surface hydrophobicity and surfactant release, the adhesive and non-adhesive behavior towards PEGylated surfaces differs even amongst single *P. aeruginosa* strains as demonstrated by Roosjen et al. [174]. To validate the anti-adhesive potential of the PEGylated NPs, further experiments with other *P. aeruginosa* strains as well as gram-positive pathogens might be envisaged. However, in light of the individual and complex surface interactions with bacteria, the presented results suggest that PEGylated coatings can only give a limited, strain-dependent solution to prevent surface-adhesion.

5.2 Contact-active non-leaching surfaces based on polymeric quaternary ammonium compounds

5.2.1 Quaternary ammonium compounds – state of the art

The bactericidal properties of cationic biocides, also known as quaternary ammonium compounds (QACs), were discovered in the 70s by Isquith et al. [175]. The authors functionalized different substrates with organosilicon quaternary ammonium chloride salts and exposed them to different microorganisms (*E. coli, S. faecalis*). Multiple washing cycles proved the stability of the functionalized surfaces. Therefore, the antimicrobial activity was attributed to a contact-interaction with the surface-bound material. Based on those findings, molecules containing quaternary nitrogen atoms, quickly found their way into the list of disinfectants, used in hospitals for surgical instrumentation and preoperative disinfection of healthy skin. In general gram-negative bacteria are less susceptible towards QAC-based antiseptics and disinfectants than gram-positive strains because of compositional differences in the outer lipopolysaccharide membrane [176].

In the last decade, the concept of QACs has been introduced to polymeric materials by some pioneering work of Tiller, Klibanov and co-workers [12, 13, 16, 177-180]. Several generations of cationic polyelectrolyte systems were developed by radical polymerization methods, to generate surface coatings based on brushes and complex polymeric networks from *N*-alkylated derivatives of acrylates, polyethyleneimine (PEI) and poly(4-vinylpyridine) (PVP). For instance, in one of his initial publications, Tiller et al. grafted cationic poly(4-vinyl-*N*-alkylpyridinium bromide) from functionalized glass surfaces, which exhibited very efficient growth reduction towards *E. coli, S. aureus*, and *P. aeruginosa* [13]. In another approach, polymer conetworks of polydimethylsiloxane (PDMS), 2-hydroxyethylacrylate (HEA) and acrylic acid (AA) were prepared and reversibly loaded with the antimicrobial surfactant cetyltrimethylammonium chloride (CTAC), which remained active for a period of up to 3 weeks [177]. Emulsion polymerization was used to prepare antibacterial, film-forming copolymers of styrene and butylacrylate (PS-co-PBA), which were stabilized by the antimicrobial emulsifier polystyrene-block-poly(4-vinyl-*N*-methylpyridinium iodide) (PS-b-P4VMP) [179]. Recently, Tiller et al. focused on the synthesis of biocidal macromonomers

using poly(methyloxazoline) spacers to connect acrylate polymerizable end-groups with an QAC-based terminator to synthesize a new generation of more stable antimicrobials [16].

Antibacterial and antifungal polymer brushes of alkylated 2-(dimethylamino)ethyl methacrylate (DMAEMA) were created through controlled polymerization methods by Russel and coworkers [14, 181, 182], using different alkyl chain lengths and grafting densities. Cheng et al. synthesized poly(4-vinylbenzyl chloride) (PVBC) microspheres with surface-grafted and subsequently quaternized PDMAMEA brushes [183]. The microspheres demonstrated a 5-fold log reduction of viable *E. coli* and *S. aureus* cell numbers within a couple of minutes.

A different pathway was chosen by Cakmak et al. [184]. The authors introduced the cationic charge into the main polymer chain by polycondensation of epichlorhydrin (EPH) with benzyl amine. However, the resulting polyelectrolytes revealed only limited growth inhibition against the six pathogenic strains tested. Other approaches focused on the use of natural materials, such as chitosan, or cationic polyelectrolyte networks made through layer-by-layer assembly, which have been summarized in a couple of excellent reviews [19, 26].

Various theories about the antimicrobial mechanism of action of polymeric QACs have been discussed in the literature. The PVP-surface coatings of Tiller et al. were found to have optimal antimicrobial activity for alkyl chain lengths between 3 and 8 carbon atoms [13]. Based on these results, the authors assumed that the killing mechanism is caused by membrane disruption through penetration of the aliphatic side chains into the lipid bilayer assembly. Dizman et al. found an increase of antimicrobial activity from butyl to hexyl alkyl chain lengths of pendant quaternary ammonium moieties in 1,4-di-azabicyclo-[2.2.2]-octane (DABCO) monomer derivatives [185]. In contrast, Kügler et al. proposed a destabilization mechanism of the bacterial membrane based on the displacement of stabilizing counterions by cationic polymeric chains [186]. Similarly, Murata et al. synthesized high density QAC surface brushes with experimental evidence strongly favoring a charge density related mechanism [182]. Binder investigated the interaction of lipid bilayer membranes with polymeric materials [187]: Depending on the polymer structure, four different mechanisms of polymer-induced pore formation within lipid bilayer membranes were proposed. With regard to polymeric QACs, the so-called barrel-face mechanism, where the polymeric backbone is aligned to the membrane surface under insertion of its hydrophobic side chains into the

membrane structure, could explain the lysis of bacterial cell walls. Alternatively, the carpet model, which includes a pore formation, with amphiphilic charged polyelectrolytes covering both membrane ends, fits as well (Fig. 15).

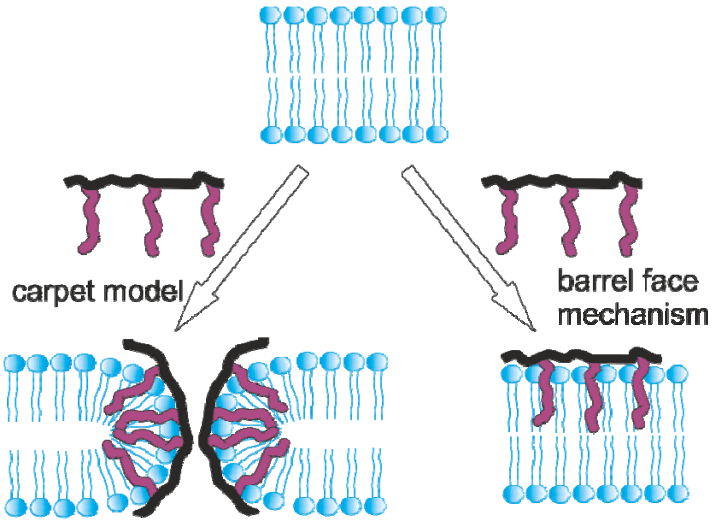

Fig. 15. Schematic illustration of polymer-induced pore formation into lipid bilayer membranes.

Recently, Palermo et al. [15] described very interesting results concerning the interaction of copolymers containing primary, secondary and quaternary polymeric amines with model membrane systems. They found that careful fine-tuning of the hydrophobic and hydrophilic groups increased the pronounced interactions of the polymers with biomembranes, including possible amine-phosphate complexation after initial binding of the polymer to the membrane. In summary, the antibacterial performance of polymeric QACs appears to be related to the alkyl chain length, the polarity of the system and most importantly the hydrophilic/hydrophobic balance.

With regard to the aforementioned factors, surface coatings based on colloidal polymer systems seem quite advantageous because they offer a high surface area as a basic requirement for a maximum of functionalization. To compete with the grafted contact-active surfaces, a non-leaching approach should be considered, which disqualifies the use of surfactants that are not covalently bound to the surface.

Surfmers (SURFactant monoMERS) have been widely used in emulsion polymerization methods to impart surface functionalities directly into the bulk polymer network and to stabilize latex particles in addition to or even without the use of surfactants [56]. Caillier et al.

[188] investigated the antimicrobial properties of different polymerizable quaternary ammonium compounds based on DMAEMA-derivatives with varying spacer and alkyl chain lengths. All studied compounds were active against *S. aureus* and *P. aeruginosa* strains. The results indicated a parabolic dependence of the minimum inhibitory concentration (MIC) with respect to the length of the alkyl chain, with an optimum activity for 12 carbon atoms. The authors attributed the antibacterial activity to a so-called "cut-off-effect/concept of free volume", a model that is similar to the barrel face mechanism, where hydrophobic side chains insert into the membrane. They assumed that if the chain length lied within a range slightly smaller than the phospholipids of the cell, a free volume could be created, which would induce membrane lysis.

Following the above-stated study [188], DMAEMA was selected as a starting monomer, subsequently quaternized with an alkyl chain of 12 carbon atoms and integrated into two different systems for the formulation of polymeric NPs. In the first approach, the quaternized monomer (further referred to as qDMAEMA) served as costabilizer for styrene to create novel, surfactant-free QAC-functionalized polystyrene-co-(poly(2-methacryloyloxyethyl)-dodecyldimethylammonium methacrylate) (PS-co-PqDMAEMA) NPs by miniemulsion polymerization (2^{nd} generation of materials). In the second approach, qDMAEMA was polymerized by free radical polymerization and used to generate pure PqDMAEMA NPs by the miniemulsion/solvent evaporation technique (3^{rd} generation of materials). Both approaches aimed at simultaneously exploiting the surface-active and antimicrobial potential of qDMAEMA or PqDMAEMA respectively, to covalently stabilize novel systems of highly functional polymer NPs with anticipated biocidal activity.

5.2.2 Synthesis and characterization of PS-co-PqDMAEMA nanoparticles by miniemulsion polymerization (2^{nd} generation of materials)

Functional NPs can be created in different ways by (*i*) imparting the desired function to ready-made polymeric NPs by surface coupling reactions, (*ii*) adsorption processes of suitable molecules or (*iii*) copolymerization with a functional comonomer [189]. The formation of the 2^{nd} generation of materials is based on the synthesis of copolymer NPs from styrene and qDMAEMA, which is schematically displayed in Fig. 16. In a first step, the functional comonomer qDMAEMA was synthesized by nucleophilic substitution of dodecylbromide

with the commercially available DMAEMA according to Hamid and Sherrington [145]. The second step comprised the free-radical copolymerization of styrene with qDMAEMA in direct miniemulsion (o/w) to generate functional NPs. To explore the stabilizing potential of the surfmer qDMAEMA, the miniemulsion was conducted in a further denoted "surfactant-free" mode, i.e. no additional surfactant molecules were added apart from the qDMAEMA monomer.

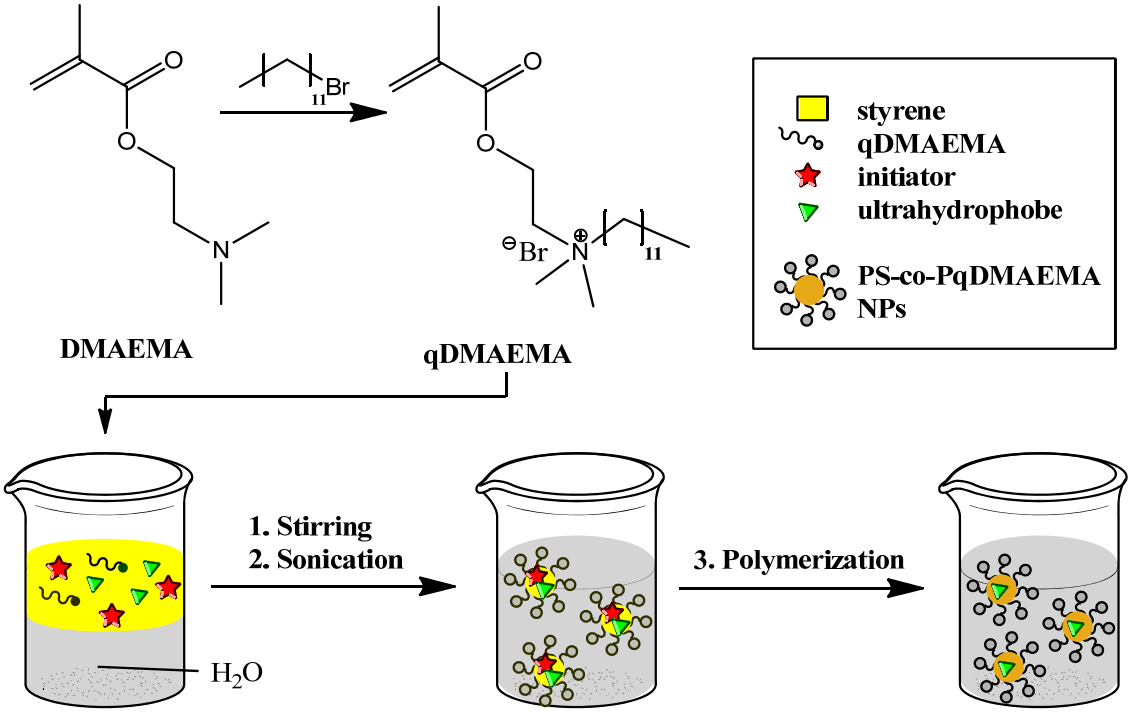

Fig. 16. Schematic presentation of the synthetic route for the formation of PS-co-PqDMAEMA NPs by surfactant –free copolymerization in direct miniemulsion.

The surface-active properties of quarternized DMAEMA monomers with various alkyl chain lengths have been described in the literature [145, 188, 190]. Besides, DMAEMA copolymers with alkylmethacrylates have shown good stabilizing properties for the synthesis of polystyrene latexes in dispersion [191, 192] and miniemulsion polymerization [193]. The surfmer qDMAEMA is soluble in water at low concentrations and its CMC has been assessed in different studies as well as in our lab. The values are listed in Table 3, in comparison to common surfactants such as SDS, CTAC and CTAB. Consequently, qDMAEMA should represent a suitable candidate for the stabilization of polymeric NPs.

Table 3. CMC of PqDMAEMA and some commonly used surfactants according to the literature and surface tension measurements in our lab.

Surface-active compound	CMC in water at 25°C [mol l^{-1}]	Method	Reference
qDMAEMA	$3.6x10^{-3}$	conductivity measurements,	Hamid & Sherrington [145]
	$2.5x10^{-3}$	surface tension measurements,	
	$1.9x10^{-3}$	dye absorption measurements	
	$5.9x10^{-3}$	conductivity measurements,	Nagai et al. [190]
	$6.0x10^{-3}$	dye solubilization	
	$6.5x10^{-3}$	conductivity measurements	Caillier et al. [188]
	$3.3x10^{-3}$ (23 °C)	surface tension measurements	our lab
SDS	$8.1x10^{-3}$	conductivity measurements	Mukerjee & Mysels [194]
		light scattering	
		dye absorption measurements	
CTAC	$1.3x10^{-3}$	conductivity measurements	Mukerjee & Mysels [194]
CTAB	$9.7x10^{-4}$	conductivity measurements	Modaressi et al. [195]
	$9.2x10^{-4}$	conductivity measurements	Mukerjee & Mysels [194]

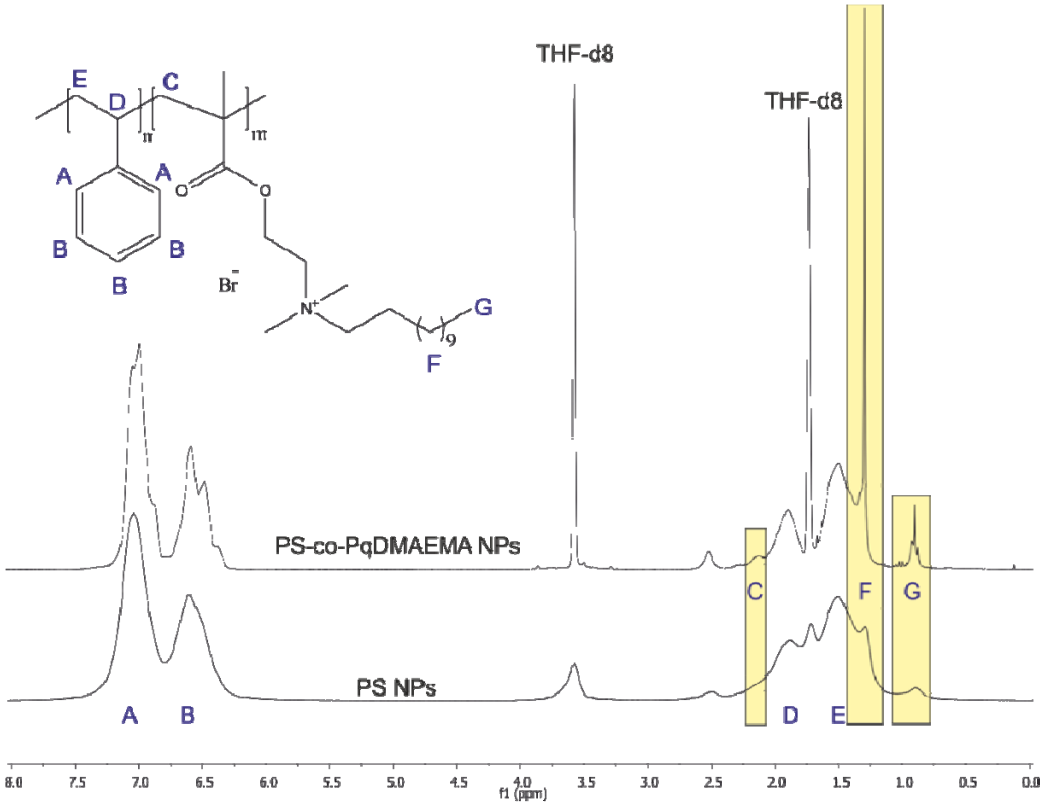

Fig. 17. Overlay of the ^{1}H-NMR spectra (250 MHz, THF-d_8) of native PS (VS23.0) and PS-co-PqDMAEMA (VS23.2, 5% qDMAEMA) NPs. The differences between both spectra are highlighted and assigned to the copolymer structure.

Different sample series of PS-co-PqDMAEMA NPs with various amounts of qDMAEMA comonomer (0-10% w/w styrene) and with and without stabilizing agents (cetyltrimethylammonium chloride, (CTAC), Lutensol AT50) were synthesized and characterized by NMR, DLS, TEM and zeta potential measurements.

The additional copolymer NPs which were stabilized with the biocidal QAC-based cationic surfactant CTAC were produced to compare with their surfmer-stabilized ("surfactant-free") analogues in terms of colloidal stability and biocidal activity. Fig. 17 shows an overlay of the NMR-spectra of pure PS NPs and copolymer NPs (5% of qDMAEMA), both stabilized with CTAC. The absence of vinylic protons in both spectra indicates the successful (co)polymerization. Furthermore, a marked increase of the signals which can be attributed to different aliphatic protons within the qDMAEMA monomer (Fig. 17, C, F, G) can be observed. However, there is no clear distinction between those signals and the ones caused by the aliphatic protons of the ultrahydrophobe hexadecane and CTAC, which are present in both systems. Thus, it is difficult to derive the actual content of qDMAEMA within the PS backbone from the NMR spectra. Yet, stable miniemulsions with and without surfactant were obtained up to 10% qDMAEMA content. The CTAC-stabilized and surfmer-stabilized samples did not show any coagulation and their high solid contents suggest a full conversion. Since no vinylic protons could be detected by NMR, it can be assumed that the qDMAEMA has been integrated quantitatively into the PS backbone. In contrast, the polymerization of both components under stabilization with the non-ionic surfactant Lutensol yielded clotty, gel-like samples at the experimental conditions studied.

5.2.2.1 Effect of comonomer content and additional surfactant stabilization on the size and size distribution of the resulting NPs

The transmission electron micrographs of copolymer NPs with 5% comonomer as well as native CTAC-stabilized PS NPs are displayed in Fig. 18. The images reveal the presence of spherical NPs in the range of 40-70 nm for all NP samples with no marked difference in morphology between surfactant-stabilized, surfactant-free copolymer NPs or native PS NPs. Table 4 compares the hydrodynamic diameters of CTAC-stabilized, Lutensol-stabilized and surfactant-free copolymer NPs, as measured by DLS, to the diameters obtained from TEM particle analysis. The values evidence a slight decrease of the NP size with increasing amounts of comonomer within the surfactant-free sample series. The same, though much

more pronounced effect is noted for the CTAC-stabilized sample series. This observation is similar to the general effect seen in miniemulsions with increased amounts of surfactants [57], clearly reflecting the surface-active potential of qDMAEMA to stabilize smaller droplets at higher qDMAEMA concentrations. Although this trend is also visible within the Lutensol-stabilized sample series, the DLS data should be interpreted with caution due to the pronounced coagulation, which was observed for both Lutensol-stabilized copolymer samples.

As expected, the hydrodynamic diameters of the CTAC-stabilized copolymer NPs are smaller compared to their surfactant-free analogues. This can be attributed to the higher amounts of surface-active agents in the CTAC-stabilized system and thus consecutive formation of smaller droplets/particles [57].

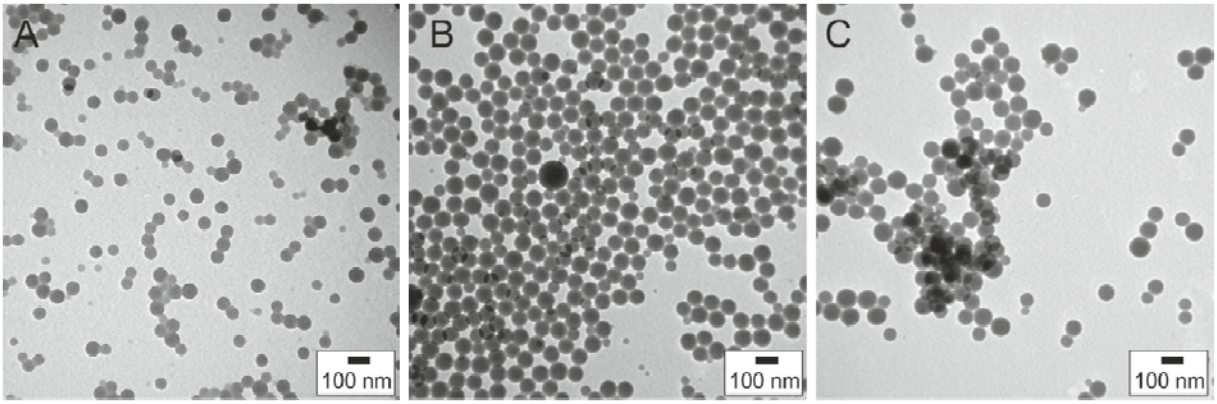

Fig. 18. Transmission electron micrograph of (A) CTAC-stabilized (VS23.2), (B) surfactant-free (VS28.2) PS-co-PqDMAEMA NPs with 5% (w/w styrene) of comonomer and (C) CTAC-stabilized native PS NPs (VS23.0).

Similar to the PS-co-PEGMA NPs (see section 5.1) increasing amounts of qDMAEMA led to an increased sample viscosity, independently from the applied stabilization method. The high viscosity of the qDMAEMA-concentrated NP dispersions most probably results from increased charge repulsion between qDMAEMA entities and surface-adsorbed cationic surfactant in case of the CTAC-stabilized NPs. Thus, in order to ensure sufficiently dilute, stable NP dispersions, the optimum amount of qDMAEMA comonomer is limited to 5-8% for the copolymerization in miniemulsion.

Table 4 additionally summarizes the measured zeta-potentials for the different PS-co-PqDMAEMA NPs. The values span between +30 to +40 mV, thus demonstrating sufficient stability of the colloidal dispersions for both surfactant-free and surfactant-stabilized systems. Furthermore, the positive zeta potentials of all NPs indicate the presence of surface-oriented quaternary ammonium groups, which either results from covalently integrated qDMAEMA comonomer units or stabilization by surface-adhered CTAC molecules. Indeed, the data confirm a successful functionalization of the surfactant-free NP with charged comonomer entities.

Table 4. Effect of the functional qDMAEMA amount on the solid content, the average particle size as determined by DLS (D_H) and TEM (d) analysis and zeta potential of the dialysed samples.

Sample name	Amount of qDMAEMA[1]	Additional surfactant	Solid content	Size		Zeta potential
	[%]		[%]	D_H [nm]	d [nm]	ζ [mV]
VS23.0	0	CTAC	20.1	97±13	65±9	+43
VS23.1	3		21.6	61±6	62±20	+32
VS23.2	5		20.5	68±7	51±20	+28
VS23.3	10		25.7	38±4	50±10	+28
VS28.1	3	none	20.8	110±16	76±9	+40
VS28.2	5		21.6	97±12	58±12	+31
VS28.3	8		22.9	95±12	51±17	+24
VS24.2	10		22.1	83±13	53±11	+29
VS25.0	0	LutensolAT50	20.1	251±29	-	-
VS25.1	5		22.0	102±12	-	+8
VS25.2	10		21.7	46±6	-	+9

[1](w/w, styrene)

The molecular weight of the copolymer NPs has been assessed by SEC. The measurements showed relatively broad molecular weight distributionts for all copolymer NP samples. Assuming similar reactivity ratios of styrene and qDMAEMA to styrene and methyl methacrylate (r_1 = 0.4-0.5, r_2 =0.42-0.5) [172], which to our knowledge is the closest relative to qDMAEMA with published copolymerization values, statistical copolymerization of both monomers is to be expected. Yet, since the local concentrations of both components differ significantly, the formation of styrene-rich chains is supposedly much more favored than the incorporation of qDMAEMA units. Hence, this would explain the broad molecular weight

distributions for all samples, independently of the stabilization agent used. In contrast to the surfactant-free copolymer samples, bimodal molecular weight distributions, starting from comonomer amounts of 5%, were obtained in the CTAC-stabilized NP series only. The SEC elugrams of both a CTAC-stabilized (A) and surfactant-free sample (B) including the UV as well as the RI signal are presented in Fig. 19. While the surfactant-free sample shows a monomodal distribution in accordance with both detector signals, the elugram of the CTAC-stabilized NPs evidences two peaks. Furthermore, both detector signals are not congruent. These results suggest the presence of different polymeric fractions in the CTAC-stabilized copolymer NP sample. Yet, as a matter of fact, both elugrams are not very well defined, most probably due to interactions of the charged nitrogen atoms with the column material. The bimodal molecular weight distribution of the CTAC-stabilized samples could be attributed to the presence of free copolymer chains in the water phase in addition to the polymer NPs. But, since the water solubility of styrene and qDMAEMA is very limited, this option seems rather improbable.

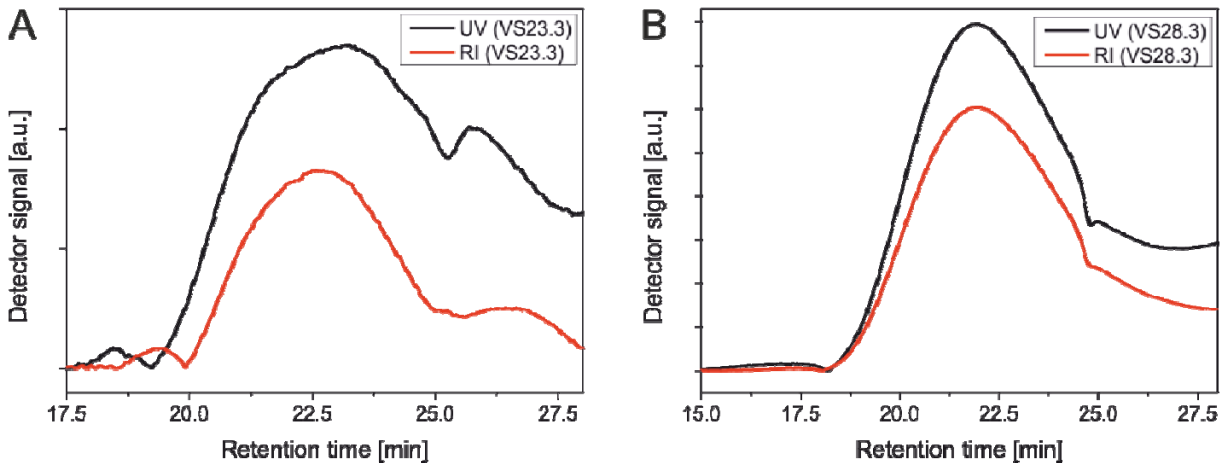

Fig. 19. SEC elugrams including both detector signals (UV, RI) from (A) CTAC-stabilized PS-co-PqDMAEMA (10% qDMAEMA) and (B) surfactant-free PS-co-PqDMAEMA NPs (8% qDMAEMA).

On the other hand, the bimodal molecular weight distribution could also result from a hindered integration of qDMAEMA into the polystyrene backbone due to additional charge repulsion from the cationic surfactant. In this case, secondary nucleation producs could be formed from either CTAC-stabilized PS or surfactant-free copolymer NPs. Indeed, the latter assumption is supported by the TEM results since the particle size distribution of the CTAC-stabilized NPs by TEM is slightly higher than for the surfactant-free analogues. Furthermore,

close observation of the TEM images of both NP species reveals the presence of very small CTAC-stabilized copolymer NPs, which are scattered in between a majority of larger species. In conclusion, the surfmer qDMAEMA has demonstrated its efficiency to adequately stabilize und functionalize PS NPs in miniemulsions up to a maximum of 10% comonomer content.

5.2.2.2 Investigation of the antibacterial properties of the PS-co-PqDMAEMA NPs

The antibacterial properties of the copolymer NPs were assessed by OD measurements in collaboration with the University Clinic Cologne (UKK). For this purpose, freeze-dried samples of copolymer NPs (5% qDMAEMA), stabilized by CTAC, Lutensol AT50 or synthesized without additional surfactant were redispersed in TSB medium (Trypticase Soy Broth) with a final concentration of 0.5 mg mL^{-1} and incubated with *S. aureus* (MSSA476) at 37 °C for 24 h. Subsequently, the bacterial growth was monitored by OD measurements at 600 nm within a period of 24 h. The OD of various sample dispersions is plotted against the measuring time in Fig. 20. According to Fig. 20, the control, which was composed of NP-free, sterile medium, follows a standard bacterial growth cycle: In the initial lag phase, bacteria adapt to their growth conditions. The subsequent log phase or exponential growth is characterized by multiple cell divisions, followed by a stationary phase. Prolonging the time scale of the experiment would induce a death phase, which occurs when all nutrients are consumed [196]. Similar growth curves were observed for the surfactant-free and Lutensol AT50-stabilized copolymer NP dispersions. In contrast, the log phase of the bacteria seemed to be retarded by the presence of CTAC-stabilized PS NPs for approximately 5 h although the final population reached the same level than the control. Furthermore, a considerable growth inhibition with a difference in optical density of 55% was detected for the CTAC-stabilized copolymer NP dispersions after 24 h of incubation.

The different copolymer NP samples were investigated at the same concentrations and the same qDMAEMA content of 5%. Consequently, the different effects on the bacterial growth, observed in the OD measurements, can be related to the presence/absence of surfactant or the charge density, respectively, and the concentration of the NP dispersions. Indeed, CTAC is a known biocide with a MIC_{100} within 3-5 µg mL^{-1} for *S. aureus* (MSSA476) as determined at the UKK and in accordance with the literature [177]. The standard miniemulsion protocol utilizes 5.2 mg mL^{-1} of CTAC which, even when reduced by dialysis of the samples, is supposedly higher than the MIC_{100} value. The observed growth retardation for the CTAC-

stabilized PS samples can therefore be attributed to the presence of the biocidal surfactant. Conversely, the bacteriostatic activity of the CTAC-stabilized copolymer NPs implies a combined biocidal effect of CTAC and the quaternary ammonium entities of the qDMAEMA comonomer.

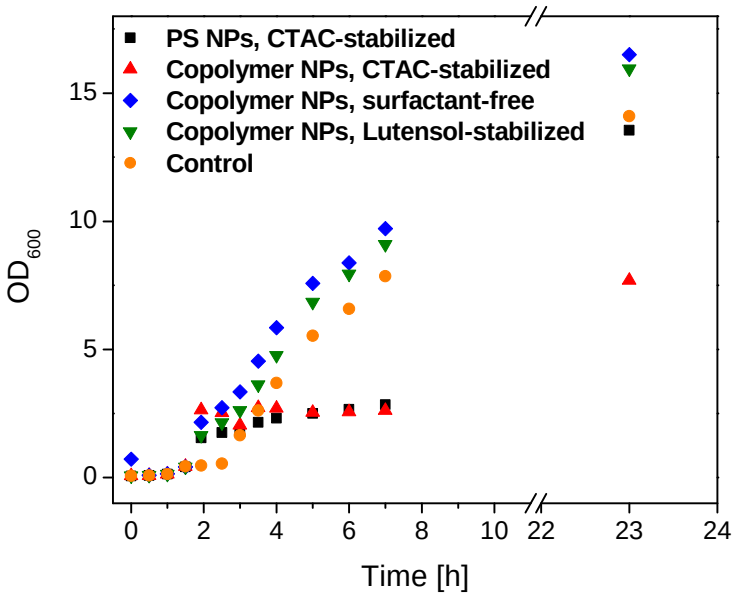

Fig. 20. Growth curve of *S. aureus*, incubated in TSB medium at 37 °C with differently stabilized PS-co-PqDMAEMA NP dispersions (0.5 mg mL^{-1}, 5% qDMAEMA), expressed by OD measurements at 600 nm over a time period of 24 h. NP-free media served as negative, pure PS NPs served as positive control [UKK].

Kügler et al. [197] found that the killing efficiency of *E. coli* and *S. Epidermidis* was strongly influenced by the number of positive charges on their surface-grafted, butyl-quarternized PVP surfaces. Consequently, they proposed the existence of a biocidal charge density threshold for polycations of 10^{13} N^+ cm^{-2} against *S. epidermidis* and 10^{13} N^+ cm^{-2} against *E. coli*, respectively. However, in a more recent study, Palermo et al. [15] observed that the membrane-lysing potential of cationic polymers appeared to be related to the interplay of hydrophilic and hydrophobic components - charged end groups versus the hydrophobic moieties. This indicates that the absolute number of cationic charges in the polymers do not uniquely determine the overall antimicrobial performance.

In the present system, the antimicrobial tests have been carried out in dispersion. Hence, apart from the balance of functional hydrophilic/hydrophobic moieties, the antimicrobial

performance is significantly dependent on the NP concentration. However, the OD measurements rely on the turbidity of the sample solutions. Therefore, in order to ensure an adequate contrast between the viable cell number and the NP suspensions, only NP concentrations lower than 0.5 mg mL^{-1} could be considered. On the other hand, OD measurements do not necessarily reflect the number of viable cells. More precise, dead bacteria could also contribute to the turbidity of the sample dispersion and thus falsify the growth curve. Therefore, future bacterial assays need to be optimized to allow for the investigation of a larger concentration range of NPs.

The question wether the copolymer NPs are able to induce any damage towards *S. aureus*, independently of the presence of biocidal CTAC molecules, cannot be answered easily. The concentration of the surfactant-free copolymer NPs might just have been too low to cause any detrimental effect under the experimental conditions studied. Yet, due to the increased viscosity of the NP dispersions in relation to higher comonomer contents (more than 8%), the amount of biocidal entities on the PS NP surface is limited by default when using miniemulsion copolymerization. The access to more densely functionalized NPs requires another route (3rd generation of materials, next chapter). Although the CTAC-stabilized NPs exerted bacteriostatic properties towards *S. aureus*, the ultimate aim of this approach is to discard any physically adsorbed surfactant.

5.2.2.3 Conclusions

The main concept of this approach was to synthesize novel, non-leaching bioactive NPs based on PS by introducing the multifunctional comonomer qDMAEMA, capable of stabilizing the colloidal system as well as providing biocidal quaternary ammonium moieties to the resulting NP surface. This has been achieved through copolymerization of both components in miniemulsion without additional stabilizing agents. Stable, surfactant-free PS-co-PqDMAEMA NPs were obtained with comonomer contents of 3-8% (w/w styrene) and compared to copolymer NP analogues, which were formulated under the additional stabilization of a cationic (CTAC) and non-ionic (Lutensol AT50) surfactant. Morphological analysis of the NPs by TEM revealed the presence of spherical shapes in the size range of 40-70 nm for all NP variations. Increasing comonomer contents within the surfactant-free NP series led to smaller NP sizes in analogy to surfactant-stabilized systems, thus emphasizing the stabilization potential of the qDMAEMA monomer. The presence of surface-oriented quaternary ammonium moieties for the surfactant-free NPs was confirmed by zeta potential

measurements. The bimodal molecular weight distributions observed for the copolymer latexes that were stabilized by the cationic surfactant may reflect the occurrence of secondary nucleation due to charge-repulsion between the comonomer and the surfactant. OD measurements of various copolymer NP dispersions in contact with *S. aureus* MSSA476 demonstrated bacteriostatic effects for CTAC-stabilized copolymer NPs as a result of the biocidal properties of CTAC. Conversely, the bacterial growth did not appear to be affected by the presence of surfactant-free copolymer NPs. Whether the inactivity of the surfactant-free NPs either results from an insufficient concentration or functional group density, or both, could not be distiniguished in the OD experiment due to the concentration limits set by the measuring technique. Thus, further optimization of the antimicrobial assays is needed. On the other hand, since the comonomer content it limited to 8% by the current polymerization method, an exploration of an alternate approach appears more favorable to maximize the amount of functional quaternary ammonium groups at the NP surface.

5.2.3 Synthesis and characterization of surfactant-free PqDMAEMA nanoparticles by combination of miniemulsion and solvent evaporation techniques (3rd generation of materials)

5.2.3.1 Synthesis and characterization of PqDMAEMA by radical polymerization

Cationic polyelectrolytes with quaternary nitrogen atoms can be synthesized by the polymerization of suitable monomers or by polymer analogous modification of an amine-functionalized polymer. The first method guarantees 100% functionalities, but often leads to characterization problems due to conformational changes of the polymer that depend on the ionic strength of the solution. The second method has the disadvantage of incomplete functionalization because of steric hindrance, especially when dealing with long alkyl chains [198]. Therefore, taking into account the alkyl chain length of 12 carbon atoms, the first method was selected to polymerize the qDMAEMA monomer in free radical polymerization.

Several protocols for the polymerization of qDMAEMA in various media (THF, water, ethanol) were tested and optimized. High monomer conversions after polymerization above the CMC of the monomer were observed by Hamid & Sherrington [199] and Nagai et al. [200] who postulated that the favorable thermodynamics of micelle formation could overcome charge repulsion. Since the water solubility of qDMAEMA is quite low, best yields were obtained from polymerization in THF and ethanol at 70 °C with AIBN as initiator.

Fig. 21 shows the ^{1}H-NMR spectra of the PqDMAEMA polymer, synthesized in ethanol. The pronounced absence of vinylic protons and characteristic broadening of all other signals outlines the successful polymer formation. Further characterization by TGA and DSC measurements revealed a degradation temperature around 200 °C and a melting domain of 110-130 °C, which is in accordance with the literature data [201]. The solubility of the polyelectrolyte is limited to polar organic solvents, in contrast to the monomer, which is additionally soluble in water. Only one batch was used for the subsequent NP formulation to ensure adequate reproducibility independently from the molecular weight distribution.

The solubility and structure formation of polyelectrolytes strongly depends on their acid/base strength, the charge density, the location of the charged sites (backbone or side groups), and the nature of the counterion [202]. Dissociation of the ionic groups depending on the ionic

strength of the solvent is to be expected. The intensive electrostatic interactions between all species disturb all methods of characterization. Yet, most of these effects can be suppressed by the addition of low-molecular weight salts to screen the electrostatic interactions [202]. Thus, a relatively narrow molecular weight distribution was obtained from SEC measurements under addition of high amounts of LiBr with a mean number average of molecular weight of M_n = 108 400 g mol^{-1} (DMF, PS standard) and a PDI of 1.95.

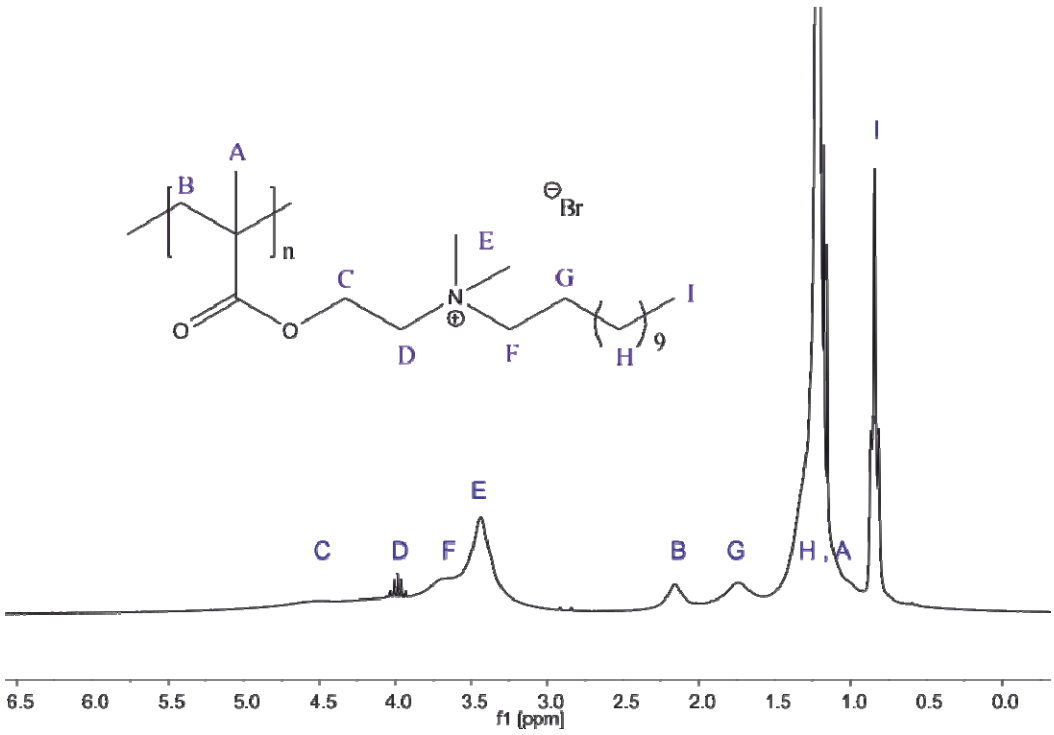

Fig. 21. ^{1}H-NMR (250 MHz, $CDCl_3$) of PqDMAEMA including structure and designated peaks.

The determination of the molecular weight proved to be quite challenging. Initial SEC measurements under variation of different parameters (solvent, column, salt addition) lead to unsatisfactory results or no signal at all, corroborating the aforementioned charge-mediated polymer-solvent-column material interactions in the literature. As concerns the final combination of solvent and column parameters, which yielded a reproducible signal, only PS standards were available. Because the solution properties of the polymer are affected by the salt concentration, thus altering the Kuhn-Mark-Houwink-Sakurada coefficients [203], a universal calibration could not be calculated for this system. Hence, the obtained value for the molecular weight is not accurate. In general, light scattering is the most frequently used technique to determine the molecular mass of polyelectrolytes. However, experiments require

a lot of care and the results have to be reviewed critically in the presence of aggregates larger than 100 nm. DLS experiments of PqDMAEMA in different solvents revealed the formation of numerous aggregates. Eventually, the implementation of further light scattering experiments was restrained because the presence of those aggregates would have influenced the quality of the measurement.

5.2.3.2 Synthesis and characterization of surfactant-free PqDMAEMA NPs by combination of miniemulsion and solvent evaporation techniques

The PqDMAEMA NPs were synthesized from the preformed homopolymer by combination of miniemulsion and solvent evaporation techniques. The 2-step concept of the homopolymerization and subsequent NP formation served several purposes. Firstly, because of its amphipathic structure, a transition from the qDMAEMA surfmer towards a PqDMAEMA "surfpolymer", which could act as potential stabilizing agent for its own NPs, was anticipated. This could allow for the generation of highly functional NPs devoid of any additional stabilization agent. Second, the polymerization was employed to transform a known biocidal homopolymer into polymeric NPs with expected biocidal activity. To this end, a given amount of PqDMAEMA was dissolved into chloroform, mixed with either water or an aqueous solution of CTAC and miniemulsified under ultrasonication as illustrated in Fig. 22. The excess of solvent in the preformed droplets was evaporated, which lead to the precipitation of the polyelectrolyte NPs. Additional PS NPs, which were stabilized with CTAC, were produced as control for the feasibility of the process, as well as antimicrobial control agent due to the biocidal properties of CTAC. In analogy to the previous approach (see section 5.2.2), the CTAC-stabilized polyelectrolyte NPs served as control particles to evaluate the colloidal stability of their surfactant-free analogues.

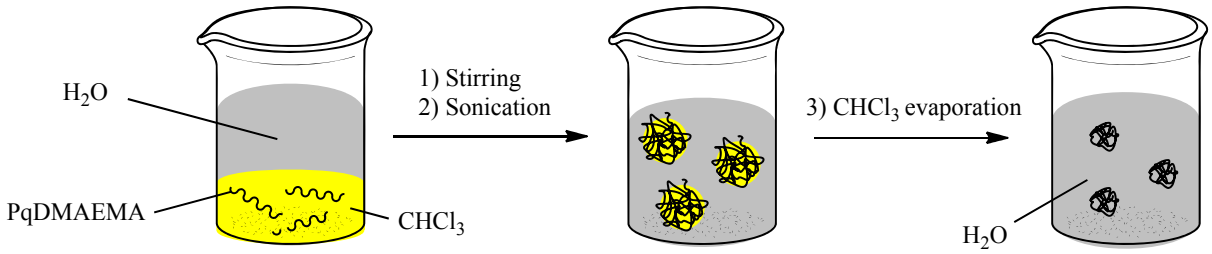

Fig. 22. Schematic representation of the formulation of surfactant-free PqDMAEMA NPs by combination of miniemulsion and solvent evaporation technique.

The process yielded polydisperse polyelectrolyte NPs in the size range of 200-400 nm as confirmed by DLS measurements and TEM. Fig. 23 shows the transmission electron micrographs of CTAC-stabilized PS control NPs as well as of various PqDMAEMA NPs, which were stabilized by different amounts of CTAC or synthesized without additional surfactant. In contrast to the spherical, much smaller PS NPs, the polyelectrolyte particles formulated from PqDMAEMA displayed a slightly angular shape. The similar images suggest that the NP size, shape and size distribution did not depend on the amount of stabilizer used.

The size and size distribution of latex particles obtained by emulsion/solvent evaporation can be influenced by many parameters such as the concentration, the molecular weight and PDI of the polymer, the solvent and the volume fraction of the solvent, the nature and the amount of employed stabilizer, and the homogenizer speed and evaporation time [49].

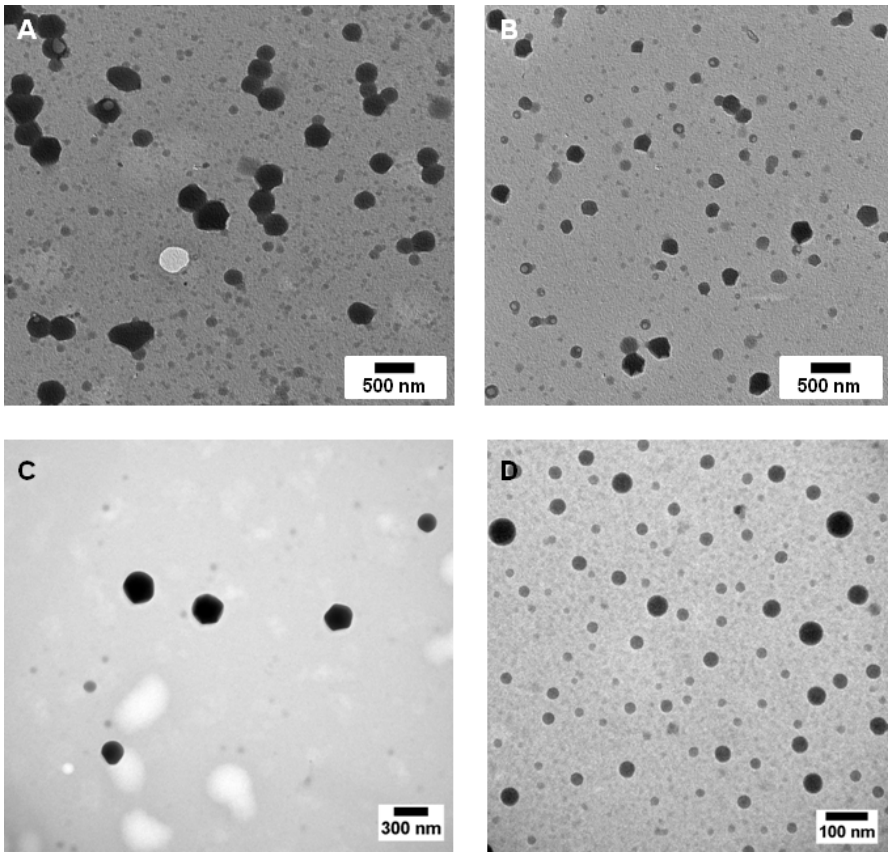

Fig. 23. Transmission electron micrograph of PqDMAEMA NPs stabilized by A) 42% (w/w polymer) CTAC, B) 17% CTAC, C) no surfactant. D) PS NPs stabilized by 42% CTAC.

Many of these parameters were investigated by Mistlberger et al. [204] for the synthesis of inorganic/polymeric magnetic nanosensors via miniemulsion/solvent evaporation. In this study, hybrid polymer NPs were obtained from four different polymers, including a copolymer of acrylic and methacrylic acid esters with approximately 10% of quaternary ammonium groups. One of their most critical findings showed that the PDI of the obtained NPs increased linearly if a certain threshold concentration of polymer was reached. In contrast, the PDI diminished drastically once a specific amount of emulsifier was used, which resulted in a moderate decrease of the particle size. Conversely, the PDI was little influenced by the volume of the organic phase and the type of polymer used. Furthermore, other studies demonstrated that the rate of homogenizer and evaporation as well as the molecular weight were less critical in their systems [83, 205]. In brief, polymer and emulsifier concentration appear to be the most crucial determinants for the polydispersity of the resulting latexes. In comparison, much lower polymer concentrations than the reported experimental threshold concentrations by Mistlberger et al. [204] were utilized in the present approach. Hence, it is reasonable to hypothesize that the polydispersity of the polylelectrolyte particles is not related to the polymer concentration at the experimental conditions studied.

Table 5 summarizes the characteristics of selected PqDMAEMA and PS NPs as measured by DLS, which were synthesized with various amounts of CTAC (0, 2.1 and 5.2 mg mL^{-1}). The borad size distributions of the polyelectrolyte NPs observed in TEM analysis were supported by the average particle sizes between 150 and 350 nm obtained from DLS. Similarly, no specific trends could be traced with regard to the particle size distribution although the amount of additional surfactant varied drastically from no surfactant at all to 42% of CTAC (w/w PqDMAEMA). These results indicate that the polydispersity of the PqDMAEMA particles does not significantly depend on the amount of cationic surfactant. In general, the precipitation of the NPs upon solvent evaporation is driven by hydrophobic effects. Considering the special case of a polyelectrolyte, secondary effects related to charge repulsion have to be taken into account. Zeta potential measurements confirmed the presence of positive charges on all NPs. Therefore, charge-mediated effects are very likely to be the source of the experimentally observed broad size distributions. For instance, charge repulsion between distinct polymer fragments could induce a budding effect to disengage smaller fragments and thus reduce the overall charge of a larger fragment in case of the surfactant-free NPs.

Secondly, upon addition of cationic surfactant, charge repulsion might encourage the separation of small, surfactant-stabilized NPs and larger surfactant-free particles.

Table 5. Effect of different amounts of CTAC on the average size of the solid polymeric NPs (PqDMAEMA and PS) as determined by DLS and ζ-potential measurements.

Sample name	Polymer	Surfactant		Size	ζ-Potential
		Type	Amount [%][1]	D_H [nm]	[mV]
VS70.1	PqDMAEMA	CTAC	42	143±18 319±46	+38
VS70.3	PqDMAEMA	CTAC	17	110±13 326±42	+31
VS78.1	PqDMAEMA	none	0	295±41	+36
VS72.5	PS	CTAC	42	68±9	+22

[1] w/w polymer

As concluded from the DLS data, the CTAC-stabilized PS NPs proved to be much smaller and less polydisperse than the corresponding PqDMAEMA NPs. As mentioned above, previous studies have demonstrated little influence of the type and molecular weight on the PDI of the resulting particles. Accordingly, the more homogeneous particle size distribution of the PS latexes is most probably due to favorable stabilization of the PS NPs by CTAC in the absence of charge repulsion and conformational changes in aqueous solution.

Finally, the surfactant-free colloidal dispersions of PqDMAEMA exhibited adequate colloidal stability for at least several weeks before showing any signs of flocculation. In comparison, the colloidal dispersions of CTAC-stabilized counterparts proved to be slightly more robust against coagulation (months). The zeta potential values in the range of +30 to +40 mV attest sufficient colloidal stability for the surfactant-free NPs as well as their surfactant-stabilized analogues. Furthermore, the positive values indicate the presence of surface-oriented quaternary ammonium groups.

In summary, the successful formation of polydisperse, functional polyelectrolyte NPs in the presence and absence of surfactants has been demonstrated. Although the colloidal stability of the polyelectrolyte NPs is slightly enhanced by the addition of stabilizing agents, the PqDMAEMA homopolymer has affirmed its potential as “surfpolymer” for the intrinsic stabilization of its NPs. With regard to their biocidal properties, the size distribution of the PqDMAEMA NPs is of minor importance as will be shown in the following chapters.

5.2.3.3 Investigation of the antimicrobial and cytotoxic properties of the PqDMAEMA NPs in vitro

The antimicrobial properties of the PqDMAEMA homopolymer and its corresponding NPs have been assessed in a modified version of a standardized testing method [206]. This assay was specially designed to evaluate the antimicrobial performance of surfaces. As a general approach, biocide-coated surfaces are inoculated with various bacteria and covered by a sterile foil to ensure constant contact without drying out the culture medium. After incubation at 37 °C for 24 h, the surfaces are thoroughly rinsed to remove any adhered species. The viable bacterial cells in the collected washings are then determined by a surface spread-plate method.

Generally, the assay allows a reliable evaluation of the surface interactions between the designed material and the pathogen since they are kept in close contact to each other. Yet, a reduced amount of colony forming units (CFUs) in the final step could potentially mask incomplete detachment of the bacteria during the rinsing process in case of a strong adhesion to the surface. However, the degree of adhesion can be determined by plating out aliquots of the supernatant at various time-intervals and comparing the resulting bacterial counts with the initial amount.

"Proof-of-concept": Antimicrobial activity of the PqDMAEMA homopolymer

The antifungal and antimicrobial activity of PqDMAEMA homopolymer against several bacterial strains has been demonstrated in the literature [181, 201]. Yet, due to the previously discussed complexity of bacteria-substratum interactions and individual attributes of each bacterial strain (see section 5.1.3), the antimicrobial activity of the PqDMAEMA homopolymer was analyzed for *P. aeruginosa* (PAO1) and *S. aureus* (MSSA476) strains, used in the following investigations.

The antimicrobial properties of the PqDMAEMA homopolymer against *S. aureus* (MSSA476) and *P. aeruginosa* (PAO1) was assessed in collaboration with the UKK. For this purpose, PS culture dishes were coated with ethanolic solutions of various polymer concentrations by spin-coating and subsequently analyzed. After sample processing according to the modified antibacterial assay, the surviving bacterial colonies were counted and used to calculate the mean CFUs per mL relative to the control, as summarized in Fig. 24. Inspection

of Fig. 24A reveals a killing efficiency against *S. aureus* of 99.97% for the 1.5% (w/v ethanol) films and 100% for higher PqDMAEMA concentrations. In contrast, as outlined in Fig. 24B, the CFUs of *P. aeruginosa* augmented significantly with respect to the control. Considering the high standard deviations at higher polymer concentrations (5, 10%), which result from a growth reduction between 0 – 100% in the raw data, the high number of CFUs can be explained by assuming a growth inhibition of the surface. Following a standard bacterial growth phase (see section 5.2.2.2), the bacteria on the control surface have most likely passed the stationary phase after 24 h of incubation. Therefore, their number is diminishing due to the lack of additional nutrients. In contrast, if we assume bacteriostatic properties of the polymer-coated surface, the initial lag phase will be retarded. By the end of the experiment, the bacteria should be at the end of their exponential growth phase and therefore show higher CFU compared to the control. In general, the presence of high standard deviations within the control samples of one experiment are relatively normal for a standard experiment because the initial bacterial count is only roughly adjusted to ~10^5 CFU mL^{-1}.

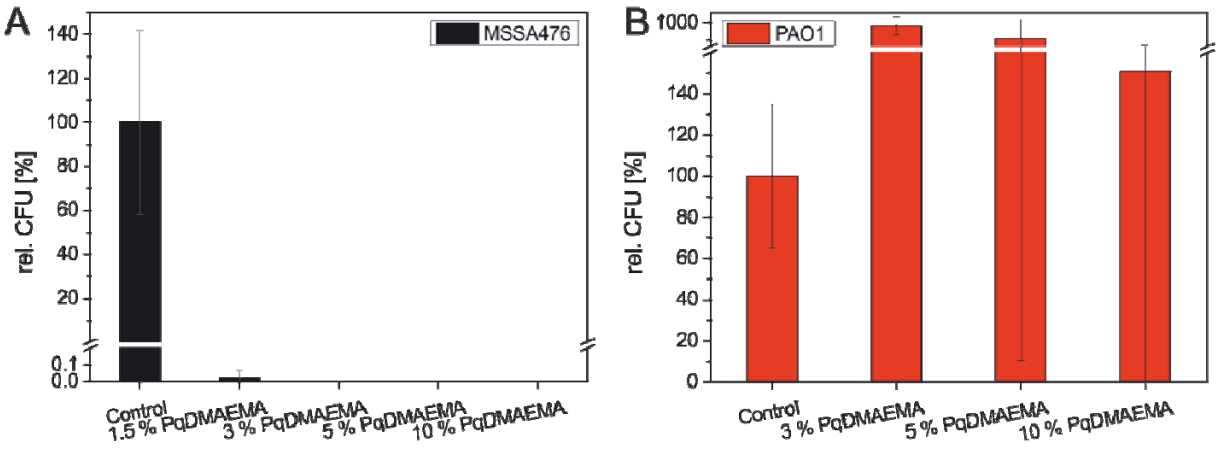

Fig. 24. The effect of PqDMAEMA homopolymer layers in different concentrations (0-10% w/v ethanol) on the growth of *S. aureus* (MSSA476) and *P. aeruginosa* (PAO1) expressed as relative colony forming units (CFUs) compared to the control [UKK].

Complementary studies were performed by staining the surfaces after 2 h of incubation with *S. aureus* at 37 °C with a specific dye that allows to differentiate between living and dead bacteria under the microscope. Yet, bacteria and the PqDMAEMA layers were equally stained, which prevented the formation of a visible fluorescent contrast between dead and viable species. Therefore, the surfaces were additionally characterized by optical microscopy.

Fig. 25 shows images of an uncoated (A) and coated petri dish (B), 2 h after inoculation with *S. aureus*. A bacterial lawn, visualized by the small punctual structures (CFUs), can be observed on the control surface (Fig. 25A). In this experiment, the polymer, which was dropcasted onto the activated culture dish, formed ring-like structures after drying. Closer examination of these rings suggested that the bacteria are concentrated outside, in the polymer-free interstice similar to results reported from Lu et al. [201]. Since the polymer is insoluble in water, it is very unlikely that it detaches from the surface as a result of the charge-mediated adhesion process on the plasma-activated culture dishes. Besides, soaking experiments of a previous study [181] did not show any visible delamination of PqDMAMEA films on culture dishes.

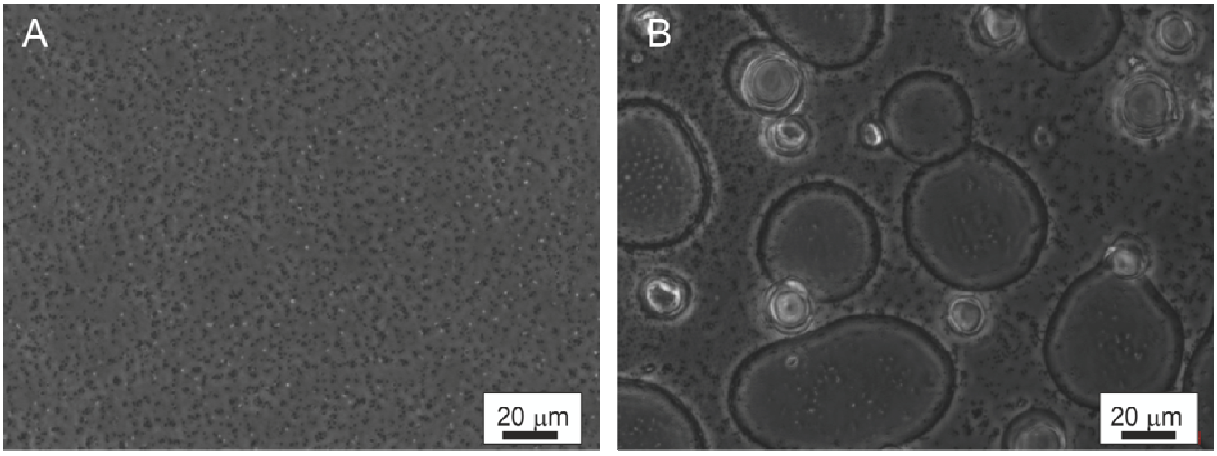

Fig. 25. Optical micrographs of (A) uncoated and PqDMAEMA-coated (B) (3%, w/v ethanol) petri dishes after 2 h of inoculation with *S. aureus* MSSA476 [UKK].

In conclusion, the "proof-of-concept" experiments have shown bactericidal properties of PqDMAEMA polymer films against *S. aureus* at relatively low concentrations. In accordance with the literature, the gram-negative strain *P. aeruginosa* has been less affected by the polyelectrolyte although punctual growth reductions were observed for distinct samples. Consequently, the following investigations of the PqDMAEMA were focused on *S. aureus* only.

"Proof-of-concept": Cytotoxicity of the PqDMAEMA homopolymer

To our knowledge, no reports are available in the literature about the cytotoxic properties of the PqDMAEMA homopolymer towards mammalian cells. Consequently, the cytotoxicity of

PqDMAEMA has been investigated in parallel to find out if its biocidal properties are selectively restricted to microorganisms only.

The cytotoxicity of the PqDMAEMA homopolymer against mammalian cells (NIH/3T3 Swiss mouse fibroblasts) was assessed in collaboration with the UKK. To this end, polymer-coated culture dishes were prepared in analogy to the antimicrobial tests. The NIH/3T3 cells were seeded onto the polymeric surfaces and incubated at 37 °C for 24 h in 5% CO_2. Fig. 26 outlines the successful attachment, spreading and viability of the cells on both, the uncoated control surface (A) and PqDMAMEA-coated surface (B). Although the image of the PqDMAEMA-coated surface indicates minor cluster formation of a few distinct cellular species, subsequent analysis according to the alamarBlue© staining assay ensured a significantly high viability of the cells in comparison to the control. The main component of this staining assay is the non-fluorescent dye resazurin. In metabolic active cell, resazurin will be reduced to its fluorescent form resofurin, thus indicating healthy cell proliferation.

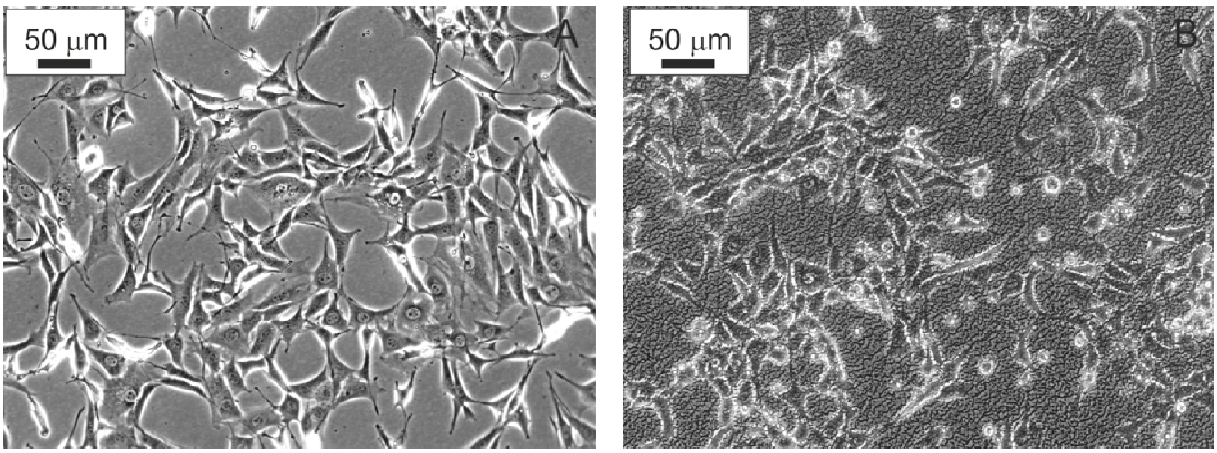

Fig. 26. Optical micrograph of NIH/3T3 Swiss mouse fibroblasts after 24 h of incubation on (A) uncoated and (B) 3% (w/v ethanol) PqDMAEMA-coated culture dishes [UKK].

Antimicrobial activity of the surfactant-free PqDMAEMA NPs

Microbiological training was provided at the UKK to investigate the antimicrobial properties of surfactant-free PqDMAEMA NP-coated surfaces according to the previously-mentioned modified standard assay [206]. The short and long-term antimicrobial tests against *S. aureus* (MSSA476) were conducted as follows: PS culture dishes were coated with 3% (w/w) of aqueous surfactant-free PqDMAEMA NP suspensions. Uncoated culture dishes and culture dishes coated with PS NPs, stabilized by different surfactants (CTAC, SDS), served as control. After sample processing according to the modified antibacterial assay, the surviving bacterial colonies were counted and used to calculate the number of surviving cells. Similarly, long-term studies over a period of up to 5 days were conducted on selected samples. In this experiment, the surfaces were inoculated with fresh cells every day after removing the previous supernatant for plating and determination of the viable cells. The results are summarized in Fig. 27.

Fig. 27A outlines the results of at least three different experiments after 24 h of incubation for different sample series of surfactant-free PqDMAEMA NPs. The number of viable cells is expressed as relative CFUs with respect to the control. As expected, bacterial suspensions incubated on the control surface showed a considerable bacterial growth including the usual fluctuation in the number of viable cells. In contrast, a $6\log_{10}$ reduction in CFUs of *S. aureus* was observed for the surfactant-free PqDMAEMA NP coatings, i.e. the absence of CFUs is indicative of 100% of bacterial cell death. Similar results, with a 99.99% killing efficiency were recorded for PS NPs, stabilized with CTAC. PS NPs, stabilized with SDS also exhibited antibacterial activity with a growth reduction of 61%, although high variations in the viable cell numbers occurred within the different experiments as reflected in the high standard deviation. Fig. 27B depicts the number of viable cells after 24 h of incubation in contact with selected PqDMAEMA and PS samples as compared to the control, in a total period of 5 days. The number of viable cells detected on the both sample surfaces is practically zero at all times. These results remarkably point out that both surfaces, coated with 3% (w/w) PqDMAEMA NPs and CTAC-stabilized PS NPs, were able to maintain their bactericidal potential for an extended period of 5 days.

Regarding the antimicrobial activity of the PqDMAEMA homopolymer, the antimicrobial activity of the corresponding NPs is to be expected. The novelty of the present system lies in

the demonstration of the biocidal activity of a surfactant-free and therefore non-leaching, colloidal approach. Their pronounced long-term toxicity with comparable efficiency to a common disinfectant (CTAC) denotes the potential of these highly functional polyelectrolyte NPs for biomedical applications such as implant coatings.

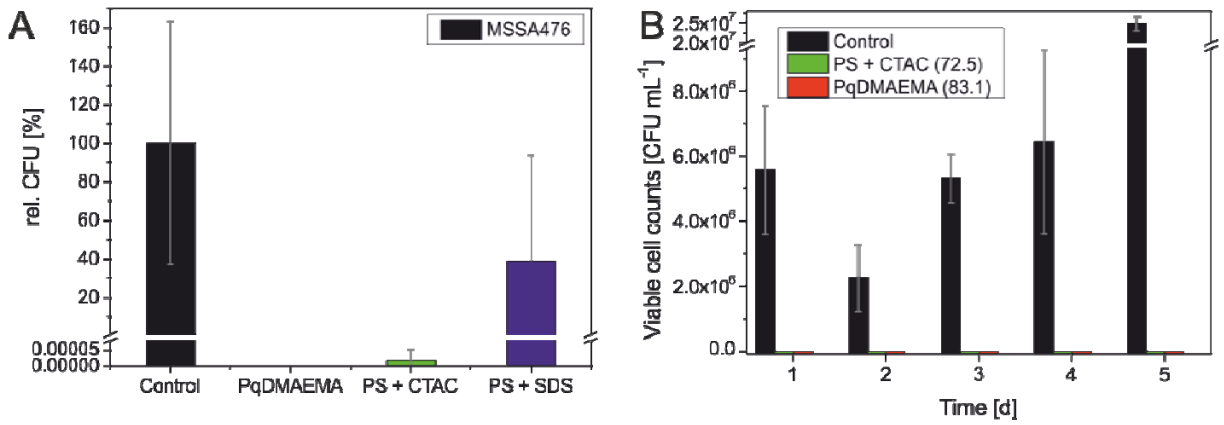

Fig. 27. (A) The effect of surfactant-free PqDMAEMA NPs and CTAC or SDS-stabilized PS NPs on the growth of *S. aureus* (MSSA476) after 24 h of incubation, expressed as relative CFUs in comparison to the control. (B) Long-term study of the effect of selected samples on the growth of *S. aureus* (MSSA476) presented by the number of viable cell counts [UKK].

The surfactant-stabilized PS NPs primarily served as positive control to show the effectiveness of the testing method. Both surfactants (CTAC and SDS) have been reported to induce membrane damage to prokaryotes and eukaryotes [176, 207]. The cationic surfactant CTAC, in clinical studies also known as cetrimonium chloride, and the more commonly used cetrimonium bromide (CTAB) are widely used as disinfectants in hospital environments with MICs against *S. aureus* ranging from 1 to 8 µg mL^{-1}, depending on the specific strain [196, 208, 209]. MIC measurements of aqueous CTAC-solutions in the presence of MSSA476 displayed an MIC_{100} between 2-3 µg mL^{-1} (Fig. 28), which is in good agreement with the value of 2 µg mL^{-1} reported by Tiller et al. [177]. The PS NPs were stabilized with an initial concentration of 3.1 mg mL^{-1} of CTAC, which exceeds the MIC by 10 orders of magnitude. The results of the antimicrobial experiments imply that even after dialysis, the concentration of CTAC is sufficiently above its MIC. As mentioned before and confirmed by additional MIC measurements, the gram-negative bacteria *P. aeruginosa* is less affected by the cationic surfactant.

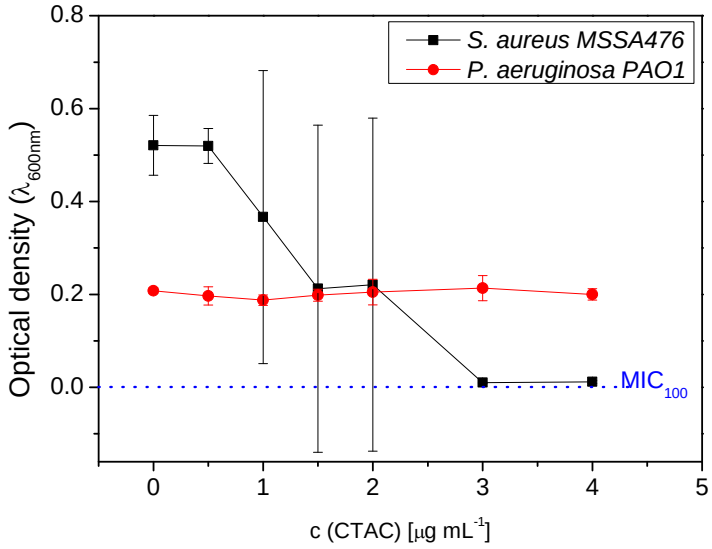

Fig. 28. Minimal inhibitory concentrations (MIC) of aqueous CTAC-solutions in the presence of *S. aureus* (MSSA476) and *P. aeruginosa* (PAO1) [UKK].

Due to its insolubility in water and DMSO, the actual MIC of the PqDMAEMA NPs could not be determined in solution. Therefore, the antibacterial activity of the surfactant-free PqDMAEMA NPs and CTAC-stabilized PS NPs is not directly comparable. Alternatively, the number of charges per particle of both NPs could be compared. But, due to the polydispersity of the PqDMAEMA NPs, the determination of the amount of N^+ equivalents would only give a meaningless average value of charges per particle including a high standard deviation. However, as mentioned before, recent advances on highlighting the antimicrobial mechanism of cactionic polymers suggest that the biocidal activity should not be quantified by the charge density only [15]. Instead, the overall performance of those polymers appears to be governed by the interplay of cationic and hydrophobic groups. Thus, CTAC-stabilized PS NPs can only provide a qualitative picture on the effectiveness of our system.

Cytotoxicity of the surfactant-free PqDMAEMA NPs

The evaluation of the cytotoxic behavior of PqDMAEMA NPs and CTAC-stabilized PS NPs was performed in collaboration with the UKK. For the fluorescence intensity measurements, the resafurin-stained NIH/3T3 Swiss mouse fibroblasts were harvested from NP-coated surfaces after 24 h and 5 d respectively, in separate experiments. The test was carried out 4 times for each parameter. Uncoated culture dishes served as control. The results are

summarized in Fig. 29. The analysis of the fluorescent intensity depicted a slight decrease in the number of viable cells in similar levels for the surfactant-free PqDMAEMA NPs coatings as well as for the CTAC-stabilized PS NPs after 24 h of incubation. In contrast, after 5 days of incubation, the number of viable cells on the PqDMAEMA surface was reduced by $2\log_{10}$ units, whereas no viable cells could be detected on the CTAC-stabilized PS NPs. These numbers indicate moderate cytotoxic properties for the surfactant-free PqDMAEMA NPs to high cytotoxicity caused by the CTAC stabilized PS NPs.

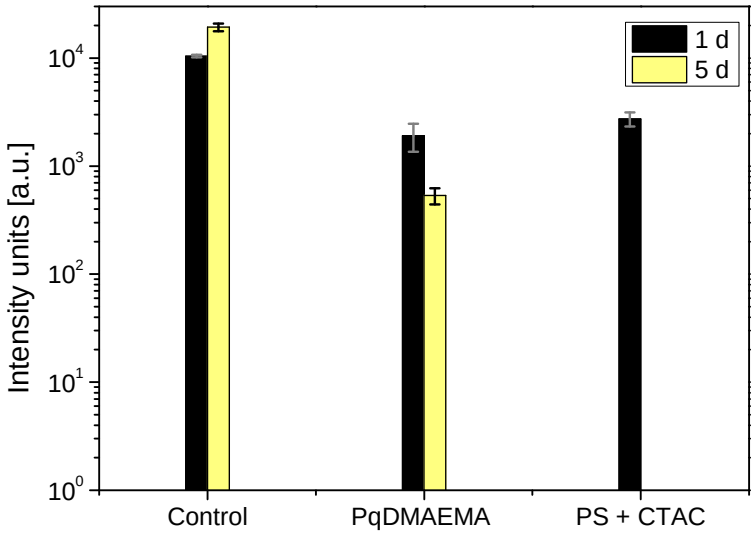

Fig. 29 Fluorescent intensity signal of stained mouse fibroblasts (NIH/3T3) which were harvested from NP coated surfaces after 24 h and 5 days of incubation. The surfaces were coated with different samples of 3% (w/w) surfactant-free PqDMAEMA NPs (78.2, 83.1) and CTAC-stabilized PS NPs (72.5). [UKK].

For more detailed information, the cell morphology was documented by light microscopy as outlined in Fig. 30. The micrographs taken after 24 h revealed a healthy attachment and spreading on the control (A) and in a decreased measure also on the PqDMAEMA NPs surface (B). Although, the fluorometric assay displayed a similarly high viability of the cells in contact with CTAC-stabilized PS NPs, the microscopic images clearly depicted cluster formation (C), indicative of restricted proliferation. The microscopic documentation of the cell morphology after 5 days of incubation looked quite different (D-F). In comparison to the control surface, the cells on the PqDMAEMA surfaces did not show healthy proliferation, but

some of them appeared to have grown into the surface (E). In contrast, no living cells could be observed on the CTAC-stabilized PS surface (F).

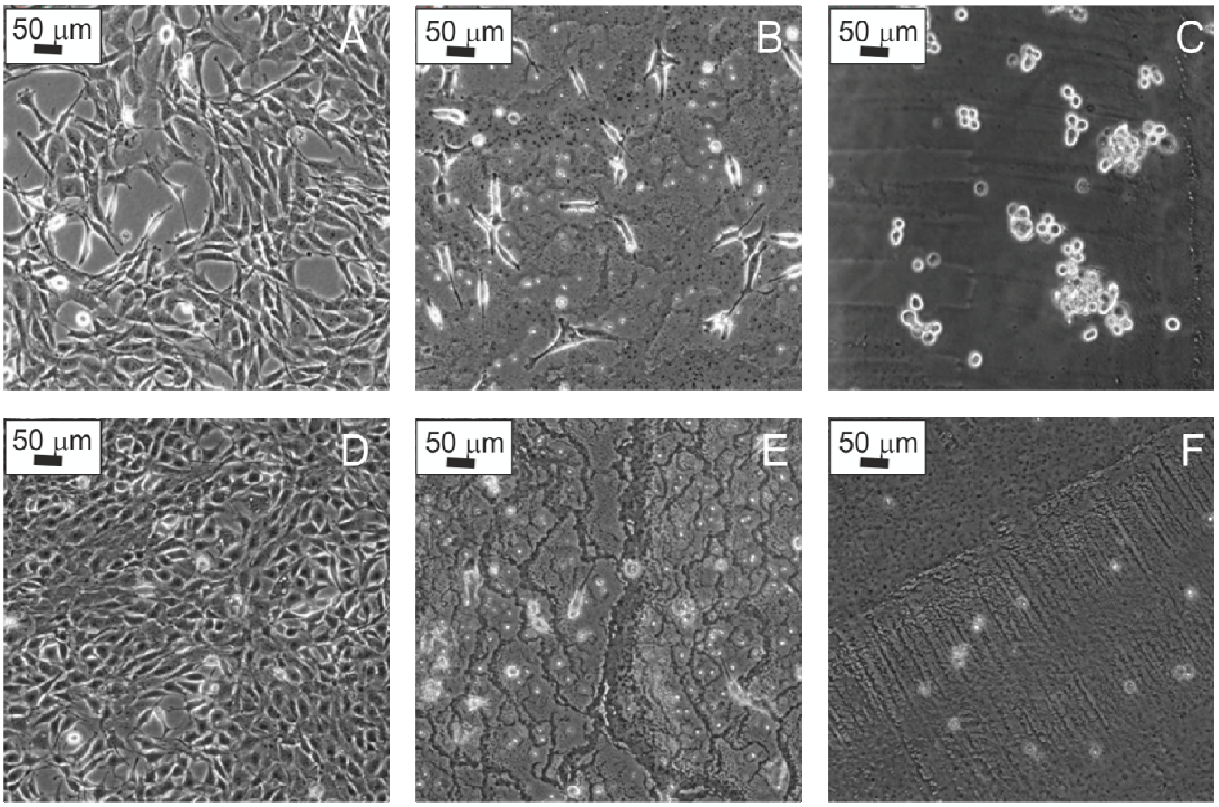

Fig. 30. NIH/3T3 Swiss mouse fibroblasts cultivated on (A, D) uncoated, (B, E) PqDMAEMA NPs-coated and (C,F) CTAC-stabilized PS NPs-coated surfaces after 24 h (A-C) and 5 d (D-F) of incubation [UKK].

The combined results of the fluorometric and microscopic investigation indicate that the surfactant-free PqDMAEMA NPs coatings exhibit short-term non-cytotoxic properties to moderate cytotoxic properties after an extended period of 5 days at bactericidal concentration levels. In this light, an important insight has been provided by the complementary microcopic characterization of the cell morphology. Although, the fluorometric assay displayed a high level of viability for both NPs after 24 h, the micrographs clearly outlined healthy proliferation features for the PqDMAEMA NPs only, in contrast to cluster formation on the PS NP surfaces. Yet, for the fluorescent assays, the cells could only be detached from the PqDMAEMA NPs surface with some difficulties. The possibility of the cells to grow in or under the surface, respectively, or to form a strong junction with the PqDMAEMA surface cannot be excluded. Taking this into account, the lack of proliferation after 5 days may reflect the inability of those attached cells to retrieve nutrients, which might not have been able to

diffuse into the intercalated cells. The cytotoxic properties of the CTAC-stabilized PS NPs are not surprising considering that the initial concentration of CTAC (3.1 mg mL^{-1}) exceeds its MIC against *S. aureus*.

The differences in the cell wall structure of prokaryotes and eukaryotes generally afford a gap between bactericidal and cytotoxic behavior of the majority of antimicrobials. The bandwith of selective toxicity towards both species determines the quality of any antimicrobial agent. Comparing both antimicrobial and cytotoxic experiments, the results have demonstrated a selective toxicity of the PqDMAEMA NP-coated surfaces towards *S. aureus*. While maintaining bactericidal properties for 5 days, the PqDMAEMA NP-coated surfaces exerted only moderate cytotoxic behavior on the long term, thus qualifying them as potential candidates for biomedical applications. Although the selectivity between both species is not outstanding, the colloidal PqDMAEMA provide a suitable antimicrobial prototype for further optimization.

Since the CTAC-stabilized PS NPs were primarily used as qualitative control to validate the feasibility of the antimicrobial tests, their selectivity has not been probed. The determination of their therapeutic values, i.e. the ratio of antimicrobial dose to cytotoxic dose, requires further investigation of PS NPs with different concentrations of CTAC, which was not the focus of this study.

5.2.3.4 Conclusions

A biocidal, surfactant-free and thus non-leaching colloidal system was developed based on highly functional polyelectrolyte NPs with quaternary ammonium moieties. The surfactant-free as well as CTAC-stabilized NPs were formulated by miniemulsion and solvent evaporation of the previously synthesized PqDMAEMA polyelectrolyte. Thus, angular-shaped polyelectrolyte latex particles of 200-400 nm in size were obtained. The relatively large size distribution was attributed to charge-mediated effects within the cationic chains. Zeta potential measurements of the surfactant-free PqDMAEMA NPs confirmed the presence of surface-oriented quaternary ammonium groups. As compared to their CTAC-stabilized analogues, the surfactant-free NPs demonstrated adequate colloidal stability for several weeks, evidencing the surface-active and consecutive autostabilization potential of the PqDMAEMA homopolymer. Different protocols were applied to analyze the bacterial and cellular growth of mammalian cells on the surfactant-free PqDMAEMA NPs in collaboration

with the UKK. Self-assembly of the 3% (w/w, water phase) colloidal PqDMAEMA on adequate substrates lead to engineered surfaces that exhibited bactericidal properties against *S. aureus* (MSSA476) for a period of up to five days. Short-term interactions of the PqDMAEMA NPs with mammalian cells within 24 h permitted attachment and proliferation, while moderate cytotoxic effects could be observed after long-term studies of 5 days. The differential toxic response towards prokaryotes and eukaryotes designates a promising potential for the PqDMAEMA NPs as novel colloidal, contact-active antimicrobials and provides a suitable platform for further optimization.

5.3 Contact-active leaching surfaces based on inorganic/polymer nanocomposites

5.3.1 State-of-the-art

Inorganic nanoparticles (NPs) have shown great potential in the biomedical sector due to their unique optical, catalytical and antimicrobial properties [210-212]. Compared to organic agents, inorganic antibacterial materials such as metal oxides have the key advantage of improved durability and stability, particularly at high temperature or pressure conditions which are used in sterilization processes [99].

The most studied broad-spectrum antibiotic is silver [213], which has a long history of antiseptic applications related to the treatment of burn wounds. Silver NP-impregnated products such as wound dressings, textile fabrics and catheters have rapidly conquered the market [33, 214]. However, there have been concerns about dose-related nanotoxicity towards healthy tissue [215] and the uncontrolled release of silver ions into the environment [216]. Yet, other inorganic NPs have shown efficient antibiotic properties. These include gold [217], copper and CuO [218-220], TiO_2 [35, 221], MgO [222], and ZnO [10]. Nanosized ZnO is of particular interest due to its comparably modest cost and its established use in cosmetic dermatology [223] in combination with numerous technological applications as (photo)catalyst, gas sensor, semiconductor, field-emission display, and UV-shielding material, to name a few [224, 225]. Recently, several studies have demonstrated quite efficient antimicrobial activity of ZnO NPs against gram-positive and gram-negative bacteria [36, 226-230]. Based on some pioneering work of Sawai and coworkers [45], subsequent studies have independently shown that the antimicrobial action is clearly governed by the NP size and corresponding large specific surface area respectively, and possibly by light activation as well as the nature of the capping agent used [229, 231-233].

Several mechanisms of antibacterial action have been proposed based on the reaction of ZnO with water to generate either reactive oxygen species (ROS) or free zinc ions and labile zinc complexes. Both processes supposedly lead to harmful interactions with the bacterial cell membrane due to oxidative or osmotic stress [234, 235]. Complementary TEM investigations by Applerot et al. demonstrated an increased cellular internalization and subsequent cell

damage depending on the NP size [37]. Nevertheless, the exact interplay between microorganism and nanomaterial is still not completely understood.

Controversial reports can be found concerning the nanotoxicity of nanoscale ZnO towards healthy tissue [227, 236-238]. However, various sizes of the NPs, capping agents, media and assays employed, make it difficult to correlate and trace a general trend in the structure-property relation, thoroughly suggesting the necessity for a case-to-case study. In particular, the choice of surfactant has been shown to affect the NP properties considerably, especially when using membrane-lysing agents such as SDS, CTAC or CTAB [239-241]. Uniform ZnO nanocrystals with a controlled particle size can be produced by sol-gel methods [99, 242]. Yet, owing to their high surface-to-volume ratio, pristine nanoscale ZnO generally displays poor colloidal stability in aqueous media. On the other hand, colloidal stability is mandatory for biomedical applications and can be achieved in different ways i.e. by using suitable polymeric surfactants [243] or by incorporating the ZnO NPs into an appropriate matrix. The matrix covers any kind of system from polymeric brushes, biomolecules, mesoporous inorganic materials, colloidal systems or fibers [113, 244].

In the following chapter, two different approaches of transferring ZnO NPs into a suitable template for biomedical applications will be presented. The first approach comprises the formulation of novel, colloid-based hybrid nanocapsules which are composed of a ZnO core within a poly(L)-lactide (PLLA) NP shell (4^{th} generation of materials). PLLA is one of the most intensively investigated biocompatible and biodegradable materials for drug delivery [245, 246]. Currently, PLLA and its various derivatives (e.g. PLGA (poly(lactid-co-glycolic acid)) are being used in numerous surgical devices such as resorbable sutures, screws and stents [247-249] as well as scaffolds in bone tissue engineering [250]. Additionally, the fabrication of hybrid inorganic/PLLA composite materials including filler material of hydroxyapatite, TiO_2, MgO and SiO_2 has been widely explored for structural reinforcement and cell attachment [251]. Several approaches have been reported to encapsulate silver NPs [252] or antibiotics [253] into PLLA or PLLA-based nanoparticles. Yet, the combination of ZnO NPs and PLLA in the context of biomedical applications is new and to our knowledge has not been reported in the literature. The selected approach aims at the beneficial exploration of the combined properties of biocompatibility and biodegradability for PLLA and photocatalysis and biocidal characteristics of ZnO, i.e. photoactivating ZnO to catalyze

the degradation of PLLA and thereby trigger the release of ZnO to exploit its antimicrobial potential.

The second approach involves the incorporation of ZnO NPs into a poly(*N*-isopropylacrylamide) (PNIPAAm) hydrogel layer to generate novel antimicrobial nanocomposite thin film surfaces (5^{th} generation of materials). Hydrogel surface coatings have been extensively used as support or protecting layer in food packaging [254] and tissue engineering [255-258]. Other important applied fields of hydrogels, described in the literature, are surface coatings for biocompatibilization, anti-fouling properties [259] and lubrication of implants, stents and other medical devices, wound dressings, and controlled release in drug delivery [260-262]. The combination of inorganic NPs and hydrogel networks has already led to the generation of new composite materials where the hydrogel matrix can benefit from the physical (mechanic, magnetic, optical, conducting, catalytic) and biomedical (antimicrobial, anticancer) properties of the embedded NPs with unprecedented applications in biotechnology [122]. Yet, to our knowledge, the presented orginial combination of both bioactive components has not been explored to date. As concerns the PNIPAAm hydrogel, the focus of this study was set on using it as biocompatible reservoir for the ZnO NPs independently of its thermoresponsive properties, which have already been well characterized in the literature [146, 263, 264].

5.3.2 Synthesis and characterization of ZnO nanocrystals

The ZnO NPs were synthesized via high-temperature decomposition of zinc acetylacetonate in a binary surfactants medium, namely oleylamine and oleic acid. The high temperature process induces nucleation and permits a controlled growth of the resulting ZnO nanocrystals [99]. Owing to their hydrophobic organic coating, the ZnO NPs display a good dispersibility and long-term stability (at least several months) in non-polar solvents (e.g. chloroform).

The transmission electron micrograph in Fig. 31A shows the angular, slightly anistropic morphology of the ZnO NPs in a rather homogeneous size distribution of the sample with an average particle size of 23±3 nm as determined by particle analysis from TEM images (Fig. 31C). The size range of the ZnO NPs was intentionally adjusted to be much smaller than 100 nm to ensure successful encapsulation into PLLA and incorporation into the PNIPAAm surface layer, respectively. HRTEM investigations of distinct NPs confirmed their single

crystalline structure (Fig. 31B) as can be observed from the lattice-fringes and the corresponding fourier transform patterns (inset) which are characteristic of the Wurtzite structure of bulk ZnO. The nanocrystalline character of ZnO was also confirmed by complementary X-ray powder diffraction (XRD) measurements (Fig. 31D). Indeed, the distinct fine reflections, which correspond well to the Bragg reflections of the standard Wurtzite structure, indicate the ultrafine nature of the crystallites (hexagonal phase, space group: $P6_3mc$, with lattice constants $a = b = 3.249$ Å, $c = 5.206$ Å, JCPDS, Card No. 36-1451).

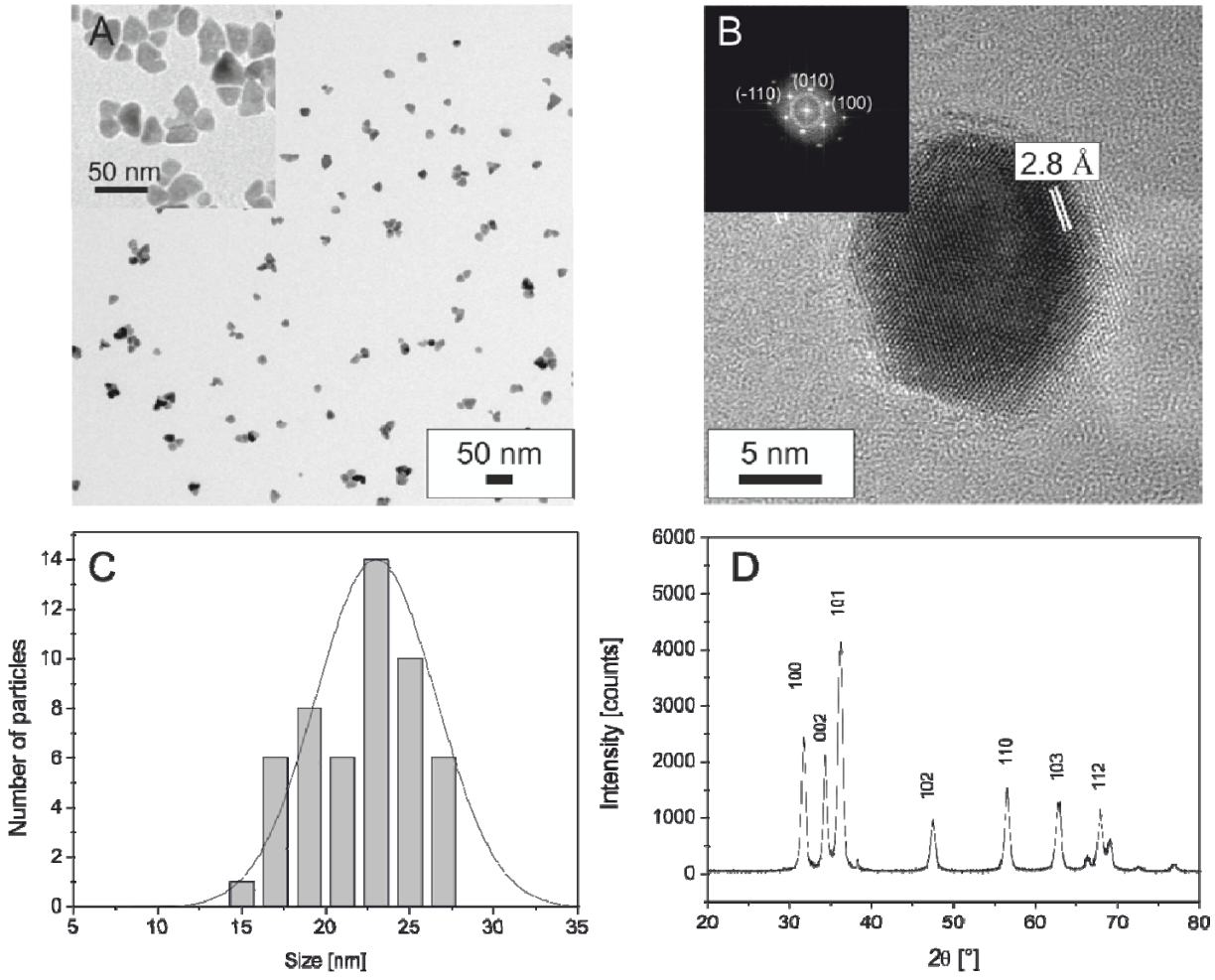

Fig. 31. (A) Transmission electron micrograph of ZnO NPs. Inset: higher magnification. (B) Lattice-fringes HRTEM micrograph of a distinct ZnO nanocrystal. Inset: corresponding fourier transform pattern confirming the single crystalline character of the material, which corresponds well to the Wurtzite structure of bulk ZnO (hexagonal phase, space group: $P6_3mc$, with lattice constants $a = b = 3.253$ Å, c=5.213 Å, JCPDS, Card No. 76-704). (C) Particle size distribution of 23±3 nm, as determined by particle counts from TEM images (Gaussian fit). (D) X-ray powder diffraction pattern of the ZnO NPs with marked indexations of the reflections according to the Wurtzite structure from the JCPDS database.

5.3.3 Synthesis of novel nanocomposite colloidal ZnO/PLLA nanoparticles via miniemulsion/solvent evaporation (4th generation of materials)

Biodegradable ZnO/PLLA nanocomposite particles were formulated from the preformed components via combined miniemulsion and solvent evaporation methods as illustrated in Fig. 32. To this end, a given amount of commercially available PLLA was dissolved in ZnO/chloroform dispersion, mixed with an aqueous solution of SDS and miniemulsified under ultrasonication. The excess of solvent in the preformed droplets was evaporated, which lead to the precipitation of polymer and formation of the hybrid polymeric NPs. Since the size and size distribution of latex particles obtained by emulsion/solvent evaporation methods can be influenced by many parameters (see section 5.2.3.2), the initial protocol was inspired from previously published data within our group [84, 265] with respect to the amount of polymer and surfactant used. The hydrophobic coating of the ZnO NPs ensured a good compatibility of all components within the dispersed phase (ZnO, PLLA, chloroform). Therefore, prior to combining aqueous and organic phase, the latter was subjected to short intervals of sonication to ensure a homogeneous distribution of ZnO within the PLLA/chloroform solution. Control samples of pure PLLA and SDS-dispersed ZnO were formulated the same way. The ZnO content was adjusted to a maximum of 14% (w/w) with respect to the polymer, which corresponds to a ZnO concentration of 1.75 mg mL^{-1} in water. The amount of ZnO was limited by the concentrations of the initial ZnO NP dispersions since the NPs were stored in chloroform to prevent coagulation.

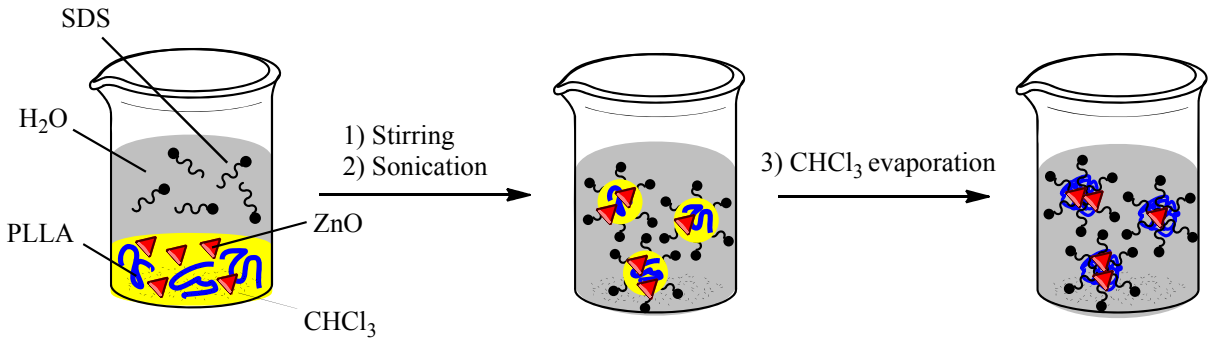

Fig. 32. Schematic presentation of the ZnO/PLLA nanocomposite particle formulation by miniemulsion and solvent evaporation methods.

Morphology and size distribution of the resulting hybrid NPs were characterized by TEM and DLS, which exhibited spherical, uniform nanocomposite particles in the range of 160-230 nm. The transmission electron micrographs in Fig. 33 image selected samples of SDS-dispersed ZnO (A), ZnO/PLLA nanocomposite particles (B) and pure PLLA particles (C). Inspection of Fig. 33B reveals the presence uniform PLLA spheres with a diameter of ~180 nm and darker, much smaller structures of ZnO NPs. The ZnO NPs are remarkably well dispersed in the polymer matrix and do not show any pronounced agglomeration. Furthermore, the TEM investigations indicate that the majority of the ZnO is associated to PLLA polymer because very few traces of free, non-bound ZnO NPs or NP agglomerates could be observed. Yet, although the images tend to suggest a ZnO@PLLA core-shell structure, it is not possible to clarify at this stage of the investigations if the ZnO NPs are located on the outer surface or encapsulated within the polymer. In contrast to the composite latexes, the similarly uniform spheres obtained from the pristine PLLA NPs (C) appear quite bare. Interestingly, upon miniemulsification the pure ZnO NPs formed SDS-stabilized spherical, cauliflower-like clusters of ~100 nm in water (Fig. 33A). The clusters precipitated after a couple of days, confirming the instability of neat ZnO in aqueous media. In addition to the nanocomposite latexes of ~180 nm, more detailed TEM investigations of various nanocomposite samples revealed the presence of much smaller, pure PLLA NPs in the size range of 100 nm or below. Therefore, it appears that the encapsulation process requires a certain threshold polymer size of about 180 nm under the present experimental conditions.

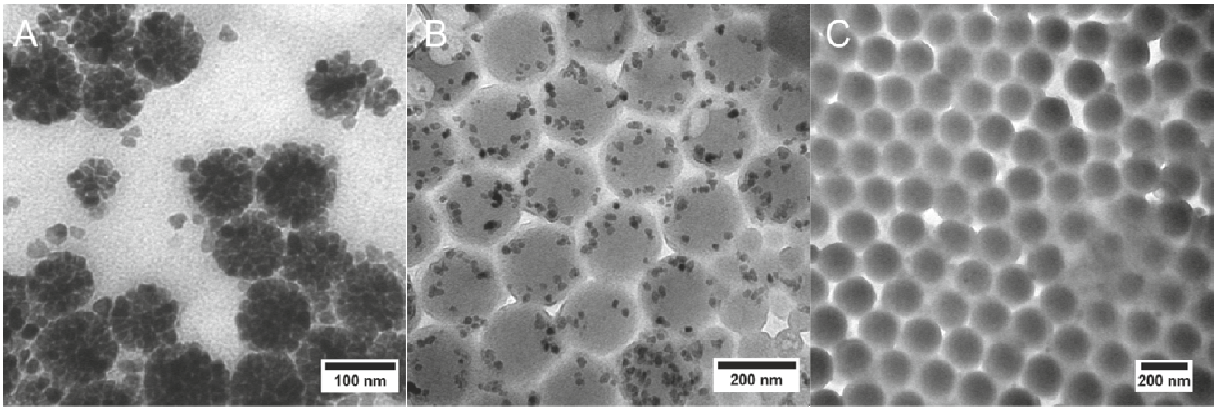

Fig. 33. Transmission electron micrograph of unpurified (A) SDS-stabilized ZnO NPs clusters, (B) ZnO/PLLA nanocomposite particles, (C) pure PLLA NPs.

The observations on the TEM images raise several questions in the context of (*i*) the location of the ZnO NPs: Have they been encapsulated inside of the polymer or did they precipitate on the outer PLLA surface? (*ii*) What is the encapsulation efficiency?

To clarify the first question, SEM studies were performed on samples of native ZnO, ZnO/PLLA nanocomposite particles and pure PLLA NPs. The pictures of purified and unpurified composite and pure PLLA NPs are presented in Fig. 34. The first image (Fig. 34A) displays the unpurified hybrid NPs, which correspond to the particles seen on the transmission electron micrograph in Fig. 33B. Close examination of the surface of the PLLA spheres shows that they are covered in a raspberry-like fashion with ZnO NPs. A similar surface coverage of ZnO NPs on PLLA was observed for the purified sample (Fig. 34B) although it appears that the surface coverage is lower. The inset shows the corresponding TEM image, which was not listed in Fig. 33. Compared to the surface of the nanocomposite samples, the surface of the pristine PLLA NPs (Fig. 34C) is very smooth. A few spherical PLLA NPs can be observed to occupy the interstices between larger PLLA NPs but they can be clearly distinguished from the ZnO surface coverage of the composite particles. Whereas the SEM investigations demonstrate a raspberry-like ZnO surface coverage of the PLLA latex, the TEM images (Fig. 33B, inset of Fig. 34B) rather denote the encapsulation of ZnO into PLLA. Taken together, both TEM and SEM investigations strongly indicate a „ZnO@PLLA@ZnO“ core-shell-shell geometry of the nanocomposite particles with ZnO simultaneously located inside and on the outer surface of the PLLA NPs. Hence, it also offers a logical explanation for the apparent difference in surface coverage of purified and unpurified hybrid latexes. The purification step, which involves the centrifugation of the composite samples at low rotational speed (2000 rpm), is intended to remove potential non-encapsulated inorganic material due to its higher density compared to the inorganic/polymer hybrid latexes. During the NP formation upon chloroform evaporation of the miniemulsified nanodroplets, the driving force for the phase separation within the water phase solely stems from the hydrophobicity of both components (ZnO, PLLA). Thus, the SEM investigations tend to prove that the purification step partially removes surface-adhered ZnO NPs since there is no obvious covalent linking between the ZnO nanostructures and PLLA. Consequently, the purification process leads to ZnO@PLLA core-shell NPs.

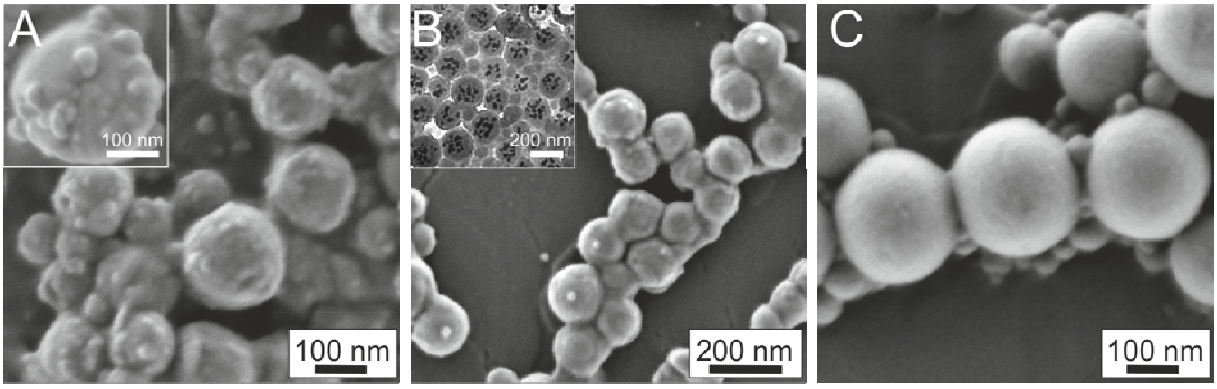

Fig. 34. Scanning electron micrographs of (A) unpurified ZnO/PLLA nanocomposite particles (inset: higher magnification of a selected NP) (B) purified ZnO/PLLA nanocomposite particles (inset: corresponding TEM micrograph) and (C) pure PLLA NPs. Samples (A) and (B) represent the corresponding SEM images of the TEM micrographs (B) and (C) in Fig. 32.

Several examples of colloidal ZnO/polymer (PS, PMMA) hybrids can be found in the literature. For example, Liu et al. [266] fabricated ZnO@PS core-shell NPs by microemulsion polymerization. In their work, the oleic acid-stabilized ZnO NPs were mixed with the monomer solution and integrated into the polymeric network by partial linkage between the double bond of oleic acid and styrene during the polymerization process. Tang et al. [267] reported the successful encapsulation of ZnO into polymeric NPs of styrene and butylcyanoacrylate by miniemulsion polymerization, using 3-aminopropyltriethoxysilane (APTES)-capped ZnO to increase the monomer compatibility. In another study, Agrawal et al. demonstrated the fabrication of PS@ZnO colloidal nanocomposites [268]. ZnO was reduced *in situ* on the surface of seed PS latexes, which were functionalized with small amounts of the zinc complexing agent acetoacetoxyethyl methacrylate (AAEM).

In contrast to those literature examples, the convenience and novelty of the presented ZnO/PLLA system lies in the combination of the biocompatibility of PLLA as opposed to other polymers (PS, PMMA), and the possibility to trigger the release of ZnO via an enhanced photocatalytic degradation of PLLA as will be shown later.

5.3.3.1 Determination of the encapsulation efficiency of ZnO

The encapsulation efficiency of ZnO into PLLA nanoparticles was determined by TGA as well as ICP-OES. The TGA curves of SDS-stabilized ZnO, unpurified and purified ZnO/PLLA nanocomposite particles and pure PLLA are presented in Fig. 35. As the temperature increases, a weight loss resulting from the decomposition of the organic

components (oleic acid, PLLA) is observed for all samples. Pure ZnO shows a 2-step degradation with a higher weight loss between 200-300 °C, related to the decomposition of oleic acid and oleylamine [269] and a smaller decay between 500-600 °C, which most probably includes the desorption of refractory organic residues. On the other hand, the decomposition of PLLA occurs in the range of 200-330 °C due to the degasification of water and surfactant molecules [265] with a final weight residue of 9%.

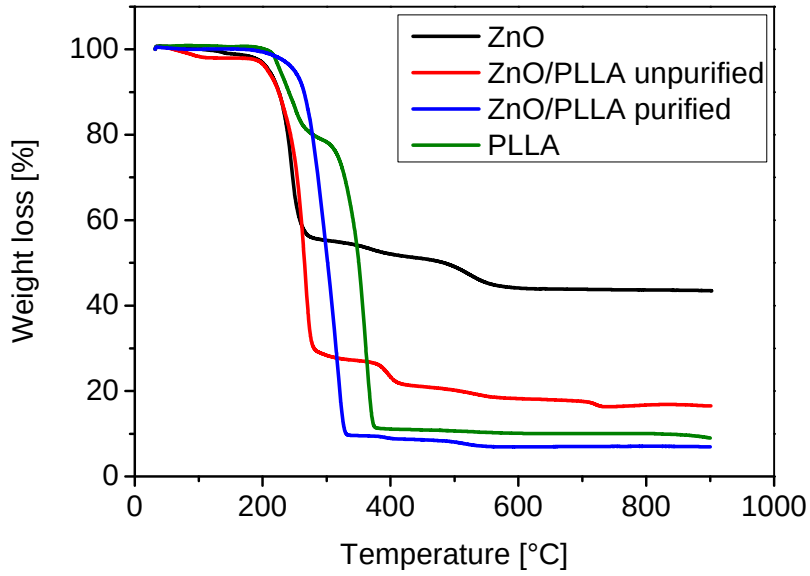

Fig. 35. Thermograph of different samples of ZnO NPs, ZnO/PLLA nanocomposite particles and pristine PLLA NPs.

Interestingly, the purified and unpurified ZnO/PLLA nanocomposite samples display a significant difference in their thermostability. Whereas the unpurified nanocomposite sample exhibits a 2-step decay to a final weight residue of 17%, the final weight residue of purified nanocomposite is much lower. Considering a weight loss of 83.5% and after addition of the residual 9% of the pure PLLA, one obtains a residual weight fraction of 7.5% for ZnO in the unpurified sample. With regard to the inital solid content of ZnO in the sample (10%), we can conclude a retainment of ~75% ZnO in the unpurified sample, including encapsulated and non-encapsulated material. In contrast, the results of the TGA analysis suggest a ZnO residue of less than 3% for the purified nanocomposite sample after normalization with the residual weight fraction of the pure PLLA sample. According to the previously-described SEM studies, some of the surface-adhered ZnO is most probably washed away during the

purification process. Consequently, a lower ZnO content is to be expected in the purified sample. Yet, with regard to the initially employed ZnO concentration and the significant amounts of encapsulated ZnO observed in TEM, the actual encapsulation efficiency appears to be surprisingly small indeed.

The most critical factor in TG experiments is gas handling [270]. Since all samples were measured under nitrogen flow, experimental disturbances might have arisen from the nitrogen flow not being perfectly adjusted to the sample. Additionally, especially when dealing with low contents of inorganic material, TGA analysis has shown to be less reliable because it cannot distinguish between inorganic particles, impurities, and organic residues [142]. Therefore, complementary analysis of purified nanocomposite samples has been conducted by ICP-OES. ICP is a well established method in food industry and environmental analysis but has rarely been used for the analysis of hybrid polymeric particles up to date. Recently, a detailed study on the determination of the concentration of metal complexes encapsulated into polymeric NPs and optimization of the measuring conditions has been published within our group [143]. With regard to the experimental conditions used in their study, ZnO/PLLA nanocomposite samples were analyzed by ICP. The measurements revealed a final zinc content of 159 µg mL^{-1}, which corresponds to a zinc oxide concentration of 199 µg mL^{-1}. Consequently, the encapsulation efficiency accounts for a much more fitting value of 12% in relation to the initially employed ZnO concentration and the apparent loadings observed from the TEM images.

Reddy et al. reported a minimum inhibitory concentration (MIC) of 13 nm-ZnO NPs as little as 8 µg mL^{-1} against *S. aureus* [36]. According to the ICP analysis of the ZnO/PLLA nanocomposites, the overall ZnO NP concentration is 25 times higher than the reported MIC. Based on these considerations, the ZnO loading should be sufficiently elevated to induce significant bacterial damage even when only partially released from the PLLA matrix.

5.3.3.2 Influence of ZnO on the degradation rate of PLLA

ZnO has been widely used as a photocatalyst for the degradation of organic pollutants in water under UV irradiation, namely phenol and various azo-dyes [271, 272]. Therefore, the question arises if in addition to its anticipated biocidal properties, the incorporation of ZnO into PLLA could enhance the degradation rate of PLLA upon irradiation with UV light and thus trigger a ZnO release.

The natural degradation of PLLA relies on the hydrolysis of backbone ester groups, which results in the generation of metabolizable moieties [273] such as lactic acid. The degradation rate is generally very slow (months to years) and depends on the polymer crystallinity, the molecular weight, the processing method, and the storage conditions (temperature, pH, presence of salts) [274]. Its characteristics have been investigated in numerous studies [251, 275, 276]. For example, von Recum et al. [276] reported a weight loss of 69% after submitting low molecular PLLA membranes dispersed in PBS buffer to orbital shaking at 37 °C for 28 days. A detailed study on the degradation behavior of PLLA NPs has been carried out by Musyanovych et al. [84]. A marked weight loss of 48% for SDS-stabilized PLLA NPs with high and low molecular weight was observed in this study after 9.5 months of storage in aqueous suspensions at 4 °C.

To determine the influence of ZnO on the degradation of PLLA, UV degradation studies on both composite ZnO/PLLA NPs and pure PLLA NPs have been performed. Within a total period of 45 days, aqueous sample dispersions were irradiated with UV-light for 15 min every 48 h. In the meanwhile, the samples were stored at 4 °C under light exclusion. The irradiation wavelength of 356 nm was selected according to the absorption maximum of the pristine ZnO NPs in chloroform (see section 5.3.4). The degradation behavior of PLLA was monitored by measuring the molecular weight distribution via SEC in reasonable time intervals i.e. every two weeks. The results of the photodegradation study are summarized in Fig. 36 and Table 6.

Fig. 36 shows the SEC chromatograms of nanocomposite ZnO/PLLA and pure PLLA samples before (0 days) and after UV-irradiation (45 days). At all times, the molecular weight distributions of the main PLLA body are unimodal and relatively broad and the non-irradiated chromatograms of both samples are almost identical. Close examination of both non-irradiated samples reveals the presence of an additional small signal at a retention time of 30 min, which can be attributed to the accumulation of small molecular weight degradation products as a consequence of the ultrasonic treatment during miniemulsification [84]. In contrast, after UV-treatment, the intensity of the latter increased significantly for both samples - ZnO/PLLA nanocomposite and pure PLLA. The pronounced signal evidences the increased formation of degradation products. Furthermore, two additional shoulders at the low molecular weight tail can be spotted for the ZnO/PLLA nanocomposite sample, which do not

appear in the chromatogram of the native polymer. These additional signals point out an increased formation of oligomers or low molecular weight fragments in the presence of ZnO.

The observations in the chromatograms are supported by the molecular weight distributions which were obtained from a PS calibration curve with respect to the main PLLA body at ~22 min as summarized in Table 6. Whereas the pure PLLA sample suffered a weight loss of 65% after UV irradiation, a much higher weight loss of 83% could be detected for the ZnO/PLLA nanocomposite particles.

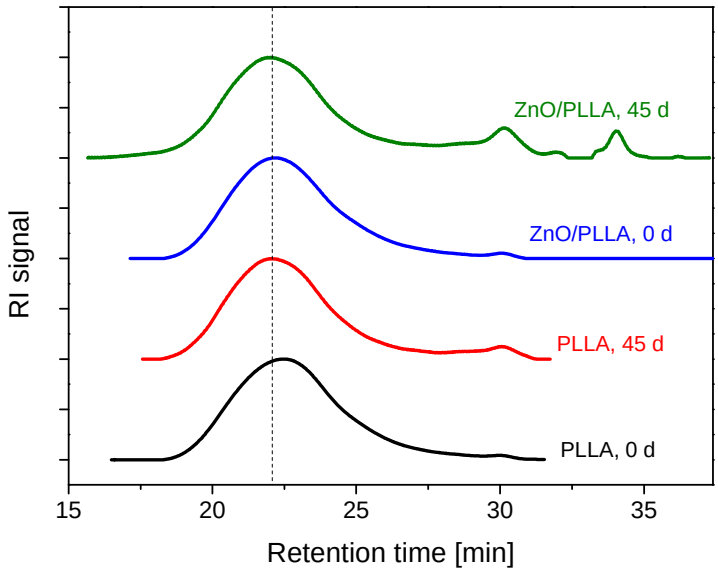

Fig. 36. Overlay of SEC elugrams from pure PLLA NPs and ZnO/PLLA nanocomposite particles before (0 days) and after UV treatment (45 days). The samples were stored at 4 °C under light exclusion.

Table 6. Molecular weight distribution of PLLA and ZnO/PLLA nanocomposite particles obtained from SEC measurements before (0 days) and after UV-treatment (45 days).

Sample	Before UV treatment		After UV-treatment	
	M_n [g mol^{-1}]	M_w/M_n	M_n [g mol^{-1}]	M_w/M_n
PLLA	30835	2.89	10650	8.32
ZnO/PLLA	33306	2.81	5113	20.22

In summary, two conclusions can be drawn from the aforementioned results. First of all, compared to the data published by Musyanovych et al. [277], the degradation rate of pure

PLLA increases upon UV irradiation. Second, the degradation rate of PLLA is significantly enhanced by the presence of ZnO.

The first observation is not surprising, considering that polymeric materials in general are affected by UV light, which for example can be exploited to induce crosslinking processes [146]. Previous studies on the influence of UV irradiation on PLLA have shown that the exposure of the polymer to UV-light basically leads to the excitation of carbonyl groups, entailing a rapid decrease in molecular weight and racemization of the fragmented chains [278]. However, the second observation evidences the photocatalytic potential of ZnO to enhance the PLLA degradation upon irradiation with UV-light, in addition to the simple hydrolytic cleavage in aqueous solution. The photocatalytic reaction mechanism relies on electron-hole pair generation upon UV-irradiation on the surface of ZnO. Subsequent reactions with water lead to radical formation with strong oxidization potential to the surrounding material [279]. Consequently, the resulting radicals are able to induce the breakage of adjacent polymer chains and therefore catalyze the degradation process.

In short, the degradation of PLLA has been significantly enhanced via light activation of the ZnO photocatalyst, which is encapsulated in the polymer matrix. The degradation process allows for a release of the ZnO NPs with the possibility to trigger and thereby control the release rate by applying a UV-light stimulus.

5.3.3.3 Investigation of the antimicrobial activity of the ZnO/PLLA nanocomposite particles

The antimicrobial assay to evaluate the antimicrobial activity of the as-synthesized ZnO/PLLA nanocomposite particles was developed in collaboration with the University Medical Center of Mainz, using an agar dilution method as follows: *S. aureus* (MSSA476) and *P. aeruginosa* (PAO1) were spread on agar plates as sketched in Fig. 37. Subsequently, circular holes were cut out from the agar surface with a sterile pipette and filled with 30 µL of sample solution. After 20 h of incubation at 37 °C, the agar plates were examined for zones of inhibition close to the sample holes.

The test was carried out with five different samples with their assigned numbers summarized in Table 7 according to their blanking position on the agar plates. Ultrapure water served as negative control. The SDS solution used for the NP stabilization served as second control to

differentiate between any surfactant-related and ZnO-related effects, since SDS is known for its cell-lysing properies at elevated concentrations [207]. Furthermore, dialyzed ZnO/PLLA and pure PLLA NPs with reduced amounts of SDS were tested in comparison to non-dialysed ZnO/PLLA samples.

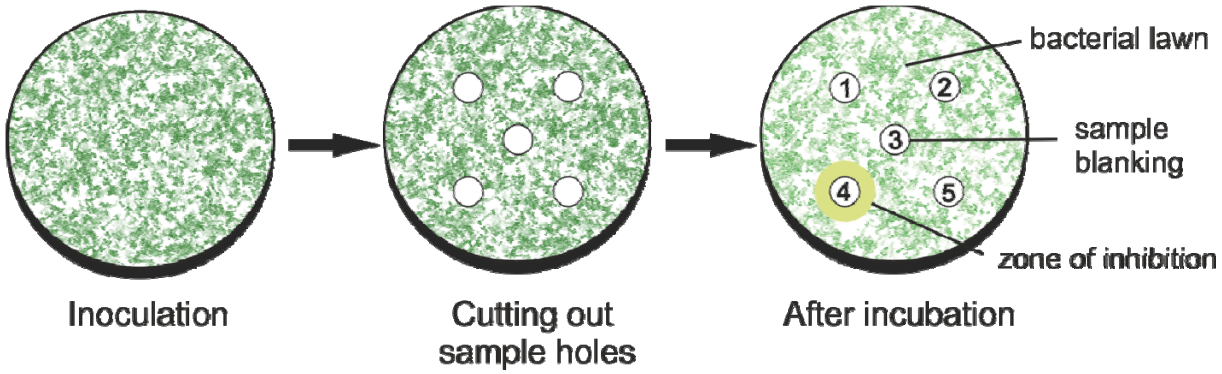

Fig. 37. Schematic illustration of the agar dilution assay used for the evaluation of the antibacterial activity of different ZnO/PLLA nanocomposite samples.

Table 7. The effect of ZnO/PLLA nanocomposite particles on the growth of *S. aureus* and *P. aeruginosa* expressed by the presence of inhibition zones on inoculated agar plates.

Position	Sample name	Type	SDS amount [mg mL^{-1}]	Zone of inhibition	
				***S. aureus* (MSSA476)**	***P. aeruginosa* (PAO1)**
1	VS87.4	ZnO/PLLA NPs	< 3.1	No	No
2	VS87.6	PLLA NPs	< 3.1	No	No
3	VS90.1	ZnO/PLLA NPs	3.1	Yes	No
4	Control	SDS solution	3.1	Yes	No
5	Control	H_2O	-	No	No

The results of the agar assay are presented in Table 7 and Fig. 38. Fig. 38 shows the photographs taken after incubation of the different samples on inoculated surfaces with *S. aureus* and *P. aeruginosa*. Close observation of the sample blankings reveals a small zone of inhibition within the *S. aureus*-colonies for undialyzed ZnO/PLLA nanocomposite particles as well as for the SDS solution. On the other hand, *S. aureus* does not appear to be affected by the dialyzed ZnO/PLLA and pure PLLA NPs. As concerns *P. aeruginosa*, only a slightly visible ring of inhibition could be observed for the SDS solution and no other inhibition zones were seen for all other samples. In brief, both *S. aureus* and *P. aeruginosa* do not show any growth inhibition in the presence of the as-synthesized ZnO/PLLA nanocomposite particles.

The effect seen for the undialysed composite sample can be attributed to the high amounts of surfactant (SDS, 25% w/w PLLA) used to ensure the colloidal stability of the system.

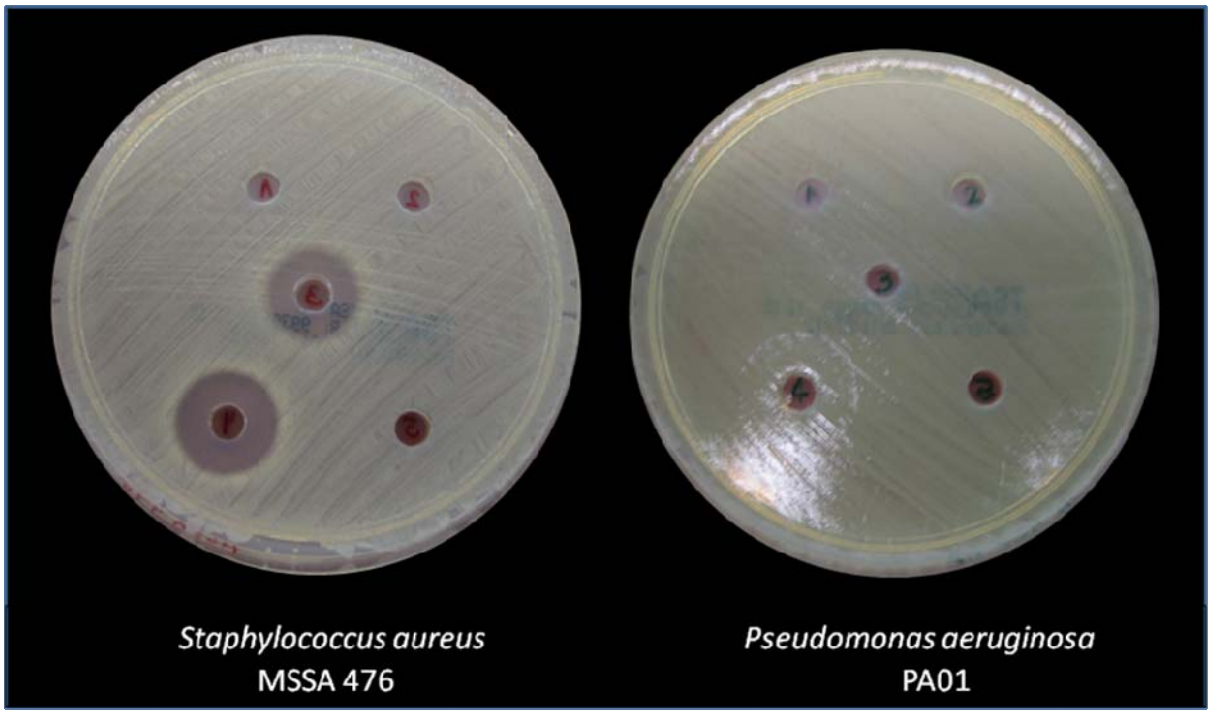

Fig. 38. The effect of ZnO/PLLA nanocomposite particles on the growth of *S. aureus* and *P. aeruginosa* visualized by photographs of the inoculated agar plates including the zones of inhibition for sample 3, 4 (*S. aureus*) and 4 (*P. aeruginosa*).

Eventually, several conclusions can be drawn from this experiment. Firstly, there is a clear distinction between the sensitivity of both microbial strains towards SDS, which is related to the fact that *P. aeruginosa* is able to degrade and metabolize SDS [280] while *S. aureus* is not. This has to be kept in mind to be able to differentiate between surfactant-related and ZnO-related antibacterial effects when dealing with *S. aureus*. Therefore, the amount of SDS should be adjusted to a minimum of colloidal stability as can be easily achieved by dialysis of the hybrid latexes. Secondly, the as-synthesized ZnO/PLLA nanocomposite samples do not exhibit any antimicrobial activity within the extent of the experimental conditions, i.e. an incubation period of 24 h.

The apparent inactivity of the nanocomposite samples in this experiment can be explained as follows: (*i*) The incubation period of the as-synthesized composite latexes is too short to ensure adequate degradation of PLLA and consecutive release of ZnO, (*ii)* the viscosity of the

agar does not promote diffusion of the ZnO NPs in case of a release and (iii) the amount of encapsulated material is below the MIC for both strains, even when fully released.
Considering the results obtained from the SEM investigations and UV degradation studies, the explanations of (*i*) are much more likely than (*ii*) and (*iii*). With regard to the first point (*i*), the experimental results of the aforementioned antimicrobial assay have been obtained from as-synthesized nanocomposite samples, which have not been subjected to any treatment apart from dialysis. Yet, the photocatalytic degradation studies of nanocomposite samples (see 5.3.3.2) have demonstrated a degradation of more than 50% only after 45 days of continuous exposure to short intervals of UV light. Consequently, with regard to the comparably short incubation time of 24 h in the antimicrobial assay, the results suggest that the inactivity of the nanocomposite samples is merely based on the fact that the ZnO NPs are still trapped in the PLLA matrix. The points mentioned under (*ii*) and (*iii*) can be easily discarded because a complete release of ZnO from the as-synthesized latexes is very unlikely at the present experimental conditions (24 h of incubation). Besides, ICP analysis of the nanocomposite latexes has shown an overall ZnO NP concentration which is 25 times higher than the reported MIC of 8 µg mL^{-1} against *S. aureus* [36]. Therefore, significant antibacterial activity is to be expected in case of a complete release of the ZnO loading and has already been demonstrated against *E. coli* for a another composite system (see next chapter, 5.3.4).

Several comparable systems have been reported in the literature. For example, the antimicrobial activity of ZnO@PS core-shell systems was investigated by Tang et al. [267]. Antimicrobial properties were reported with increasing ZnO concentration and exposure to light when mixing the hybrid ZnO@PS into commercial latexes. However, it is not very clear how the encapsulated ZnO is supposed to be in contact with the microorganism since the PS latexes are neither porous nor biodegradable. In contrast, Xu et al.[281] presented a profound study on the insertion of 30 nm-silver NPs into 1 µm-PLLA fibers by electrospinning. Tunable loadings and steady release of silver after an initial burst of 4 days were quantified by atomic absorption spectroscopy. The authors suggested that the release mechanism is related to the diffusion of silver ions, owing to the porous nature of the fiber. It is generally believed that the antibacterial mechanism of action of silver is based on its interaction with thiol groups within the respiratory chain of the microorganism upon internalization into the cell membrane [33]. Yet, the mechanism for silver NPs differs from the ones proposed for zinc oxide. Most hypotheses favor a antibacterial mechanism based on a reaction of the ZnO

surface with water thereby generating ROS, notably the highly reactive hydroxyl radical, which induce oxidative stress and subsequent cell damage [37]. In general, the degradation process of PLLA particles results from matrix erosion in the interior part of the particles through water diffusion and subsequent increase of carboxylic acid functions [277]. The *in vitro* degradation of PLGA microspheres was visualized in SEM studies by Cohen et al. [207]: Starting from an intact outer surface, small pores with increasing diameter emerged within 4 days, proceeding to surface crevasses after 14 days of suspension in PBS at 37 °C. Theoretically, even small pores in the PLLA layer could promote water diffusion and initiate the ROS production by ZnO. Yet, with regard to the time frame of the previously described UV degradation study of the present system and the generally slower degradation rate of PLLA as opposed to PLGA [84], pore formation in the current system will certainly take longer than 24 h.

Finally, the absence of bactericidal effects of the as-synthesized, non-degraded ZnO/PLLA nanocomposite particles after 24 h of incubation results from the fact that the majority of ZnO NPs are enclosed in the PLLA matrix. Conversely, the photocatalytic properties of ZnO introduce the option to trigger their release by UV irradiation as shown in the UV degradation experiments. Consequently, a variety of perspectives are conceivable to optimize the triggered release as a function of time by playing around with different parameters (UV irradiation time, nature of the polymer, molecular weight of the polymer, shape of the ZnO NPs). For instance, the degradation of PLLA could be initiated by an intense pretreatment of the ZnO/PLLA nanocomposite particles with UV light. The pretreated system could then be surrendered to the enzymatic degradation of lipases which are secreted from *S. aureus* [282] to induce the full ZnO release and consecutively get killed. Alternatively, the natural degradation rate of the polymer could be enhanced by replacing PLLA with low molecular weight PLGA and increasing the photocatalytic activity of ZnO by selecting differently-shaped ZnO NPs with a different aspect ratio (e.g. nanorods).

5.3.3.4 Conclusions

In summary, the formulation of a novel, UV-responsive, biocompatible and biodegradable system of hybrid ZnO/PLLA NPs in the size range of 160-230 nm has been successfully demonstrated. Angular hydrophobic ZnO NPs were obtained by classical sol-gel methods and combined with preformed PLLA polymer to generate hybrid NPs by miniemulsion/solvent

evaporation methods. Morphological characterization by transmission and scanning electron microscopy revealed the presence of spherical PLLA NPs with a uniform distribution of the filler particles inside and on the outer surface of the polymer, indicating a threshold size of ~180 nm PLLA for efficient loading. After purification, the surface-adhered ZnO was predominantly removed so as to yield final ZnO@PLLA core-shell structures. In contrast to the TEM images, a relatively low encapsulation efficiency of less than 3% was obtained by TGA analysis, which was subsequently corrected to 12% by complementary ICP measurements. Thus, the final ZnO concentration was determined to be 25 times higher than the reported MIC against *S. aureus* for comparable ZnO NPs. A significantly increased degradation rate of PLLA (83% within 45 days) has been achieved by photocatalytic activation of ZnO, which opens up the possibility of triggering a controlled ZnO release independently of hydrolysis and thus induce bactericidal activity. The absence of antimicrobial activity of the as-synthesized, non-degraded ZnO/PLLA nanocomposite particles evidences that the ZnO NPs are inert as long as they are entrapped within the PLLA matrix. The original approach, described in this chapter provides a general and facile methodology for the fabrication of a bioactive, multicomponent inorganic/polymer hybrid system with the perspective of tailoring the light-induced ZnO release and thereby antimicrobial response as a function of time.

5.3.4 Antibacterial surface coatings from zinc oxide nanoparticles embedded in poly(*N*-isopropylacrylamide) hydrogel surface layers (5th generation of materials)

5.3.4.1 Film preparation and characterization

Many synthesis approaches of polymer-based nanocomposite materials rely on *in situ* generation of the nanomaterials inside of an appropriate matrix system such as the reduction of metal salts, ball milling, plasma polymerization in combination with metal deposition and co-evaporation of a metal and an organic component [283-286]. However, they often suffer from relatively poor control over the particle characteristics and the distribution of the filler particles [287]. The advantages of the herein presented two-step procedure include firstly an independent optimization of the synthesis conditions for the individual components, e.g. size and shape of the nanocrystals. Secondly, it allows for a detailed characterization of both components, and thirdly, the composites are easily prepared at low temperatures under mild conditions. In contrast to *in situ* precipitation methods, the polymer will not be contaminated by unconverted precursor material and by-products [119].

The PNIPAAm terpolymer was synthesized in free radical polymerization from *N*-isopropylacrylamide, methacrylic acid and 4-benzophenone methacrylate (MABP) in a molar ratio of 90:5:1 as described elsewhere [263].

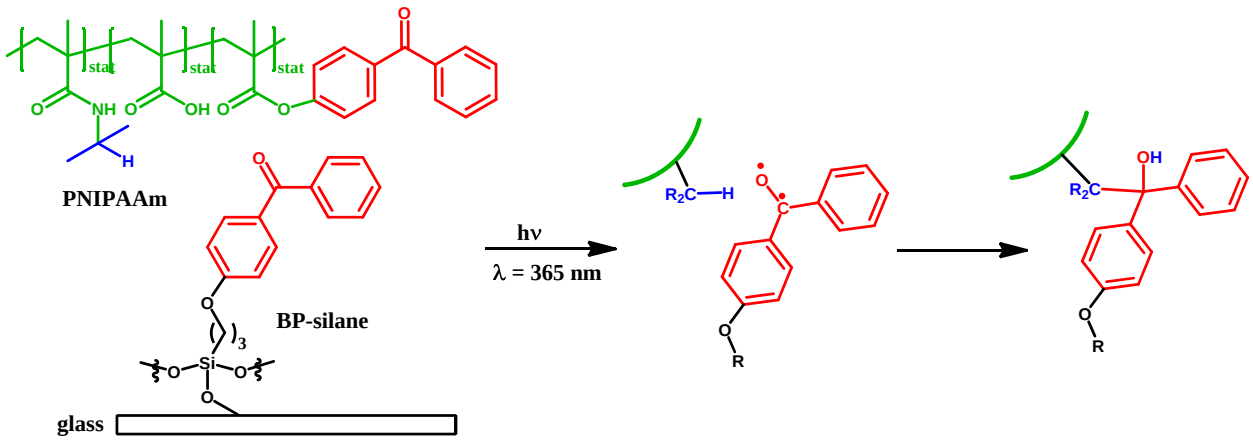

Fig. 39. Crosslinking of the PNIPAAm terpolymer and covalent surface attachment to glass upon UV-irradiation.

Subsequently, the ZnO/PNIPAAm nanocomposite films were prepared by mixing both components in different compositions of 1, 5, 10, 15, 25 and 35% ZnO in PNIPAAm (w/w) into chloroform, evaporating the solvent and redispersing the blend in ethanol. Spin-coating of these blends on functionalized glass substrates led to smooth films that were crosslinked by UV-irradiation. Whereas the MABP entity provides the basis for photocrosslinking the polymeric network, the photocrosslinkable adhesion promoter 4-(3-triethoxysilyl) propoxybenzophenone (BP-silane) was synthesized to functionalize the glass substrate and consecutively covalently link the hydrogel to the substrate. UV-irradiation of both polymer and linker resulted in a dense polymer network with tunable crosslinking density as illustrated in Fig. 39. Small amounts of methacrylic acid were introduced into the polymer backbone to provide a potential linking unit towards the NP surface. The affinity of ZnO NPs towards carboxylic acids is well known and has been exploited in previous studies as well as the current one to impart colloidal stability to the NPswhen using oleic acid as surfactant [288].

By using polymer contents of 2 or 5% (w/v), different film thicknesses were obtained, which will be further denoted as thin films (d = 60-85 nm) and thick films (d = 230-400 nm). Scanning electron micrographs of the composite film surfaces demonstrated a remarkably homogeneous distribution of the ZnO NPs at the surface of the thin films, for every NP/polymer ratio and even for very high NP loadings (Fig. 40). A cross-sectional SEM image of a 382 nm thick film also revealed a uniform distribution of the NPs throughout the hydrogel matrix. Additionally, the successful incorporation of nanocrystalline ZnO into the same thick film was supported by EDS analysis. The absence of pronounced agglomerates indicated a partial stabilization of the ZnO NPs within the hydrogel matrix by attractive interactions between the carboxylic acid groups of the polymer backbone and the NP surface, partially replacing surface-adsorbed oleic acid moieties. Indeed, ligand exchange between nanosized inorganic oxide surfaces and carboxyl or hydroxyl groups of natural organic compounds has been widely observed in aqueous environments [289].

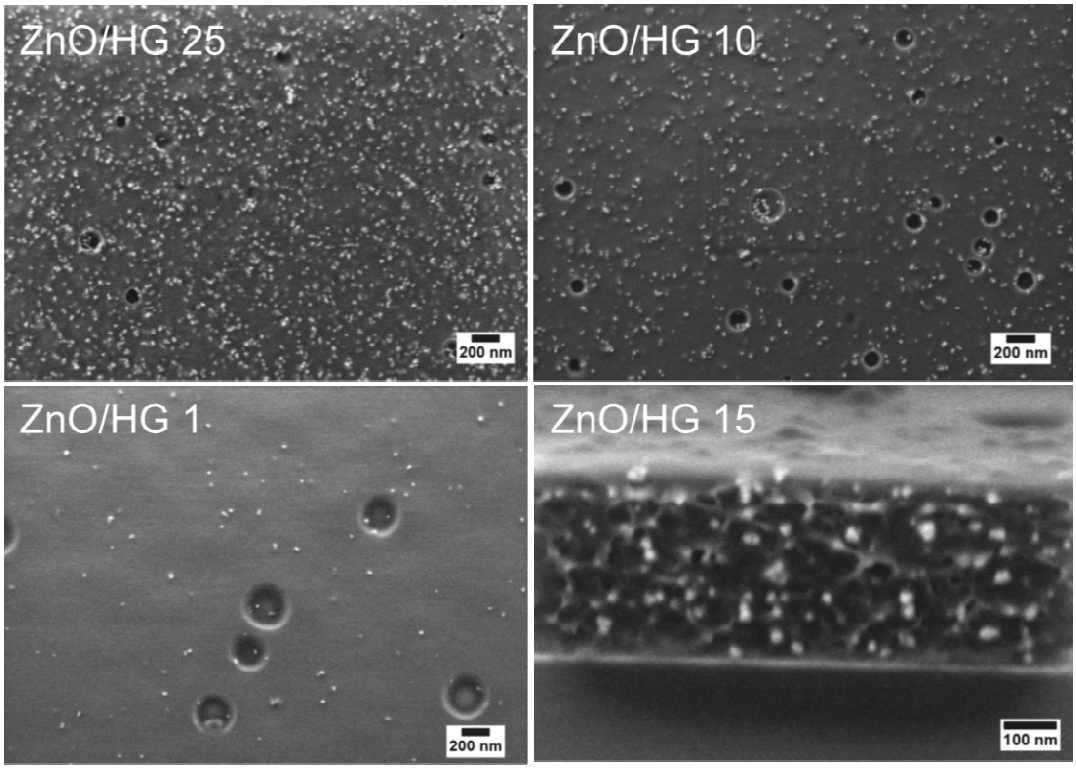

Fig. 40. Scanning electron micrographs of ZnO/PNIPAAm nanocomposite thin films (*d* = 60-85 nm) with varying ZnO contents of 25, 10 and 1% (w/w PNIPAAm) respectively. The circular holes are due to air bubbles in the spin-coating solutions. Cross-sectional image of a ZnO/PNIPAAm nanocomposite thick film (*d* = 382± 2 nm) with a ZnO content of 15%.

The assumption of favorable, stabilizing interactions between acrylic acid moieties and ZnO is supported by SEM studies of composite films, spin-coated from chloroform and ethanolic solutions (Fig. 41). The resulting thin films displayed a homogeneous NP distribution for both solvents although ethanol is a precipitating solvent for the native ZnO NPs. Besides, when dispersed into the non-crosslinked polymer during the solution mixing process, the ZnO NPs could be easily resuspended in ethanol. In short, these simple observations suggest that the NPs are not influenced by the solvents used as a result of internal stabilization within the hydrogel matrix. Due to high viscosity of the sample solutions with increasing amounts of ZnO NPs, the spin-coating procedure is limited to a production of thick composite films with a NP content of maximum 15%.

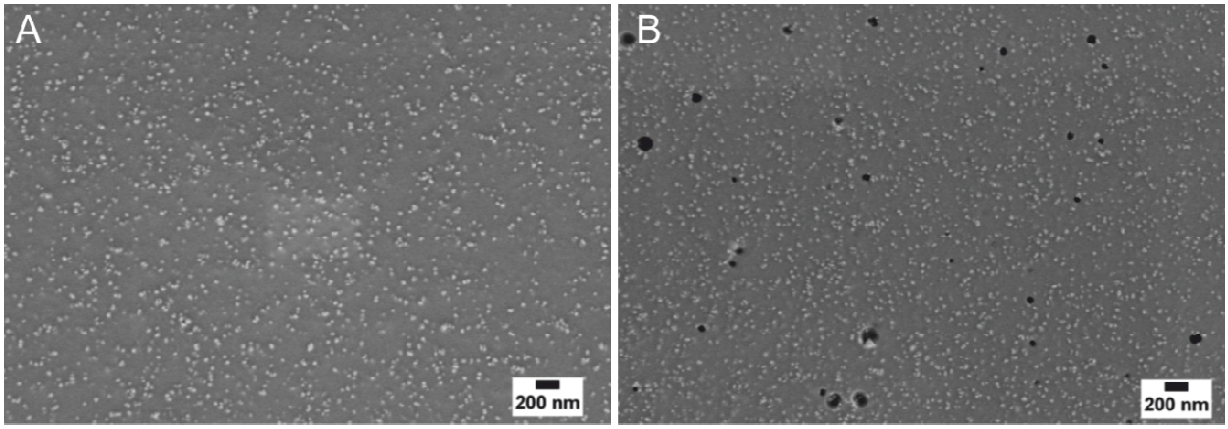

Fig. 41. Scanning electron micrographs of ZnO/PNIPAAm nanocomposite thin films (35% ZnO) spin-coated on Si from (A) chloroform and (B) ethanol.

5.3.4.2 Investigation of the optical properties of the nanocomposite films

The photoluminescent properties of ZnO nanomaterials with a sharp excitation edge around 370-350 nm have been widely studied [243, 290, 291]. To investigate whether the optical properties of the NPs are changed upon embedding them into the hydrogel, UV-Vis absorption spectra of different ZnO/PNIPAAm nanocomposite thin films with varying NP content were recorded on quartz glass (Fig. 42A) and compared to the UV-absorbance of native ZnO NPs in chloroform. Inspection of Fig. 41A reveals an absorption edge around 356 nm of the ZnO/PNIPAAm nanocomposite thin films with decreasing intensity related to the NP content. The nanocomposite spectra are in good agreement with the absorption signal of the free NPs in chloroform. Similar results were obtained for thicker films (data not shown). As a proof-of-principle, the intensity of the excitation edge was plotted against the NP content (Fig. 42B) for thin and thick composite films to verify the linear relation according to Beer-Lambert law. Although the relation is valid for the thick films, the linear extrapolation of the fitted thin film data does not cross the x-axis at zero-% of ZnO. These results can be most likely attributed to material losses at higher ZnO concentrations due to synergistic effects of centrifugal forces and the low viscosity of the thin film sample solutions. Yet, the absorption spectra clearly indicate that the incorporation of the ZnO NPs into the hydrogel matrix does not alter their optical properties, suggesting no chemical modification of the ZnO NPs.

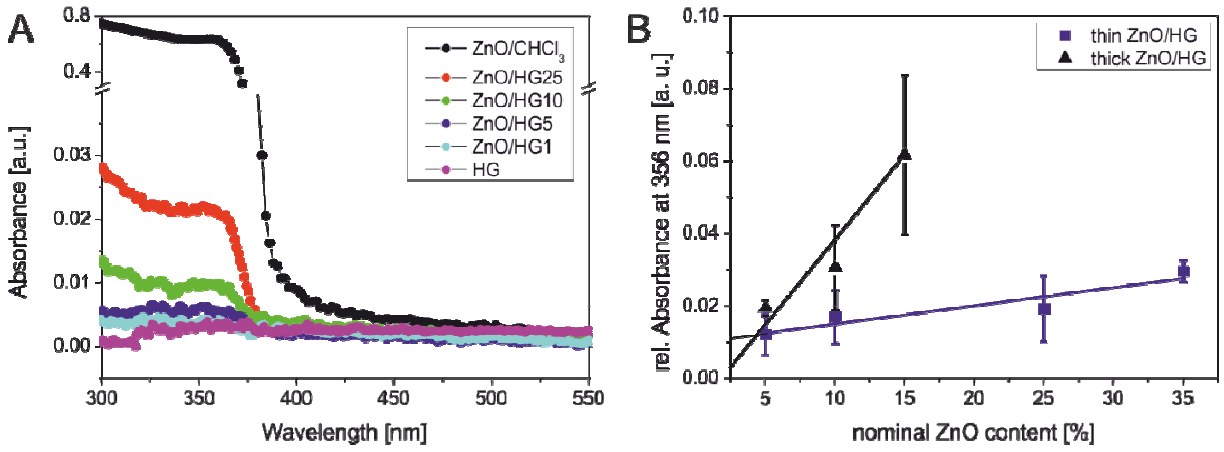

Fig. 42. Absorption spectra of (A) thin ZnO/hydrogel (HG) nanocomposite films with varying ZnO NP content (1-25% w/w HG) compared to native ZnO NPs in chloroform. (B) Absorbance at 356 nm of thin and thick films plotted versus the NP content within the hydrogel layers.

5.3.4.3 Quantification of the NP loading within the hydrogel layers

The loading of zinc within the hydrogel layers was measured by elemental analysis using ICP-OES. The resulting volume concentrations within the hydrogel were calculated by normalizing the measured amount of zinc with the total surface area of the coated glass slides multiplied with the film thickness in the dry state (Fig. 43A). The thickness of the dry thin films scales with other NP-polymer composite thin films documented in the literature, e.g. plasma-polymerized films and polyelectrolyte multilayers [283, 292]. Hence, the zinc amount was additionally expressed as loading per surface area (Fig. 43B) to facilitate direct comparison with published data. Inspection of Fig. 43A reveals a good correlation between the ZnO content used for the film preparation and the final zinc content measured by ICP. Second, it denotes similar volume concentrations in both thin and thick films of the same NP content in line with the error bars, suggesting the volume concentration to be independent of the film thickness. This result is especially interesting because it demonstrates that the loading of ZnO can be tuned by simple variation of the film thickness. Hence, it opens up the possibility to conveniently adjust the ZnO concentration for a desired application as a potential antimicrobial reservoir for a wound dressing or implant coating. The exact values per surface and volume fractions are summarized in Table 8. The values obtained from 1% ZnO/PNIPAAn films have not been listed since they were close to the detection limit of the ICP method.

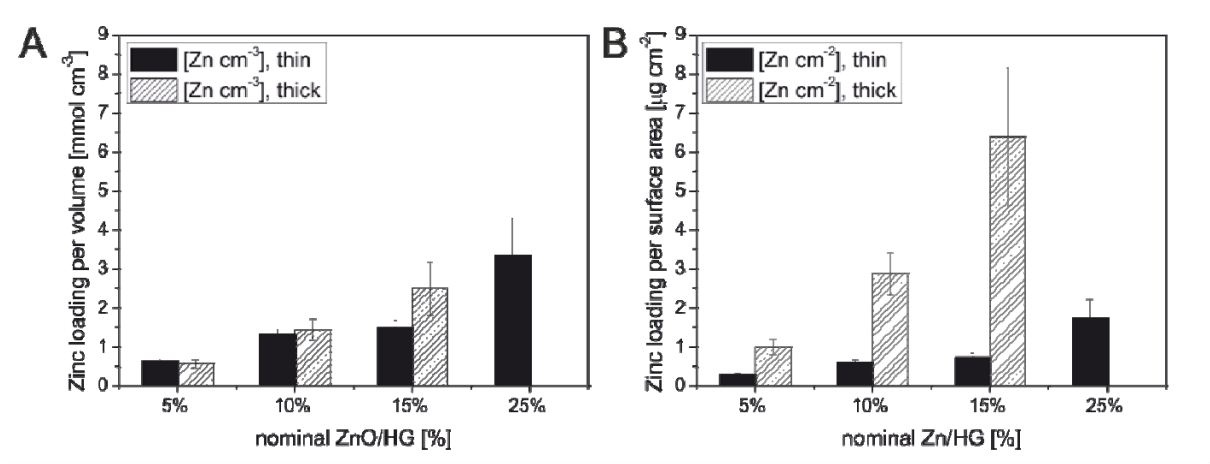

Fig. 43. Zinc loading expressed as (A) volume concentration (mmol cm^{-3}) of the hydrogel layer and (B) amount per surface area (µg cm^{-2}) as determined by ICP-OES. Due to increased viscosity of the sample solutions, the spin-coating procedure is limited to a maximum ZnO content of 15% for the thick nanocomposite films.

Table 8. Zinc loadings determined by ICP and normalized to the total coating surface (*A*) or volume of the hydrogel layer (*V*) for thin and thick films. Data expressed as mean value including the standard deviation of at least three independent measurements.

ZnO content	[Zn]/*A* [µg cm^{-2}]	[Zn]/*A* [µg cm^{-2}]	[Zn]/*V* [mmol cm^{-3}]	[Zn]/*V* [mmol cm^{-3}]
	thin films[1]	thick films[2]	thin films	thick films
5%	0.28±0.03	1.00±0.20	0.63±0,06	0.58±0.11
10%	0.60±0.06	2.89±0.54	1.33±0.13	1.45±0.27
15%	0.74±0.11	6.39±1.76	1.49±0.22	2.50±0.69
25%	1.74±0.48		3.36±0.93	

[1] *60-80 nm,* [2] *230-400 nm*

5.3.4.4 Release experiments

To understand the behavior of the composite films in aqueous media, dynamic UV-Vis experiments were performed on selected ZnO/PNIPAAm nanocomposite films in aqueous solution. The absorbance at the absorption edge provides a convenient measure to monitor a potential ZnO NP release or degradation from the swollen hydrogel through time-dependent absorption measurements on coated quarz slides in PBS buffer (0.01 M). Therefore, coated surfaces of 25% thin and 15% thick composite films were mounted into a teflon flow cell, which was rinsed with buffer at 0.1 mL min^{-1} at room temperature for 24 h. Simultaneously, absorption spectra were recorded at various time spans up to 24 h. The results are displayed in

Fig. 44A which shows the absorbance of the different films plotted against the measuring time. For 25% thin films a total loss of the ZnO absorption edge can be observed after 7 h of immersion in the buffer solution, suggesting a significant release or degradation of ZnO into the surrounding media. A slower decay of the absorption edge is found for a 15% thick film. These results confirm the previous findings via ICP measurements that the NP loading is only dependent on the layer thickness of the hydrogel. The kinetic measurements do not provide any information about the nature of the released material, whether complete NPs, some degraded species or zinc ions. However, it indicates that the bactericidal mechanism of ZnO must be related to some interaction of the cells with released species rather than surface-bound material. Furthermore, it evidences that the release rate can be modulated by the thickness of the hydrogel layer. SEM analysis of the remaining film fragments of the 25% thin film after 24 h of rinsing revealed the presence of few ZnO NPs on the quarz surface (Fig. 44B). Although the absorption signal decays to zero, the SEM image indicates that the number of ZnO NPs within the hydrogel is reduced but not completely depleted. The amount of the remaining NPs is apparently lower than the detection limit of the spectrometer. On the other hand, the size of the remaining NP scales with the previously determined crystallite size from TEM. This implies that the NPs are dispensed from the hydrogel matrix as complete entity as opposed to any dissolution products, which would be smaller in size.

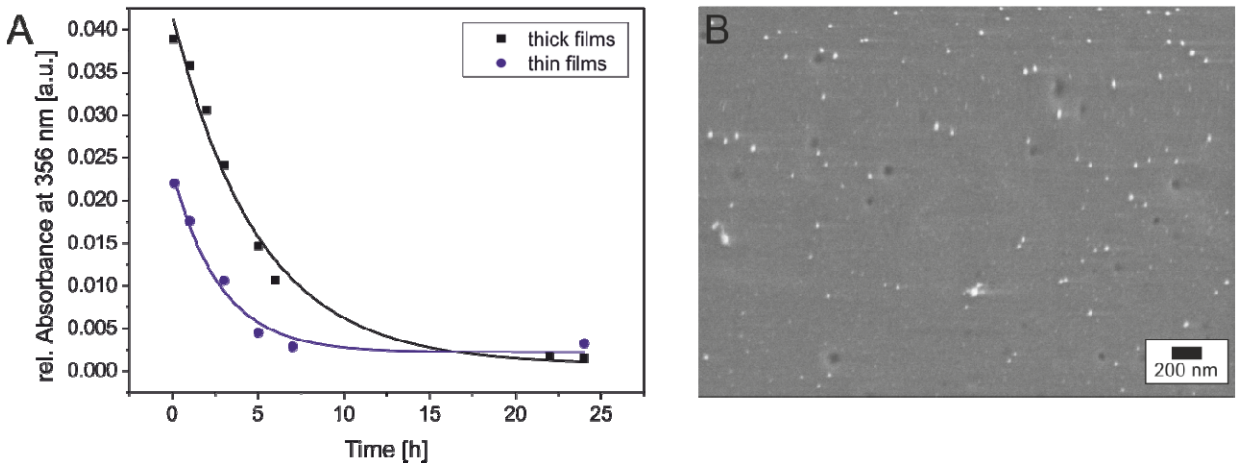

Fig. 44. (A) Absorbance at 356 nm of quartz glass coated with a thin (25%, w/w HG) and thick ZnO/HG film (15%) at different times while being rinsed for 24 h with buffer solution at room temperature. (B) Scanning electron micrograph of the same thin film (25%) on quarz after rinsing with buffer solution for 24 h.

5.3.4.5 *Antimicrobial activity of the ZnO/PNIPAAm nanocomposite films*

The evaluation of the antimicrobial activity of the ZnO/PNIPAAm nanocomposite films against *E coli* was conducted in collaboration within the MPIP. To this end, hydrogel layers of different thicknesses and varying amounts of ZnO were prepared on glass coverslips and covered with a specially designed poly(dimethyl)siloxane mask, providing a defined area of 1 cm^2. Subsequently, the reservoir on the coated surface was filled with a bacterial suspension and incubated at 37 °C for 24 h. Surviving cells were harvested from the surface and grown on agar plates for the assessment of CFUs. Uncoated glass slides and pure hydrogel-coated slides served as control surfaces. The results are presented in Fig. 45A as CFUs relative to pure hydrogel surfaces of thin and thick films plotted against increasing concentrations of ZnO NPs (1-10%). Furthermore, they are visualized by a photograph of the agar plates of undiluted and diluted material collected from a thin film samples series (Fig. 45B). Inspection of Fig. 44 allows several observations: First, the bacteria grow very well on both control surfaces, which can be readily observed by the bacterial lawn on the corresponding agar plates of the photograph. Second, there is a visible growth reduction throughout the sample series with increasing ZnO NP content: Bacterial suspensions incubated on thin ZnO/PNIPAAm nanocomposite films were bactericidal starting from 10% of ZnO relative to the polymer. Bacteriostatic behavior was still observed for NP contents as low as 1% of ZnO. Most significantly, thicker nanocomposite films exhibited even higher levels of antimicrobial activity. Whereas colonies easily formed on the pure hydrogel surfaces, a 100% reduction in CFUs of *E. coli* was observed for ZnO nanocomposite surfaces, starting from 5% ZnO films. Based on these results, the MIC amounts to ZnO contents of 10% for the thin and 5% for the thick films. Taking into account the zinc quantification by ICP (Fig. 43B**),** the MIC per surface area accounts for zinc loadings of 0.6-1.0 μg cm^{-2}.These values correspond to a ZnO concentration in suspension of 4.7-7.8 μg mL^{-1}. Currently, most studies related to ZnO NPs investigated their antibacterial effect in suspension with a MIC in the range of 1–35 mM (81–2835 μg mL^{-1}), depending on the NP size, the bacterial strain and the applied assay [232, 293]**.** Yet, only few studies are available on ZnO NPs on composite surfaces [294-296]**.** On the other hand, comparably high antimicrobial efficiencies against *S. epidermidis* with 0.4 μg cm^{-2} of silver NPs embedded into polyelectrolyte multilayers have been reported by Agarwal et al. [283]**.** Therefore, the exploration of ZnO NPs as an efficient alternative to nanoparticulate silver systems is highly recommended.

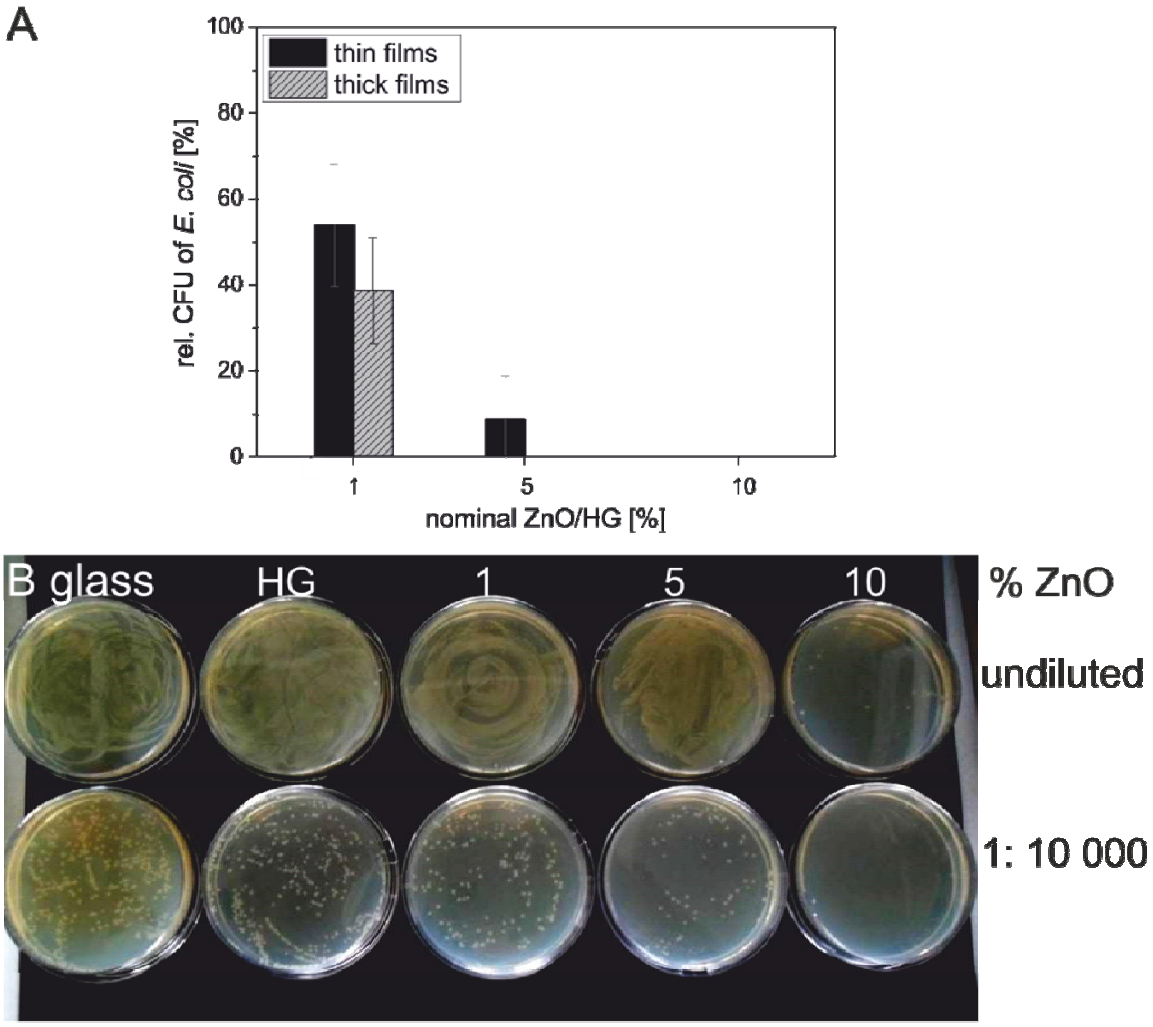

Fig. 45. (A) The effect of thin or thick hydrogels with increasing concentrations of ZnO NPs (1 - 10%, w/w HG) on the growth of *E.coli*, expressed as CFUs relative to the pure hydrogel. Mean values and standard deviation have been calculated from three independent experiments. (B) Photograph of *E.coli* colonies grown on agar plates after exposure to different thin ZnO/HG nanocomposite films.

Previous reports in the literature have shown that smaller ZnO NPs with increasing surface to volume ratios resulted in stronger antimicrobial effects against various bacteria under ambient light conditions [37, 232, 233, 293]**,** whereas the ZnO NP shape and crystalline structure seemed to have less effect [231, 297, 298]**.** Hence, the antibacterial activity of the ZnO/hydrogel nanocomposite films can be attributed to the small NP size (~23 nm), the uniform distribution of the filler particles within the hydrogel and the controlled release in aqueous media.

Several – probably accumulative - mechanisms such as direct disruptive electrostatic interactions of NPs with cell walls and membranes [234, 299] or indirect effects due to the decomposition of ZnO and the formation of reactive oxygen species, (H_2O_2, hydroxyl radicals

(●OH), singlet oxygen ($^1O_2$)) [296, 298, 300] or Zn^{2+} [235] have been discussed. Besides, the medium is known to influence the toxicity of ZnO NPs due to potential complexation of zinc ions and precipitation of zinc salts [235]. Amplified antibacterial activities were further observed by photocatalytical UV or light activation of ZnO NPs [232, 295]. Although in the current system all experiments have been conducted in the absence of light, which excludes any photoactivation processes, prominent antibacterial activity has been detected at very low ZnO loadings. It could therefore be interesting to investigate in a perspective study if the already satisfactory biocidal activity of the ZnO/PNIPAAm films could be increased by exposure to UV light. The current study provides little information on the mechanism of action. Nevertheless, the UV kinetic in aqueous medium has clearly shown a time-dependent reduction of the ZnO NPs within the hydrogel layers, suggesting a diffusional mechanism of interaction between the nanomaterial and the bacterium rather than contact-active effects of surface-bound NPs versus the microorganism.

5.3.4.6 In vitro cytotoxicity of the PNIPAAm/ZnO nanocomposite films

Cell viablility

In parallel to the antibacterial activity, the interactions of mammalian cells with the ZnO/hydrogel nanocomposite films have been evaluated in collaboration with the UMC. The attachment and spreading of NIH/3T3 Swiss mouse fibroblasts was investigated by a fluorimetric viability/proliferation test as well as by flow cytometry. For the flow cytometric analysis, the cells were cultivated on nanocomposite-coated surfaces and the viability was detected after 24 h, using Annexin V-FITC and propidium iodide staining to differentiate between viable, apoptotic and necrotic cells. Uncoated, hydrogel-coated (PNIPAAm) as well as surfaces coated with a commercially available hydrogel-based ultra low attachment surface (ULA) served as control. The results are summarized in Fig. 45. Inspection of Fig. 46 reveals that the number of vital cells decreased after exposure to different NP-free hydrogel formulations (40.8-55.5% in PNIPAAm, 22.7% in ULA) compared to uncoated control surfaces (87.0 ± 8.9%). Consequently, the rate of apoptosis (13.6-20.4% in PNIPAAm, 29.2% in ULA versus 4.0% in Control) and necrosis (29.8-44.8% in PNIPAAm, 48.1% in ULA versus 9.1% in Control) increased. Two-way ANOVA analysis, which is a statistical method of data evaluation, revealed that this highly significant effect was largely due to the presence of the hydrogels (Wilks-Lambda = 0.287, $p<0.001$), while ZnO NPs did not contribute to the

decrease in cell viability (Wilks-Lambda= 0.793, p=0.909). Tukey-corrected post hoc comparisons could not detect any significant differences between the different ZnO NPs concentrations.

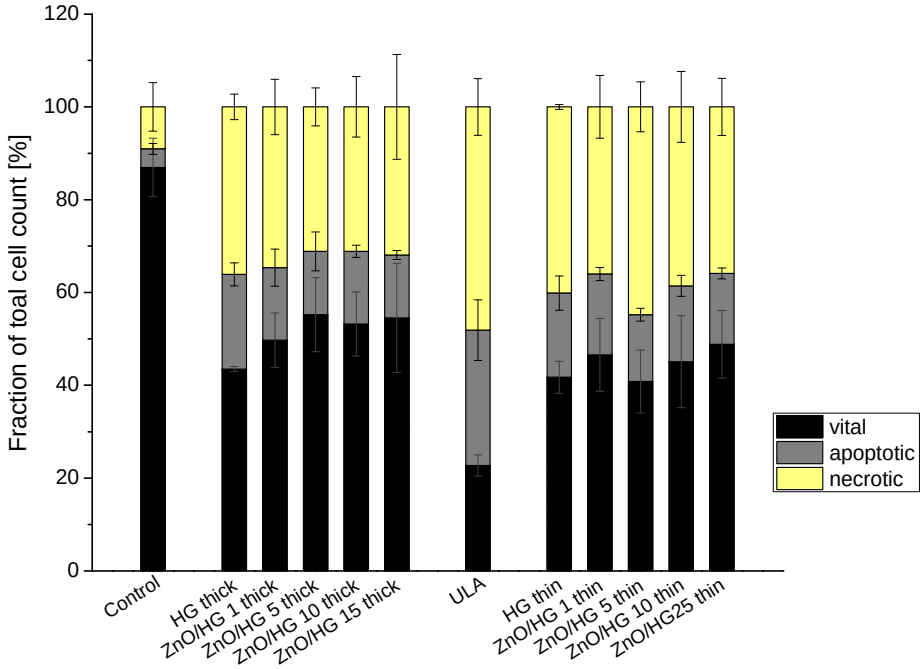

Fig. 46. Viability of NIH/3T3 Swiss mouse fibroblasts after 24 h exposure to different ZnO/hydrogel nanocomposite thin and thick films (5 – 25% of ZnO, w/w HG) as determined by flow cytometry. The "ultra low attachment surface" (ULA) is a commercially available hydrogel-coated cell culture dish/well plate, designed for non-adherent cell cultures.

The *in vitro* cytotoxicity assays demonstrated that the ZnO/ PNIPAAm nanocomposites were not generally toxic to NIH/3T3 Swiss mouse fibroblasts seeded onto the coatings for 24 h. The apparently high number of lost cells on all pure hydrogel and ZnO-doped surfaces were most likely not the result of direct hydrogel toxicity but rather stem from the cells' inability to attach to the hydrogel surface. Like most tissue-bound cells, fibroblasts are anchorage-dependent. Therefore, fibroblasts are more resistant to continued suspension than other cell types (e.g. epithelial cells), and will reversibly arrest their cell cycle, until they can attach to a surface. However, they too will eventually undergo apoptosis if kept in suspension for an extended period of time [301]. Fig. 47 outlines the cell morphology on uncoated control surfaces (Fig. 47A), PNIPAAm-coated (Fig. 47B) and a ZnO/PNIPAAm-coated thick film (15%) (Fig. 46C) after 24 h of incubation. Whereas the cells on the uncoated control surface

attached and spread out normally, the fibroblasts on the pure PNIPAAm film clustered into large clumps (marked by downward arrows in Fig. 47B). In contrast, the ZnO-doped thick film appeared to promote a slight attachment as can be seen by the formation of small cellular protrusions. The aggregation of cells exposed to PNIPAAm in our experiments may indicate the cells' attempts to adhere to their immediate environment. However, this does not fully prevent the onset of apoptosis, as shown by the flow cytometric assessment of cell viability.

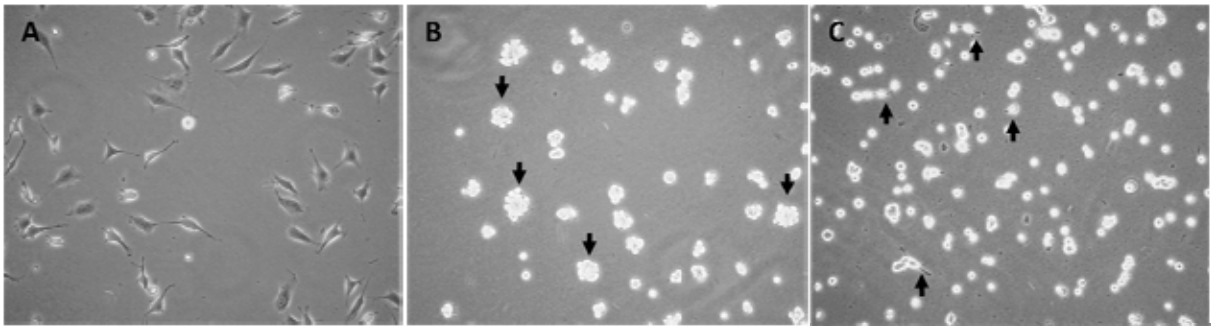

Fig. 47. NIH/3T3 Swiss mouse fibroblasts after 24 h of incubation on different surfaces. (A) Uncoated control surface, (B) PNIPAAm-coated surface with downward arrows pointing out aggregates of 20-30 cells, (C) ZnO/PNIPAAm nanocomposite thick film (15 wt-% of ZnO). Upward arrows show attached cells with small cellular protrusions.

The high rate of necrosis seen in our experiments is most likely a secondary effect due to the *in vitro* setup. *In vivo*, apoptotic cells are cleared away by macrophages which were not present in our fibroblast monoculture. A large portion of apoptotic cells are likely to have ruptured during sample preparation for FACS analysis, which involved extended exposure to trypsin and some mechanical stress in the attempt to separate cell aggregates into single cells. This secondary rupture of the cell membrane allows for the uptake of propidium iodide into the fragmented nucleus of the cell, thus rendering it difficult to distinguish from a primarily necrotic cell.

Previous studies of crosslinked PNIPAAm have shown antifouling properties both to proteins and primary human fibroblasts [257, 261, 302]. Therefore a commercially available type of hydrogel-coated culture dish was used as "positive control" in order to evaluate any effects of the expected inhibition of cell attachment on PNIPAAm coated surfaces. The positive control surface (ULA) is commonly used for suspension cultures of non-adherent cell types (e.g. leukocytes, hematopoietic stem cells) without any reported detrimental effects. Interestingly, the rate of apoptosis and (secondary) necrosis was highest in the cells seeded onto the ULA

surface. Thus, it appears reasonable to conclude from the cell experiments, that the photocrosslinked PNIPAAm used in this study is not in itself toxic to NIH/3T3 fibroblasts.

It was interesting to note that with increasing concentration of the ZnO NPs embedded in the hydrogel, the number of cells that are able to adhere to the hydrogel also increased (up to approximately 10% of all cells, Fig. 47C). The cell attachment might be a result of differences in the surface topography of the hydrogels with ZnO particles protruding from the surface, potentially enabling cell adherence. An alternative explanation might be changes in the degree of crosslinking of the terpolymer due to the UV-absorption of the ZnO-NPs, thus locally altering the non-fouling properties of the hydrogel. Although not very pronounced, this increase in cell attachment could result in an increase of cell viability that could potentially mask a minor toxic effect of ZnO NPs. However, as of now, this remains speculative.

Cell proliferation

Due to the lack of attachment of the fibroblasts, the cells were reseeded after 24 h of exposure to various ZnO/hydrogel nanocomposite films. Cell proliferation was indirectly tracked by repeated fluorometric measurements over a period of 7 days of metabolically reduced resofurin in the culture medium. As illustrated in Fig. 48A, the proliferation was unaltered by the exposure to hydrogel thin films compared to the control surface, with increasing ZnO concentrations not affecting the rate of proliferation. In contrast to the apparent absence of an immediately toxic effect seen in the FACS-analysis, long-term observation of the cells showed, that ZnO may have some influence on cell function (Fig. 48B). Exposure to concentrations higher than 10% of ZnO embedded in the thick hydrogel films led to a moderate slowing of cell proliferation. While this effect did not reach statistical significance in our experimental series due to a large variability between the separate experiments (Repeated Measures ANOVA, Greenhouse-Geisser-corrected $p = 0.155$), it is well in accordance with recent reports on the cytotoxicity of ZnO NPs towards mammalian cells [303-305]. These studies indicate a preferential toxicity of ZnO NPs to rapidly proliferating cells (i.e. cancerous cells or stem cells), while slowly or non-proliferating cells can tolerate higher concentrations of ZnO. Taccola et al. [305] suggested that this difference is caused by the more rapid ZnO-dependent production of reactive oxygen species. More interestingly, this differential effect may also provide an explanation for the apparent discrepancy between our own viability and proliferation results. As mentioned before, fibroblasts in suspension (as

caused by seeding onto our PNIPAAm hydrogel) will change into G0-Phase and thus not proliferate [301, 306-308], until they can attach. If ZnO NPs are more toxic to proliferating cells, their lack of effect on cell viability in our experiments may be a direct result of the cells' inability to adhere.

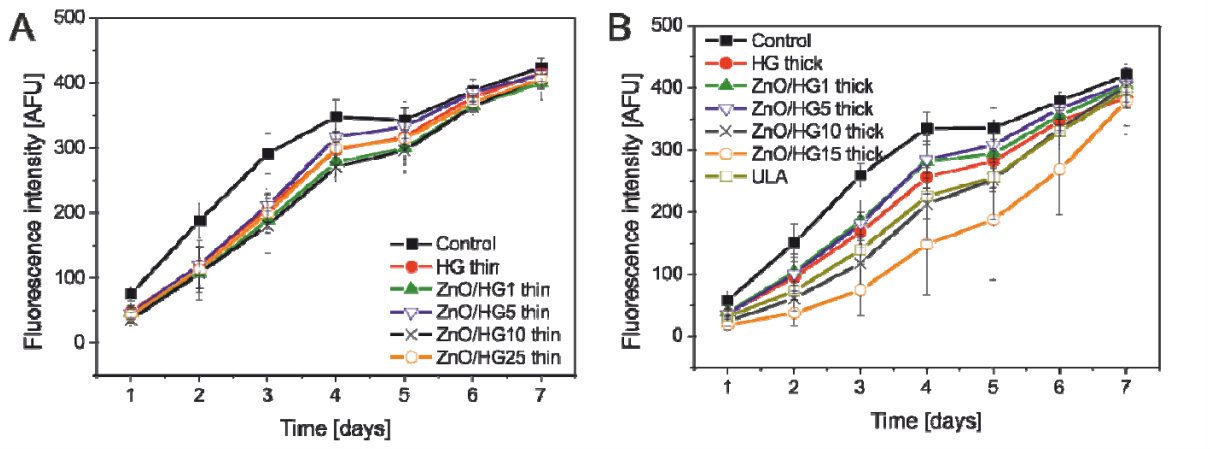

Fig. 48. Proliferation of NIH/3T3 Swiss mouse fibroblasts after 24 h exposure to different (a) thin and (b) thick ZnO/hydrogel (HG) nanocomposite films with varying ZnO NPs contents (1 - 25 wt-%). ULA: Ultra low attachment surface.

In more practical terms, the relatively higher tolerance of non-proliferating cells to ZnO NPs may be useful in clinical settings. An anti-adhesive, bactericidal coating will most likely be employed on so-called "indwelling devices" such as respiratory tubing, urinary catheters or intravenous catheters. In fact, more than two-thirds of all hospital-acquired infections are associated with the prolonged use of these three types of device [309-311]. Nanocomposite films with carefully tuned amounts of ZnO, coated onto such devices would typically come in contact with respiratory epithelium, urothelial cells or vascular endothelium. Most of these cells are well differentiated and do not proliferate.

Conclusions

In this approach, a simple and cost-effective way was demonstrated to produce novel bioactive composite materials based on ZnO NPs embedded in a biocompatible PNIPAAm hydrogel matrix. Surface and cross-sectional investigations of the composite material showed quite a uniform distribution of the filler particles within the hydrogel matrix with tunable loadings by simply varying the thickness of the thin film. Based on these results, a partial

stabilization of the NPs by ligand exchange between oleic acid and acrylic acid residues in the polymer backbone was postulated. The optical properties of the ZnO NPs did not change through incorporation into the hydrogel layers. However, depending on the NP loading, a decay of the absorption signal could be observed with time upon immersion into aqueous solution, suggesting a material release of some undefined species. The composite films exhibited efficient antimicrobial activity against *E. coli* at very low ZnO loadings of 0.74 μg cm^{-2} (1.33 mmol cm^{-3}) with bacteriostatic activity for as little as 0.1 μg cm^{-2} (0.04 mmol cm^{-3}). This contrasts to current studies with much higher ZnO NPs concentrations for a comparable performance. On the other hand, similar antimicrobial activity has been reported for nanoscopic silver/polymer composites, promoting nanoscale ZnO as an efficient alternative to nanoparticulate silver systems. Complementary to the antibacterial assay, viability studies with mammalian cells (NIH/3T3) demonstrated non-cytotoxic behavior of the nanocomposite films at bactericidal loading levels, permitting healthy proliferation for a period of 7 days. Interestingly, the ZnO-doped surfaces were found to slightly improve cell adhesion compared to pure hydrogel films. Finally, a new approach towards engineered surface coatings, which could reduce microbial contamination of biomedical devices, was successfully demonstrated.

6. Summary and outlook

The ongoing problem of undesirable, detrimental bacterial colonization on medical implants requires new material solutions capable of meeting the challenge of bacterial flexibility and resistance. In the presented work, novel functional, bioactive materials have been developed as new alternatives to existing antimicrobial surface coatings by combination of various synthetic techniques - including traditional and colloidal polymer synthesis, the synthesis of inorganic nanocrystals, and thin film processing techniques. The study comprises the thorough investigation of their structure-properties relations as well as their interactions with both prokaryotes and eukaryotes. As a result, five promising material prototypes have been engineered, three of them capable of significantly reducing bacterial colonization.

The 1st generation of materials was aimed at exploring and evaluating the anti-adhesive properties of colloidal PEGylated NPs in contact with nosocomial pathogens since PEGylated NPs have been predominantly used to repel proteins in drug delivery systems. As a versatile method to produce functional polymeric NPs, miniemulsion polymerization of styrene and PEGMA monomers of various molecular weight and chain lengths has been employed to yield stable copolymer NPs with covalently attached PEG chains in unimodal size distributions of 200-300 nm. A maximized PEGylation was achieved by additional stabilization of the NPs using a surface-adsorbed PEG-based surfactant. Microbiological training has been provided at the University of Bath to investigate the anti-fouling properties of the PEGylated NPs against *P. aeruginosa* (PAO1). Different microbiological techniques were mastered and applied to various PEGylated NP samples, notably optical density measurements, surface spread-plate and fluorescent staining methods. The results indicated that the colonization of PAO1 was not affected by the PEGylated NPs. However, they might still display anti-fouling properties towards other bacterial species because previous work indicated that the sensitivity of *P. aeruginosa* towards PEGlylated surfaces is highly dependent on the strain used.

The 2nd and 3rd generations of materials comprised a novel colloidal approach of quaternary-ammonium-functionalized polymer NPs as opposed to surface-grafted or self-assembled QAC analogues. For this purpose, a multifunctional monomer was synthesized by quaternization of DMAEMA with a long alkyl chain. The resulting monomer, qDMAEMA combines

antimicrobial and surface-active properties, including the possibility to eliminate the dependence of colloidal systems on the additional stabilization via physically-adsorbed surfactants. Stable, spherical, functional surfactant-free NPs of 40-70 nm in diameter were obtained by copolymerization of styrene and qDMAEMA in miniemulsion (2nd generation). Copolymer NPs, additionally stabilized with the surface-adhered biocidal QAC-based surfactant CTAC were produced for the purpose of comparison i.e. colloidal stability and antibacterial properties. The interactions of both NP systems with *S. aureus* were investigated in collaboration with the University Clinic of Cologne (UKK). Bacteriostatic properties were observed for the CTAC-stabilized copolymer NPs only. The inactivity of their surfactant-free analogues suggested that either the number of functional groups or the overall NP concentration did not suffice to induce a bacterial reaction at the experimental conditions studied. Because the functional group density of quaternatry ammonium moieties was limited to 8% in copolymerization with styrene, an alternate route was explored to increase the functionalization density on the NP surface (3rd generation of materials). Surface-active polyelectrolyte chains were synthesized by free radical polymerization of the functional surfmer qDMAEMA. The resulting surfactant-free PqDMAEMA NPs, which showed adequate colloidal stability for at least several weeks, were obtained in a combined process of miniemulsion and solvent evaporation. Hence, a modified assay, specially designed to evaluate the surface activity of polymeric compounds towards microorganisms, was developed in collaboration with the UKK and employed to investigate the short and long-term impact of surface-attached PqDMAEMA NPs on the colonization of *S. aureus* (MSSA476). In parallel, the interaction of the PqDMAEMA with mammalian cells (NIH/3T3 Swiss mouse fibroblasts) was analyzed in close collaboration with the UKK. The developed colloidal PqDMAEMA prototype exhibited long-lasting (up to 5 days) selective toxicity towards *S. aureus* while being non-cytotoxic to mammalian cells on a short term basis to moderatly cytotoxic after 5 days, thus demonstrating its potential as promising bactericidal contact-active agent.

In the 4th and 5th generations of materials two different leaching systems were developed based on the antimicrobial properties of nanoscale ZnO embedded into biocompatible matrices (PLLA, PNIPAAm), both systems unexplored to date: well-defined angular ZnO NPs of 23 nm diameter were synthesized by solvothermal methods and subsequently incorporated into PLLA latexes via combined miniemulsion/solvent evaporation techniques to

generate a novel bioactive, stimuli-responsive colloidal hybrid system (4th generation). Investigation of the hybrid latexes by electron microscopy revealed the presence of spherical ZnO@PLLA@ZnO core-shell-core structures of 160-230 nm in diameter. The outer shell is predominantly washed away during the purification process, yielding final ZnO@PLLA core-shell NPs. The dispersion of ZnO into PLLA ensured a remarkably agglomerate-free distribution of the distinct nanocrystals. Subsequent quantification of the encapsulated ZnO via ICP-OES attested an overall ZnO concentration sufficiently elevated to induce considerable bacterial damage, notably 25 times higher than reported MICs. The degradation of the hybrid latexes and consecutive release of ZnO was externally catalyzed by photoactivation of ZnO via UV irradiation. Consequently, a significantly increased degradation of 20 % was detected for the hybrid ZnO/PLLA NPs as opposed to the native polymer, including a weight loss of 75 % in 45 days after regular exposure to short intervals of UV light. This was especially interesting because it offered the possibility to trigger the ZnO release via its instrinsic photocatalytic capacity. Short-term (24 h) antimicrobial tests of non-degraded ZnO/PLLA hybrid NPs, which were conducted in collaboration with the University Medical Centre of Mainz (UMC), did not demonstrate any biocidal activity due to the fact that the ZnO NPs were inactive as long as enclosed in an intact, non-degraded PLLA matrix. Therefore, perspective optimization studies should focus on triggering the ZnO release as a function of time to exploit the antimicrobial properties of ZnO on a short-term basis (hours to days).

A novel, antimicrobial leaching system of ZnO/PNIPAAm nanocomposite thin films was designed as 5th generation of materials. The composite thin films were prepared in a convenient and cost-effective way by simply mixing different contents of ZnO NPs into a PNIPAAm solution, subsequently spin-coating the blend into thin nanocomposite films of 60-300 nm thickness and photocrosslinking on adequately functionalized glass slides. As opposed to *in situ* generation of inorganic materials inside a polymeric template, the selected approach allowed for the controlled blending of both preformed, well-defined components. Similar to the ZnO/PLLA hybrids, the incorporation of ZnO into a PNIPAAm hydrogel ensured a very good dispersion and protection against coalescence. The ZnO content was accurately determined by ICP-OES. Leaching experiments suggested a gradual ZnO release within several hours which can be easily tuned by varying the film thickness. In collaboration within the MPIP, an antimicrobial assay was developed which was specially suited to

determine the bacterial cell growth directly on the nanocomposite-coated glass slides. At the same time, the cytotoxic potential of the nanocomposite films was evaluated in collaboration with the UMC. The nanocomposite films demonstrated remarkable bactericidal activity of ZnO against *E. coli* at very low ZnO loadings, comparable to silver-based systems. In parallel, non-cytotoxic behavior at bactericidal loadings was observed towards mammalian cells. Thus, a versatile biocompatible nanocomposite coating has been engineered with efficiently high antimicrobial activity as competitive alternative to silver coatings.

To summarize, the present work has demonstrated the efficient combination of various synthetic strategies to develop new biocidal material prototypes based on multifunctional colloidal and inorganic/polymer nanocomposite systems. The consecutive optimization of the different generations of materials was manifested in the evolution from bacteriostatic (PS-co-PqDMAEMA) towards bactericidal systems (PqDMAEMA, ZnO/PNIPAAm) including moderate to non-cytotoxic activity towards mammalian cells. The biomedical evaluation of the materials is a result of efficient collaborations with biologists and medical doctors in this highly interdisciplinary project. Thus, several promising candidates have been engineered which are capable of reducing microbial colonization as potential implant coatings with the perspective of further optimization according to the desired application.

7. Bibliography

[1] European Centre for Disease Prevention and Control. *Annual epidemiological report on communicable diseases in Europe 20.* Stockholm: ECDC **2010**

[2] Darouiche, R.O., *Antimicrobial coating of devices for prevention of infection: Principles and protection.* The international journal of artificial organs **2007**, *30(9)*, 820-827

[3] Quin Y., Z.N., An Y. H., Wen X., *Biomaterial strategies to reduce implant-associated infections.* The international journal of artificial organs **2007**, *30(9)*, 828-841

[4] Lowy, F.D., *Staphylococcus aureus Infections.* The New England Journal of Medicine **1998**, 520-532

[5] European Centre for Disease Prevention and Control. *Antimicrobial resistance surveillance in Europe 2009. Annual Report of the European Antimicrobial Resistance Surveillance Network (EARS-Net).* Stockholm: ECDC **2010**

[6] Hetrick E. M., S.M.H., *Reducing implant-related infections: active release strategies.* Chem. Soc. Rev. **2006**, *35*, 780-789

[7] Gristina, A., *Biomaterial-centered infection: microbial adhesion versus tissue integration.* Science **1987**, *237(4822)*, 1588-1595

[8] Hall-Stoodley L., Costerton J. W., and P. Stoodley, *Bacterial biofilms: from natural environment to infecious diseases.* Nature Reviews Microbiology **2004**, *2(2)*, 95-108

[9] Ferreira, L. and A. Zumbuehl, *Non-leaching surfaces capable of killing microorganisms on contact.* Journal of Materials Chemistry **2009**, *19(42)*, 7796-7806

[10] Banerjee, I., R.C. Pangule, and R.S. Kane, *Antifouling Coatings: Recent Developments in the Design of Surfaces That Prevent Fouling by Proteins, Bacteria, and Marine Organisms.* Advanced Materials **2011**, *23(6)*, 690-718

[11] Von Eiff C., et al., *Modern strategies in the prevention of implant-associated infections.* The international journal of artificial organs **2005**, *28(11)*, 1146-1156

[12] Klibanov, A.M., *Permanently microbicidal materials coatings.* Journal of Materials Chemistry **2007**, *17(24)*, 2479-2482

[13] Tiller, J.C., et al., *Designing surfaces that kill bacteria on contact.* Proceedings of the National Academy of Sciences of the United States of America **2001**, *98(11)*, 5981-5985

[14] Lee, S.B., et al., *Permanent, Nonleaching Antibacterial Surfaces. 1. Synthesis by Atom Transfer Radical Polymerization.* Biomacromolecules **2004**, *5(3)*, 877-882

[15] Palermo, E.F., et al., *Role of Cationic Group Structure in Membrane Binding and Disruption by Amphiphilic Copolymers.* Journal of Physical Chemistry B **2011**, *115(2)*, 366-375

[16] Waschinski, C.J., et al., *Design of Contact-Active Antimicrobial Acrylate-Based Materials Using Biocidal Macromers.* Advanced Materials **2008**, *20(1)*, 104-108

[17] Lichter, J.A. and M.F. Rubner, *Polyelectrolyte Multilayers with Intrinsic Antimicrobial Functionality: The Importance of Mobile Polycations.* Langmuir **2009**, *25(13)*, 7686-7694

[18] Kim, C.H., et al., *Synthesis of chitosan derivatives with quaternary ammonium salt and their antibacterial activity.* Polymer Bulletin **1997**, *38(4)*, 387-393

[19] Rabea, E.I., et al., *Chitosan as antimicrobial agent: Applications and mode of action.* Biomacromolecules **2003**, *4(6)*, 1457-1465

[20] Zasloff, M., *Antimicrobial peptides of multicellular organisms.* Nature **2002**, *415(6870)*, 389-395
[21] Hancock, R.E.W. and H.-G. Sahl, *Antimicrobial and host-defense peptides as new anti-infective therapeutic strategies.* Nat Biotech **2006**, *24(12)*, 1551-1557
[22] Gabriel M., et al., *Preparation of LL-37-Grafted Titanium Surfaces with Bactericidal Activity.* Bioconjugate Chemistry **2006**, *17*, 548-550
[23] Costa, F., et al., *Covalent immobilization of antimicrobial peptides (AMPs) onto biomaterial surfaces.* Acta Biomaterialia **2011**, *7(4)*, 1431-1440
[24] Brogden, K.A., *Antimicrobial peptides: Pore formers or metabolic inhibitors in bacteria?* Nature Reviews Microbiology **2005**, *3(3)*, 238-250
[25] Lienkamp, K., et al., *Antimicrobial Polymers Prepared by ROMP with Unprecedented Selectivity: A Molecular Construction Kit Approach.* Journal of the American Chemical Society **2008**, *130(30)*, 9836-9843
[26] Lichter, J.A., K.J. Van Vliet, and M.F. Rubner, *Design of Antibacterial Surfaces and Interfaces: Polyelectrolyte Multilayers as a Multifunctional Platform.* Macromolecules **2009**, *42(22)*, 8573-8586
[27] Benetti, E.M., et al., *Surface-Grafted Gel-Brush/Metal Nanoparticle Hybrids.* Advanced Functional Materials **2010**, *20(6)*, 939-944
[28] Simchi, A., et al., *Recent progress in inorganic and composite coatings with bactericidal capability for orthopaedic applications.* Nanomedicine: Nanotechnology, Biology and Medicine **2011**, *7(1)*, 22-39
[29] Piozzi, A., et al., *Antimicrobial activity of polyurethanes coated with antibiotics: a new approach to the realization of medical devices exempt from microbial colonization.* International Journal of Pharmaceutics **2004**, *280(1-2)*, 173-183
[30] Raad, I., et al., *Central Venous Catheters Coated with Minocycline and Rifampin for the Prevention of Catheter-Related Colonization and Bloodstream Infections.* Annals of Internal Medicine **1997**, *127(4)*, 267-274
[31] Page, K., M. Wilson, and I.P. Parkin, *Antimicrobial surfaces and their potential in reducing the role of the inanimate environment in the incidence of hospital-acquired infections.* Journal of Materials Chemistry **2009**, *19(23)*, 3819-3831
[32] Atiyeh, B.S., et al., *Effect of silver on burn wound infection control and healing: Review of the literature.* Burns **2007**, *33(2)*, 139-148
[33] Rai, M., A. Yadav, and A. Gade, *Silver nanoparticles as a new generation of antimicrobials.* Biotechnology Advances **2009**, *27(1)*, 76-83
[34] Mary, G., S.K. Bajpai, and N. Chand, *Copper (II) ions and copper nanoparticles-loaded chemically modified cotton cellulose fibers with fair antibacterial properties.* Journal of Applied Polymer Science **2009**, *113(2)*, 757-766
[35] Kong, H., J. Song, and J. Jang, *Photocatalytic Antibacterial Capabilities of TiO2-Biocidal Polymer Nanocomposites Synthesized by a Surface-Initiated Photopolymerization.* Environmental Science & Technology **2010**, *44(14)*, 5672-5676
[36] Reddy, K.M., et al., *Selective toxicity of zinc oxide nanoparticles to prokaryotic and eukaryotic systems.* Applied Physics Letters **2007**, *90(21)*, 213902-3
[37] Applerot, G., et al., *Enhanced Antibacterial Activity of Nanocrystalline ZnO Due to Increased ROS-Mediated Cell Injury.* Advanced Functional Materials **2009**, *19(6)*, 842-852
[38] Poelstra, K.A., et al., *Prophylactic treatment of gram-positive and gram-negative abdominal implant infections using locally delivered polyclonal antibodies.* Journal of Biomedical Materials Research **2002**, *60(1)*, 206-215

[39] Skurnik, M. and E. Strauch, *Phage therapy: Facts and fiction.* International Journal of Medical Microbiology **2006**, *296(1)*, 5-14
[40] Stone, R., *Bacteriophage therapy: Stalin's forgotten cure.* Science **2002**, *298(5594)*, 728-731
[41] Cademartiri, R., et al., *Immobilization of bacteriophages on modified silica particles.* Biomaterials **2010**, *31(7)*, 1904-1910
[42] Xiong, Y. and Y. Liu, *Biological control of microbial attachment: a promising alternative for mitigating membrane biofouling.* Applied Microbiology and Biotechnology **2010**, *86(3)*, 825-837
[43] Hume, E.B.H., et al., *The control of Staphylococcus epidermidis biofilm formation and in vivo infection rates by covalently bound furanones.* Biomaterials **2004**, *25(20)*, 5023-5030
[44] *http://www.mpip-mainz.mpg.de/eu-projekte/embek1/index.php.*
[45] Sawai, J., *Quantitative evaluation of antibacterial activities of metallic oxide powders (ZnO, MgO and CaO) by conductimetric assay.* Journal of Microbiological Methods **2003**, *54(2)*, 177-182
[46] Pichot, C., *Surface-functionalized latexes for biotechnological applications.* Current Opinion in Colloid & Interface Science **2004**, *9(3-4)*, 213-221
[47] Schmid, G., *Nanoparticles: from theory to applications*. **2004,** Weinheim: Wiley-VCH
[48] Fudouzi, H. and Y. Xia, *Photonic Papers and Inks: Color Writing with Colorless Materials.* Advanced Materials **2003**, *15(11)*, 892-896
[49] Rao, J.P. and K.E. Geckeler, *Polymer nanoparticles: Preparation techniques and size-control parameters.* Progress in Polymer Science **2011**, *36(7)*, 887-913
[50] Van Herk, A.M., *Chemistry and Technology of Emulsion Polymerisation*. **2005**: Blackwell Publishing
[51] Van Herk, A.M. and K. Landfester, eds. *Hybrid Latex Particles. Preparation with (Mini)emulsion Polymerization*. Advances in Polymer Science. Vol. 233. **2010**, Springer Verlag: Berlin
[52] Chiu, T.-P. and T.-M. Don, *Synthesis and characterization of poly(methyl methacrylate) nanoparticles by emulsifier-free emulsion polymerization with a redox-initiated system.* Journal of Applied Polymer Science **2008**, *109(6)*, 3622-3630
[53] Tanrisever, T., O. Okay, and I.Ç. Sönmezoğlu, *Kinetics of emulsifier–free emulsion polymerization of methyl methacrylate.* Journal of Applied Polymer Science **1996**, *61(3)*, 485-493
[54] Cochin, D., A. Laschewsky, and F. Nallet, *Emulsion Polymerization of Styrene Using Conventional, Polymerizable, and Polymeric Surfactants. A Comparative Study.* Macromolecules **1997**, *30(8)*, 2278-2287
[55] Alain, G., *Polymerisable Surfactants.* Surfactant Science Series **2003**, *114*, 495-541
[56] Katsutoshi, N., *Radical Polymerisation and Potential Applications of Surface-active Monomers.* Trends in Polymer Science **1996**, *4*, 122-127
[57] Landfester, K., *Polyreactions in Miniemulsions.* Macromolecular Rapid Communications **2001**, *22*, 896-936
[58] Voorhees, P.W., *The theory of Ostwald ripening.* Journal of Statistical Physics **1985**, *38(1)*, 231-252
[59] Landfester, K., *Miniemulsionspolymerisation und Struktur von Polymer- und Hybrid-Nanopartikel.* Angewandte Chemie **2009**
[60] Asua, J.M., *Miniemulsion polymerization.* Progress in Polymer Science **2002**, *27(7)*, 1283-1346

[61] Baier, G., et al., *DNA Amplification via Polymerase Chain Reaction Inside Miniemulsion Droplets with Subsequent Poly(n-butylcyanoacrylate) Shell Formation and Delivery of Polymeric Capsules into Mammalian Cells.* Macromolecular Bioscience **2011**, *11(8)*, 1099-1109

[62] Aschenbrenner E. M., Weiss C. K., and K. Landfester, *Enzymatic Esterification in Aqueous Miniemulsions.* Chemistry-a European Journal **2009**, *15(10)*, 2434-2444

[63] Schiller R., Weiss C. K., and K. Landfester, *Phase stability and photocatalytic activity of Zr-doped anatase synthesized in miniemulsion.* Nanotechnology **2010**, *21(40)*

[64] Ethirajan, A., et al., *Biomimetic hydroxyapatite crystallization in gelatin nanoparticles synthesized using a miniemulsion process.* Advanced Functional Materials **2008**, *18(15)*, 2221-2227

[65] Hauser, C.P., et al., *Luminescent Polymeric Dispersions and Films Based on Oligonuclear Lanthanide Clusters.* Macromolecular Chemistry and Physics **2011**, *212(3)*, 286-296

[66] Musyanovych, A., Landfester K., *Synthesis of Poly(butylcyanoacrylate) Nanocapsules by Interfacial Polymerisation in Miniemulsions for the Delivery of DNA Molecules.* Progr. Colloid Polym. Sci. **2008**, *124*, 120-127

[67] Holzapfel V., et al., *Preparation of Fluorescent Carboxyl and Amino Functionalized Polystyrene Particles by Miniemulsion Polymerization as Markers for Cells.* Macromolecular Chemistry and Physics **2005**, *206(24)*, 2440-2449

[68] Boursier, T., et al., *Controlled radical polymerization of styrene in miniemulsion mediated by PEO-based trithiocarbonate macromolecular RAFT agents.* Polymer Chemistry **2011**, *2(2)*, 355-362

[69] Ruppert, M., K. Landfester, and U. Ziener, *Anionic polymerization of cyclic ester and amide in miniemulsion: Synthesis and characterization of poly(ε-caprolactone) and poly(ε-caprolactone-co-ε-caprolactam) nanoparticles.* Journal of Polymer Science Part A: Polymer Chemistry **2010**, *48(22)*, 4929-4937

[70] Baier, G., et al., *Cross-Linked Starch Capsules Containing dsDNA Prepared in Inverse Miniemulsion as "Nanoreactors" for Polymerase Chain Reaction.* Biomacromolecules **2010**, *11(4)*, 960-968

[71] de Barros, D.P.C., et al., *Miniemulsion as efficient system for enzymatic synthesis of acid alkyl esters.* Biotechnology and Bioengineering **2010**, *106(4)*, 507-515

[72] López-Quintela, M.A., *Synthesis of nanomaterials in microemulsions: formation mechanisms and growth control.* Current Opinion in Colloid & Interface Science **2003**, *8(137-144)*

[73] Landfester, K., *Polyreactions in Miniemulsions.* Macromolecular Rapid Communications **2001**, *22(12)*, 896-936

[74] *http://www.igb.fraunhofer.de/de/kompetenzen/grenzflaechentechnik/partikulaere-systeme/polymerisation.html.*

[75] Krauel, K., et al., *Using different structure types of microemulsions for the preparation of poly(alkylcyanoacrylate) nanoparticles by interfacial polymerization.* Journal of Controlled Release **2005**, *106(1-2)*, 76-87

[76] Charcosset, C., I. Limayem, and H. Fessi, *The membrane emulsification process—a review.* Journal of Chemical Technology & Biotechnology **2004**, *79(3)*, 209-218

[77] Matyjaszewski K., et al., *Atom transfer radical polymerization of n-butyl methacrylate in an aqueous dispersed system: A miniemulsion approach.* Polymer Chemistry **2000**, *38(S1)*, 4724-4734

[78] Grazon, C., et al., *One-Pot Synthesis of Pegylated Fluorescent Nanoparticles by RAFT Miniemulsion Polymerization Using a Phase Inversion Process.* Macromolecular Rapid Communications **2011**, *32(9-10)*, 699-705
[79] Zetterlund, P.B., Y. Kagawa, and M. Okubo, *Controlled/Living Radical Polymerization in Dispersed Systems.* Chemical Reviews **2008**, *108(9)*, 3747-3794
[80] Francis, L., et al., *Controlled Delivery of Gentamicin Using Poly(3-hydroxybutyrate) Microspheres.* International Journal of Molecular Sciences **2011**, *12(7)*, 4294-4314
[81] Dessy, A., et al., *Dead Sea Minerals loaded polymeric nanoparticles.* Colloids and Surfaces B: Biointerfaces **2011**, *87(2)*, 236-242
[82] Cun, D., et al., *Preparation and characterization of poly(dl-lactide-co-glycolide) nanoparticles for siRNA delivery.* International Journal of Pharmaceutics **2010**, *390(1)*, 70-75
[83] Zambaux, M.F., et al., *Influence of experimental parameters on the characteristics of poly(lactic acid) nanoparticles prepared by a double emulsion method.* Journal of Controlled Release **1998**, *50(1-3)*, 31-40
[84] Musyanovych, A., Schmitz-Wienke J., Mailänder V., Walther P., Landfester K., *Preparation of Biodegradable Polymer Nanoparticles by Miniemulsion Technique and Their Cell Interactions.* Macromolecular Bioscience **2008**, *8*, 127-139
[85] Bilati, U., E. Allémann, and E. Doelker, *Sonication Parameters for the Preparation of Biodegradable Nanocapsulesof Controlled Size by the Double Emulsion Method.* Pharmaceutical Development and Technology **2003**, *8(1)*, 1-9
[86] Quaglia, F., et al., *Nanoscopic core-shell drug carriers made of amphiphilic triblock and star-diblock copolymers.* International Journal of Pharmaceutics **2006**, *324(1)*, 56-66
[87] Fessi, H., et al., *Nanocapsule formation by interfacial polymer deposition following solvent displacement.* International Journal of Pharmaceutics **1989**, *55*, R1-R4
[88] Anton, N., J.-P. Benoit, and P. Saulnier, *Design and production of nanoparticles formulated from nano-emulsion templates--A review.* Journal of Controlled Release **2008**, *128(3)*, 185-199
[89] Moinard-Chécot, D., et al., *Mechanism of nanocapsules formation by the emulsion–diffusion process.* Journal of Colloid and Interface Science **2008**, *317(2)*, 458-468
[90] Murakami, H., et al., *Preparation of poly(dl-lactide-co-glycolide) nanoparticles by modified spontaneous emulsification solvent diffusion method.* International Journal of Pharmaceutics **1999**, *187(2)*, 143-152
[91] Mora-Huertas, C.E., H. Fessi, and A. Elaissari, *Polymer-based nanocapsules for drug delivery.* International Journal of Pharmaceutics **2010**, *385*, 113-142
[92] Ganachaud, F. and J.L. Katz, *Nanoparticles and Nanocapsules Created Using the Ouzo Effect: Spontaneous Emulsification as an Alternative to Ultrasonic and High-Shear Devices.* ChemPhysChem **2005**, *6(2)*, 209-216
[93] Allémann, E., R. Gurny, and E. Doelker, *Preparation of aqueous polymeric nanodispersions by a reversible salting-out process: influence of process parameters on particle size.* International Journal of Pharmaceutics **1992**, *87(1-3)*, 247-253
[94] Peter, Y., *Strategies for particle design using supercritical fluid technologies.* Pharmaceutical Science & Technology Today **1999**, *2(11)*, 430-440
[95] Sun, Y.-P., *Preparation and Processing of Nanoscale Materials by Supercritical Fluid Technology*, Y.-P. Sun, Editor **2002,** CRC Press: New York
[96] Tai, Y., et al., *Recent research progress on the preparation and application of magnetic nanospheres.* Polymer International **2011**, *60(7)*, 976-994

[97] Wang, F. and S. Hu, *Electrochemical sensors based on metal and semiconductor nanoparticles*. Microchimica Acta **2009**, *165(1)*, 1-22
[98] Wang, Y. and L. Chen, *Quantum dots, lighting up the research and development of nanomedicine.* Nanomedicine: Nanotechnology, Biology and Medicine **2011**, *7(4)*, 385-402
[99] Park, J., et al., *Synthesis of Monodisperse Spherical Nanocrystals.* Angewandte Chemie International Edition **2007**, *46(25)*, 4630-4660
[100] LaMer, V.K. and R.H. Dinegar, *Theory, Production and Mechanism of Formation of Monodispersed Hydrosols.* Journal of the American Chemical Society **1950**, *72(11)*, 4847-4854
[101] Peng, X., J. Wickham, and A.P. Alivisatos, *Kinetics of II-VI and III-V Colloidal Semiconductor Nanocrystal Growth: "Focusing" of Size Distributions.* Journal of the American Chemical Society **1998**, *120(21)*, 5343-5344
[102] Peng, Z.A. and X. Peng, *Nearly Monodisperse and Shape-Controlled CdSe Nanocrystals via Alternative Routes: Nucleation and Growth.* Journal of the American Chemical Society **2002**, *124(13)*, 3343-3353
[103] Ozin, G.A. and A.C. Arsanault, *Nanochemistry. a chemical approach to nanomaterials*. **2005,** Cambridge: The Royal Society of Chemistry
[104] Turkevich J., Stevenson P. C., and H. J., *A study of the nucleation and growth processes in the synthesis of colloidal gold.* Discussions of the Faraday Society **1951**, *11*, 55-75
[105] Frens, G., *Particle size and sol stability in metal colloids.* Colloid & Polymer Science **1972**, *250*, 736-741
[106] Kundu, S. and H. Liang, *Photoinduced Formation of Shape-Selective Pt Nanoparticles.* Langmuir **2009**, *26(9)*, 6720-6727
[107] Murray, C.B., D.J. Norris, and M.G. Bawendi, *Synthesis and characterization of nearly monodisperse CdE (E = sulfur, selenium, tellurium) semiconductor nanocrystallites.* Journal of the American Chemical Society **1993**, *115(19)*, 8706-8715
[108] Jiang, J.Z., et al., *Triangle-shape ZnO prepared by thermal decomposition.* Materials Letters **2007**, *61(16)*, 3416-3420
[109] Bourgeat-Lami E. and S.A.F. Bon, *Organic/Inorganic Composite Latexes: The Marriage of Emulsion Polymerization and Inorganic Chemistry*, in *Hybrid Latex Particles*, van Herk A. M. and L. K., Editors **2010,** Springer: Berlin, Heidelberg, 53-123
[110] Peres M and C.L. C., *A green-emitting CdSe/poly(butyl acrlytate) nanocomposite.* Nanotechnology **2005**, *16(1969-1973)*
[111] Ge, J., et al., *Superparamagnetic Composite Colloids with Anisotropic Structures.* Journal of the American Chemical Society **2007**, *129(29)*, 8974-8975
[112] Crespy, D. and K. Landfester, *Synthesis of polyvinylpyrrolidone/silver nanoparticles hybrid latex in non-aqueous miniemulsion at high temperature.* Polymer **2009**, *50(7)*, 1616-1620
[113] Agrawal, M., S. Gupta, and M. Stamm, *Recent developments in fabrication and applications of colloid based composite particles.* Journal of Materials Chemistry **2011**, *21(3)*, 615-627
[114] Tian, C., et al., *Synthesis of Ag-coated polystyrene colloids by an improved surface seeding and shell growth technique.* Journal of Solid State Chemistry **2006**, *179(11)*, 3270-3276

[115] Caruso, F., et al., *Electrostatic Self-Assembly of Silica Nanoparticle−Polyelectrolyte Multilayers on Polystyrene Latex Particles.* Journal of the American Chemical Society **1998**, *120(33)*, 8523-8524
[116] Ramsen, W., *Separation of Solids in the Surface-layers of Solutions and Suspensions.* Proceedings of the Royal Society London **1903**, *72*, 156
[117] Pickering, S.U., *Emulsions.* Journal of the American Chemical Society **1907**, *91*, 2001
[118] Balazs, A.C., T. Emrick, and T.P. Russell, *Nanoparticle Polymer Composites: Where Two Small Worlds Meet.* Science **2006**, *314(5802)*, 1107-1110
[119] Agrawal, M., et al., *Nano-Level Mixing of ZnO into Poly(methyl methacrylate).* Macromolecular Chemistry and Physics **2010**, *211(17)*, 1925-1932
[120] De Paul, S.M., et al., *Structure, Mobility, and Interface Characterization of Self-Organized Organic−Inorganic Hybrid Materials by Solid-State NMR.* Journal of the American Chemical Society **1999**, *121(24)*, 5727-5736
[121] Sanchez, C., et al., *"Chimie douce": A land of opportunities for the designed construction of functional inorganic and hybrid organic-inorganic nanomaterials.* Comptes Rendus Chimie, *13(1-2)*, 3-39
[122] Schexnailder, P. and G. Schmidt, *Nanocomposite polymer hydrogels.* Colloid & Polymer Science **2009**, *287(1)*, 1-11
[123] Loizou, E., et al., *Dynamic Responses in Nanocomposite Hydrogels.* Macromolecules **2006**, *39(4)*, 1614-1619
[124] Tokarev, I., I. Tokareva, and S. Minko, *Gold-Nanoparticle-Enhanced Plasmonic Effects in a Responsive Polymer Gel.* Advanced Materials **2008**, *20(14)*, 2730-2734
[125] Murali Mohan, Y., et al., *Hydrogel networks as nanoreactors: A novel approach to silver nanoparticles for antibacterial applications.* Polymer **2007**, *48(1)*, 158-164
[126] Schmidt, A., *Thermoresponsive magnetic colloids.* Colloid & Polymer Science **2007**, *285(9)*, 953-966
[127] Zhao, X., et al., *Active scaffolds for on-demand drug and cell delivery.* Proceedings of the National Academy of Sciences **2010**
[128] Schlegel, H.-G., *Allgemeine Mikrobiologie*, **1992,** Thieme: Stuttgart, New York
[129] Madigan, M.T., et al., *Brock-Biology of Microorganisms*. **2009,** San Francisco: Pearson International Edition
[130] Bos, R., H.C. van der Mei, and H.J. Busscher, *Physico-chemistry of initial microbial adhesive interactions – its mechanisms and methods for study.* Fems Microbiology Reviews **1999**, *23(2)*, 179-230
[131] Busscher, H.J., et al., *Interfacial re-arrangement in initial microbial adhesion to surfaces.* Current Opinion in Colloid & Interface Science **2010**, *15(6)*, 510-517
[132] Busscher, H.J., W. Norde, and H.C. van der Mei, *Specific Molecular Recognition and Nonspecific Contributions to Bacterial Interaction Forces.* Applied and Environmental Microbiology **2008**, *74(9)*, 2559-2564
[133] Busscher, H.J., et al., *Biofilm Formation on Dental Restorative and Implant Materials.* Journal of Dental Research **2010**, *89(7)*, 657-665
[134] Chen, Y., et al., *Statistical Analysis of Long- and Short-Range Forces Involved in Bacterial Adhesion to Substratum Surfaces as Measured Using Atomic Force Microscopy.* Applied and Environmental Microbiology **2011**, *77(15)*, 5065-5070
[135] Geoghegan, M., et al., *The polymer physics and chemistry of microbial cell attachment and adhesion.* Faraday Discussions **2008**, *139*, 85-103
[136] Flegler S., Heckman JW. jr. , and K.L. Klomparens, *Elektronenmikroskopie - Grundlagen, Methoden, Anwendungen*. **1995,** Heidelberg: Spektrum Verlag

[137] http://www.hitachi-hitec.com/em/.
[138] Goldstein, J.I., *Scanning electron microscopy and X-ray microanalysis*. 2nd edition ed. **1992,** New York, London: Plenum Press
[139] Schärtl, W., *Light Scattering from Polymer Solutions and Nanoparticle Dispersions*. **2007,** Berlin: Springer
[140] Müller, R.H., *Zetapotential und Partikelladung in der Laborpraxis*. **1996,** Stuttgart: Wissenschaftliche Verlagsgesellschaft mbH Stuttgart
[141] Berne B. and P. R., *Dynamic light scattering with applications to chemistry, biology and physics*. **2000,** Mineola, New York: Dover Publishing
[142] Olesik, J.W., *Elemental analysis using ICP-OES and ICP/MS.* Analytical Chemistry **1991**, *63(1)*, 12A-21A
[143] Vogel N., H.C.P., Schuller K., Landfester K., Weiss C. K., *Accurate Elemental Analysis of Metal Containing Polymer Latexes Using ICP-Optical Emission Spectroscopy.* Macromolecular Chemistry and Physics **2010**
[144] Hesse M., Meier H., and Z. B., *Spektroskopische Methoden in der organischen Chemie*. **1991,** Suttgart, New York: Thieme
[145] Hamid S. M., S.D.C., *Novel quarternary ammonium amphiphilic (meth)acrylates: 1. Synthesis, melting and interfacial behaviour.* Polymer **1986**, *28*, 325-331
[146] Beines, P.W., et al., *Responsive Thin Hydrogel Layers from Photo-Cross-Linkable Poly(N-isopropylacrylamide) Terpolymers†.* Langmuir **2007**, *23(4)*, 2231-2238
[147] Ludbrook, J., *Repeated measurements and multiple comparisons in cardiovascular research.* Cardiovasc Res **1994**, *28(3)*, 303-11
[148] Krishnan, S., C.J. Weinman, and C.K. Ober, *Advances in polymers for anti-biofouling surfaces.* Journal of Materials Chemistry **2008**, *18(29)*, 3405-3413
[149] Saldarriaga Fernández, I.C., et al., *The inhibition of the adhesion of clinically isolated bacterial strains on multi-component cross-linked poly(ethylene glycol)-based polymer coatings.* Biomaterials **2007**, *28(28)*, 4105-4112
[150] Veronese, F.M. and G. Pasut, *PEGylation, successful approach to drug delivery.* Drug Discovery Today **2005**, *10(21)*, 1451-1458
[151] Prime, K.L. and G.M. Whitesides, *Self-assembled organic monolayers: model systems for studying adsorption of proteins at surfaces.* Science (New York, N.Y.) **1991**, *252(5010)*, 1164-7
[152] Rodriguez Emmenegger, C., et al., *Interaction of Blood Plasma with Antifouling Surfaces.* Langmuir **2009**, *25(11)*, 6328-6333
[153] Jeon, S.I., et al., *Protein—surface interactions in the presence of polyethylene oxide: I. Simplified theory.* Journal of Colloid and Interface Science **1991**, *142(1)*, 149-158
[154] Szleifer, I., *Protein Adsorption on Surfaces with Grafted Polymers: A Theoretical Approach.* Biophysical Journal **1997**, *72(2, Part 1)*, 595-612
[155] Wang, R.L.C., H. Jurgen Kreuzer, and M. Grunze, *The interaction of oligo(ethylene oxide) with water: a quantum mechanical study.* Physical Chemistry Chemical Physics **2000**, *2(16)*, 3613-3622
[156] Benhabbour, S.R., et al., *Protein Resistance of Surfaces Prepared by Chemisorption of Monothiolated Poly(ethylene glycol) to Gold and Dendronization with Aliphatic Polyester Dendrons: Effect of Hydrophilic Dendrons.* Macromolecules **2008**, *41(7)*, 2567-2576
[157] Prime, K.L. and G.M. Whitesides, *Adsorption of proteins onto surfaces containing end-attached oligo(ethylene oxide): a model system using self-assembled monolayers.* Journal of the American Chemical Society **1993**, *115(23)*, 10714-10721

[158] Tedjo, C., et al., *Bacteria-surface interaction in the presence of proteins and surface attached poly(ethylene glycol) methacrylate chains.* Journal of Biomedical Materials Research Part A **2007**, *82A(2)*, 479-491
[159] Jiang, H., et al., *Synthesis of dendrimer-type poly(ethylene glycol) structures from plasma-functionalized silicone rubber surfaces.* Journal of Applied Polymer Science **2006**, *102(3)*, 2324-2337
[160] Khoo, X., et al., *Directed Assembly of PEGylated-Peptide Coatings for Infection-Resistant Titanium Metal.* Journal of the American Chemical Society **2009**, *131(31)*, 10992-10997
[161] Gillich, T., et al., *Self-Assembly of Focal Point Oligo-catechol Ethylene Glycol Dendrons on Titanium Oxide Surfaces: Adsorption Kinetics, Surface Characterization, and Nonfouling Properties.* Journal of the American Chemical Society **2011**, *133(28)*, 10940-10950
[162] Ma, H., et al., *"Non-Fouling" Oligo(ethylene glycol)- Functionalized Polymer Brushes Synthesized by Surface-Initiated Atom Transfer Radical Polymerization.* Advanced Materials **2004**, *16(4)*, 338-341
[163] Benhabbour, S.R., H. Sheardown, and A. Adronov, *Cell adhesion and proliferation on hydrophilic dendritically modified surfaces.* Biomaterials **2008**, *29(31)*, 4177-4186
[164] Tziampazis, E., J. Kohn, and P.V. Moghe, *PEG-variant biomaterials as selectively adhesive protein templates: model surfaces for controlled cell adhesion and migration.* Biomaterials **2000**, *21(5)*, 511-520
[165] Meng, F.H., G.H.M. Engbers, and J. Feijen, *Polyethylene glycol-grafted polystyrene particles.* Journal of Biomedical Materials Research Part A **2004**, *70A(1)*, 49-58
[166] Liu, Z.F., et al., *Poly(ethylene oxide) macromonomer-grafted polymer nanoparticles synthesised by emulsifier-free emulsion polymerisation.* Colloid and Polymer Science **2003**, *281(9)*, 815-822
[167] Hough D. B. and L. Thompson, *Effect of nonionic surfactants on the stability of dispersions*, in *Nonionic Surfactants: Physical Chemistry*, M.J. Schick, Editor **1987,** Marcel Dekker: New York
[168] Seebergh J. E. and B.J. C., *The effect of organic cosolvent on the aggretation stability of an aqueous polystyrene latex dispersion.* Colloids and Surfaces A: Physicochemical and Engineering Aspects **1997**, *121(1)*, 89-98
[169] Brindley, A., et al., *Polystyrene Colloids with Surface-Grafted Polyethylene Oxide as Model Systems for Site-Specific Drug Delivery: I. Preparation and Surface Chemical Characterization Using SIMS and XPS.* Journal of Colloid and Interface Science **1995**, *171(1)*, 150-161
[170] Chern, C.S., C.K. Lee, and K.C. Liu, *Synthesis and characterization of PEG-modified polystyrene particles and isothermal equilibrium adsorption of bovine serum albumin on these particles.* Journal of Polymer Research **2006**, *13(3)*, 247-254
[171] Dunn, S.E., et al., *Polystyrene-Poly(ethylene glycol) (PS-PEG2000) Particles as Model Systems for Site Specific Drug Delivery. 2. The Effect of PEG Surface Density on the In Vitro Cell Interaction and In Vivo Biodistribution.* Pharmaceutical Research **1994**, *11(7)*, 1016-1022
[172] Brandrup J., I.E.H., Grulke E. A., *Polymer Handbook*, ed. Wiley. **1999,** New York
[173] Roosjen, A., et al., *Bacterial factors influencing adhesion of Pseudomonas aeruginosa strains to a poly(ethylene oxide) brush.* Microbiology **2006**, *152(9)*, 2673-2682

[174] Cao, Z., et al., *Synthesis of raspberry-like organic–inorganic hybrid nanocapsules via pickering miniemulsion polymerization: Colloidal stability and morphology.* Journal of Polymer Science Part A: Polymer Chemistry **2011**, *49(11)*, 2382-2394
[175] Isquith A.J., A.E., Walters P.A., *Surface-bonded antimicrobial activity of an organosilicon quarternary ammonium chloride.* Applied Microbiology **1972**, *24*, 859-863
[176] McDonnell G., R.A.D., *Antiseptics and Disinfectants: Activiy, Action and Resistance.* Clinical Microbiology Reviews **1999**, *12(1)*, 147-179
[177] Tiller, J.C., C. Sprich, and L. Hartmann, *Amphiphilic conetworks as regenerative controlled releasing antimicrobial coatings.* Journal of Controlled Release **2005**, *103(2)*, 355-367
[178] Waschinski, C.J. and J.C. Tiller, *Poly(oxazoline)s with telechelic antimicrobial functions.* Biomacromolecules **2005**, *6(1)*, 235-243
[179] Fuchs, A.D. and J.C. Tiller, *Contact-Active Antimicrobial Coatings Derived from Aqueous Suspensions.* Angewandte Chemie International Edition **2006**, *45(40)*, 6759-6762
[180] Tiller, J.C., et al., *Polymer surfaces derivatized with poly(vinyl-N-hexylpyridinium) kill airborne and waterborne bacteria.* Biotechnology and Bioengineering **2002**, *79(4)*, 465-471
[181] Ravikumar, T., et al., *Surface-Active Antifungal Polyquaternary Amine.* Biomacromolecules **2006**, *7(10)*, 2762-2769
[182] Murata H., et al., *Permanent, non-leaching antibacterial surfaces--2: How high density cationic surfaces kill bacterial cells.* Biomaterials **2007**, *28(32)*, 4870-4879
[183] Cheng, Z., et al., *Polymer Microspheres with Permanent Antibacterial Surface from Surface-Initiated Atom Transfer Radical Polymerization.* Industrial & Engineering Chemistry Research **2005**, *44(18)*, 7098-7104
[184] Cakmak, I., et al., *Synthesis and characterization of novel antimicrobial cationic polyelectrolytes.* European Polymer Journal **2004**, *40(10)*, 2373-2379
[185] Dizman, B., M.O. Elasri, and L.J. Mathias, *Synthesis and antimicrobial activities of new water-soluble bis-quaternary ammonium methacrylate polymers.* Journal of Applied Polymer Science **2004**, *94(2)*, 635-642
[186] Kügler R., B.O., Rondelez F., *Evidence of a charge-density threshold for optimum efficiency of biocidal cationic surfaces.* Microbiology **2005**, *151*, 1241-1248
[187] Binder, W.H., *Polymer-Induced Transient Pores in Lipid Membranes.* Angewandte Chemie International Edition **2008**, *47(17)*, 3092-3095
[188] Caillier, L., et al., *Synthesis and antimicrobial properties of polymerizable quaternary ammoniums.* European Journal of Medicinal Chemistry **2009**, *44(8)*, 3201-3208
[189] Landfester, K., *Miniemulsion polymerization and the structure of polymer and hybrid nanoparticles.* Angewandte Chemie **2009**
[190] Nagai, K., et al., *Polymerization of surface-active monomers. I. Micellization and polymerization of higher alkyl salts of dimethylaminoethyl methacrylate.* Journal of Polymer Science: Polymer Chemistry Edition **1985**, *23(4)*, 1221-1230
[191] Baines, F.L., et al., *Use of Block Copolymer Stabilizers for the Dispersion Polymerization of Styrene in Alcoholic Media.* Macromolecules **1996**, *29(9)*, 3096-3102
[192] Creutz, S., P. Teyssie, and R. Jerome, *Living Anionic Homopolymerization and Block Copolymerization of (Dimethylamino)ethyl Methacrylate.* Macromolecules **1997**, *30(1)*, 6-9

[193] Zhang, M.Z., et al., *Kinetics of styrene miniemulsion polymerization using poly (stearyl methacrylate-co-(N,N-dimethylamino)ethyl methacrylate as surfactant.* Colloids and Surfaces a-Physicochemical and Engineering Aspects **2010**, *360(1-3)*, 190-197

[194] Mukerjee P. and M. K., *Critical Micelle Concentrations of Aqueous Surfactant Systems*, **1971,** U. S. Department of Commerce, National Bureau of Standards: Washington

[195] Modaressi, A., et al., *CTAB aggregation in aqueous solutions of ammonium based ionic liquids; conductimetric studies.* Colloids and Surfaces A: Physicochemical and Engineering Aspects **2007**, *296(1-3)*, 104-108

[196] Pons, J.L., et al., *Evaluation of antimicrobial interactions between chlorhexidine, quaternary ammonium compounds, preservatives and excipients.* Journal of Applied Microbiology **1992**, *73(5)*, 395-400

[197] Kügler, R., O. Bouloussa, and F. Rondelez, *Evidence of a charge-density threshold for optimum efficiency of biocidal cationic surfaces.* Microbiology **2005**, *151(5)*, 1341-1348

[198] Jaeger, W., J. Bohrisch, and A. Laschewsky, *Synthetic polymers with quaternary nitrogen atoms--Synthesis and structure of the most used type of cationic polyelectrolytes.* Progress in Polymer Science **2010**, *35(5)*, 511-577

[199] Hamid S. M., S.D.C., *Novel quarternary ammonium amphiphilic (meth)acrylates: 2. Thermally and photochemically initiated polymerizations.* Polymer **1986**, *28*, 332-339

[200] Katsutoshi, N. and O. Yoshiyuki, *Polymerization of surface-active monomers. II. Polymerization of quarternary alkyl salts of dimethylaminoethyl methacrylate with a different alkyl chain length.* Journal of Polymer Science Part A: Polymer Chemistry **1987**, *25(1)*, 1-14

[201] Lu, G., D. Wu, and R. Fu, *Studies on the synthesis and antibacterial activities of polymeric quaternary ammonium salts from dimethylaminoethyl methacrylate.* Reactive and Functional Polymers **2007**, *67(4)*, 355-366

[202] Dautzenberg, H., et al., *Polyelectrolytes-formation, characterization, and application*. **1994,** Munich, Vienna, New York: Hanser Publisher

[203] Spychaj, T., M. Bohdanecký, and D. Berek, *A viscometric study of solutions of poly(methyl methacrylate) and polystyrene in N,N-dimethylformamide and its mixtures with inorganic salts.* Acta Polymerica **1986**, *37(2)*, 93-96

[204] Mistlberger, G., et al., *Mini-emulsion solvent evaporation: a simple and versatile way to magnetic nanosensors.* Microchimica Acta **2011**, *172(3-4)*, 299-308

[205] Lemoine, D. and V. Préat, *Polymeric nanoparticles as delivery system for influenza virus glycoproteins.* Journal of Controlled Release **1998**, *54(1)*, 15-27

[206] *Plastics-Measurement of antibacterial activity on plastics surfaces*, in *ISO22196* **2007,** ISO copyright office: Switzerland

[207] Bishop D. G., Rutberg L., and S. B., *The solubilization of the cytoplasmic membrane of Bacillus subtilis by sodium dodecyl sulphate.* Eur. J. Biochem. **1967**, *2(4)*, 454-9

[208] Mandy Wootton, P., et al., *Evaluation of the Effectiveness of Common Hospital Hand Disinfectants Against Methicillin-Resistant Staphylococcus aureus, Glycopeptide-Intermediate S. aureus, and Heterogeneous Glycopeptide-Intermediate S. aureus* • Infection Control and Hospital Epidemiology **2009**, *30(3)*, 226-232

[209] O'Neill, A.J., et al., *Comparison of assays for detection of agents causing membrane damage in Staphylococcus aureus.* Journal of Antimicrobial Chemotherapy **2004**, *54(6)*, 1127-1129

[210] Quarta, A., et al., *Multifunctional Nanostructures Based on Inorganic Nanoparticles and Oligothiophenes and Their Exploitation for Cellular Studies.* Journal of the American Chemical Society **2008**, *130(32)*, 10545-10555
[211] Jafry, H.R., et al., *Simple Route to Enhanced Photocatalytic Activity of P25 Titanium Dioxide Nanoparticles by Silica Addition.* Environmental Science & Technology **2010**
[212] Prucek, R., et al., *The targeted antibacterial and antifungal properties of magnetic nanocomposite of iron oxide and silver nanoparticles.* Biomaterials **2011**, *32(21)*, 4704-4713
[213] Monteiro, D.R., et al., *The growing importance of materials that prevent microbial adhesion: antimicrobial effect of medical devices containing silver.* International Journal of Antimicrobial Agents **2009**, *34(2)*, 103-110
[214] Roe, D., et al., *Antimicrobial surface functionalization of plastic catheters by silver nanoparticles.* Journal of Antimicrobial Chemotherapy **2008**, *61(4)*, 869-876
[215] AshaRani, P.V., et al., *Cytotoxicity and Genotoxicity of Silver Nanoparticles in Human Cells.* ACS Nano **2008**, *3(2)*, 279-290
[216] Geranio, L., M. Heuberger, and B. Nowack, *The Behavior of Silver Nanotextiles during Washing.* Environmental Science & Technology **2009**, *43(21)*, 8113-8118
[217] Naik, A.J.T., et al., *Antimicrobial activity of polyurethane embedded with methylene blue, toluidene blue and gold nanoparticles against Staphylococcus aureus; illuminated with white light.* Materials Chemistry and Physics **2011**, *129(1-2)*, 446-450
[218] Zhang, W., et al., *Antimicrobial polyethylene with controlled copper release.* Journal of Biomedical Materials Research Part A **2007**, *83A(3)*, 838-844
[219] Akhavan, O. and E. Ghaderi, *Cu and CuO nanoparticles immobilized by silica thin films as antibacterial materials and photocatalysts.* Surface and Coatings Technology **2010**, *205(1)*, 219-223
[220] Cady, N.C., J.L. Behnke, and A.D. Strickland, *Copper-Based Nanostructured Coatings on Natural Cellulose: Nanocomposites Exhibiting Rapid and Efficient Inhibition of a Multi-Drug Resistant Wound Pathogen, A. baumannii, and Mammalian Cell Biocompatibility In Vitro.* Advanced Functional Materials **2011**, *21(13)*, 2506-2514
[221] Mihailovic, D., et al., *Functionalization of polyester fabrics with alginates and TiO2 nanoparticles.* Carbohydrate Polymers **2010**, *79(3)*, 526-532
[222] Makhluf, S., et al., *Microwave-Assisted Synthesis of Nanocrystalline MgO and Its Use as a Bacteriocide.* Advanced Functional Materials **2005**, *15(10)*, 1708-1715
[223] Morganti, P., *Use and potential of nanotechnology in cosmetic dermatology.* Clinical, Cosmetical and Investigational Dermatology **2010**, *3*, 5-13
[224] Ozgur, U., et al., *A comprehensive review of ZnO materials and devices.* Journal of Applied Physics **2005**, *98(4)*
[225] Wu, J.S. and D.F. Xue, *Progress of Science and Technology of ZnO as Advanced Material.* Science of Advanced Materials **2011**, *3(2)*, 127-149
[226] Brayner, R., et al., *Toxicological Impact Studies Based on Escherichia coli Bacteria in Ultrafine ZnO Nanoparticles Colloidal Medium.* Nano Letters **2006**, *6(4)*, 866-870
[227] Hanley C., L.J., Punnose A., Reddy K M., Coombs I., Coombs A., Feris K., Wingett D., *Preferential killing of cancer cells and activated human T cells using ZnO nanoparticles.* Nanotechnology **2008**, *19*, 295103
[228] Huang, Z., et al., *Toxicological Effect of ZnO Nanoparticles Based on Bacteria.* Langmuir **2008**, *24(8)*, 4140-4144

[229] Padmavathy, N. and R. Vijayaraghavan, *Enhanced bioactivity of ZnO nanoparticles-an antimicrobial study.* Science and Technology of Advanced Materials **2008**, *9(3)*
[230] Karunakaran, C., P. Gomathisankar, and G. Manikandan, *Preparation and characterization of antimicrobial Ce-doped ZnO nanoparticles for photocatalytic detoxification of cyanide.* Materials Chemistry and Physics **2010**, *123(2-3)*, 585-594
[231] Zhang, L., et al., *Investigation into the antibacterial behaviour of suspensions of ZnO nanoparticles (ZnO nanofluids).* Journal of Nanoparticle Research **2007**, *9(3)*, 479-489
[232] Raghupathi, K.R., R.T. Koodali, and A.C. Manna, *Size-Dependent Bacterial Growth Inhibition and Mechanism of Antibacterial Activity of Zinc Oxide Nanoparticles.* Langmuir **2011**, *27(7)*, 4020-4028
[233] Jones, N., et al., *Antibacterial activity of ZnO nanoparticle suspensions on a broad spectrum of microorganisms.* FEMS Microbiology Letters **2008**, *279(1)*, 71-76
[234] Zhang, L.L., et al., *Mechanistic investigation into antibacterial behaviour of suspensions of ZnO nanoparticles against E. coli.* Journal of Nanoparticle Research **2010**, *12(5)*, 1625-1636
[235] Li, M., L.Z. Zhu, and D.H. Lin, *Toxicity of ZnO Nanoparticles to Escherichia coil: Mechanism and the Influence of Medium Components.* Environmental Science & Technology **2011**, *45(5)*, 1977-1983
[236] Nair, S., et al., *Role of size scale of ZnO nanoparticles and microparticles on toxicity toward bacteria and osteoblast cancer cells.* Journal of Materials Science-Materials in Medicine **2009**, *20*, 235-241
[237] Song, W., et al., *Role of the dissolved zinc ion and reactive oxygen species in cytotoxicity of ZnO nanoparticles.* Toxicology Letters **2010**, *199(3)*, 389-397
[238] De Berardis, B., et al., *Exposure to ZnO nanoparticles induces oxidative stress and cytotoxicity in human colon carcinoma cells.* Toxicology and Applied Pharmacology **2010**, *246(3)*, 116-127
[239] Zhang, M.M., et al., *Synthesis, characterization and application of well-defined environmentally responsive polymer brushes on the surface of colloid particles.* Polymer **2007**, *48(7)*, 1989-1997
[240] Cho, K.-H., et al., *The study of antimicrobial activity and preservative effects of nanosilver ingredient.* Electrochimica Acta **2005**, *51(5)*, 956-960
[241] Soukupova, J., et al., *Comprehensive study on surfactant role on silver nanoparticles (NPs) prepared via modified Tollens process.* Materials Chemistry and Physics **2008**, *111(1)*, 77-81
[242] Kwon, S.G. and T. Hyeon, *Colloidal Chemical Synthesis and Formation Kinetics of Uniformly Sized Nanocrystals of Metals, Oxides, and Chalcogenides.* Accounts of Chemical Research **2008**, *41(12)*, 1696-1709
[243] Xiong H.-M., et al., *Stable Aqueous ZnO@Polymer Core-Shell Nanoparticles with Tunable Photoluminescence and Their Apllication in Cell Imaging.* Journal of the American Chemical Society **2008**, *130*, 7522-7523
[244] Lu X., et al., *Nanocomposites of poly(l-lactide) and surface-grafted TiO2 nanoparticles: Synthesis and characterization.* European Polymer Journal **2008**, *44(8)*, 2476-81
[245] Soppimath, K.S., et al., *Biodegradable polymeric nanoparticles as drug delivery devices.* Journal of Controlled Release **2001**, *70(1-2)*, 1-20
[246] Hong, Y., et al., *Synthesis and properties of poly(D,L-lactide) drug carrier with maghemite nanoparticles.* Materials Science & Engineering: C (Materials for Biological Applications) **2010**, *30(4)*, 618-623

[247] Cichinelli LD, Gonzales S. J. M., and A.T. J., *Current concepts of absorbable fixation in first ray surgery.* Clin Podiatr Med Surg **1996**, *13(3)*, 533-47
[248] Garg S. and S. P., *Biodegradable stents and non-biodegradable stents.* Minerva Cardioangiologica **2009**, *57(5)*, 537-65
[249] Wijdicks, C., et al., *Biomechanical evaluation of a medial knee reconstruction with comparison of bioabsorbable interference screw constructs and optimization with a cortical button.* Knee Surgery, Sports Traumatology, Arthroscopy **2010**, *18(11)*, 1532-1541
[250] Burg, K.J.L., S. Porter, and J.F. Kellam, *Biomaterial developments for bone tissue engineering.* Biomaterials **2000**, *21(23)*, 2347-2359
[251] Ma, F., et al., *Nanocomposites of poly(l-lactide) and surface modified magnesia nanoparticles: Fabrication, mechanical property and biodegradability.* Journal of Physics and Chemistry of Solids **2011**, *72(2)*, 111-116
[252] Xu X., et al., *Fabrication of biodegradable electrospun poly(L-lactide-co-glycolide) fibers with antimicrobial nanosilver particles.* Journal of Nanoscience and Nanotechnology **2008**, *8(10)*, 5066-5070
[253] Lecaroz M. C., et al., *Poly(D,L-Lactide-Coglycolide) Particles Containing Gentamicin: Pharmacokinetics and Pharmacodynamics in Brucella melitensis - Infected Mice.* Antimicrobial Agents and Chemotherapy **2007**, 1185-1190
[254] Incoronato, A.L., et al., *Agar hydrogel with silver nanoparticles to prolong the shelf life of Fior di Latte cheese.* Journal of Dairy Science **2011**, *94(4)*, 1697-1704
[255] Yamashita, T., et al., *Cultivation and recovery of vascular endothelial cells in microchannels of a separable micro-chemical chip.* Biomaterials **2011**, *32(10)*, 2459-2465
[256] Yang, J., et al., *Reconstruction of functional tissues with cell sheet engineering.* Biomaterials **2007**, *28(34)*, 5033-5043
[257] Duarte, A.R.C., J.F. Mano, and R.L. Reis, *Thermosensitive polymeric matrices for three-dimensional cell culture strategies.* Acta Biomaterialia **2011**, *7(2)*, 526-529
[258] Nash M. E., C.W.M., Nikoloskya N., Yang R., O'Connell C., Gorelov A. V., Docery P., Liptrot C., Lyng F. M., Garcia A., Rochev Y. A., *Straightforward, One-Step Fabrication of Ultrathin Thermoresponsive Films from Commerically Avialbable pNIPAm for Cell Culture and Recovery.* Applied Materials & Interfaces **2011**
[259] Ista, L.K. and G.P. Lopez, *Lower critical solubility temperature materials as biofouling release agents.* Journal of Industrial Microbiology & Biotechnology **1998**, *20(2)*, 121-125
[260] Mano, J.F., *Stimuli-Responsive Polymeric Systems for Biomedical Applications.* Advanced Engineering Materials **2008**, *10(6)*, 515-527
[261] Cole, M.A., et al., *Stimuli-responsive interfaces and systems for the control of protein-surface and cell-surface interactions.* Biomaterials **2009**, *30(9)*, 1827-1850
[262] Peppas, N.A., et al., *Hydrogels in biology and medicine: From molecular principles to bionanotechnology.* Advanced Materials **2006**, *18(11)*, 1345-1360
[263] van den Brom, C.R., et al., *The swelling behaviour of thermoresponsive hydrogel/silica nanoparticle composites.* Journal of Materials Chemistry **2010**, *20(23)*, 4827-4839
[264] Gianneli, M., et al., *Dynamics of swollen gel layers anchored to solid surfaces.* Soft Matter **2008**, *4(7)*, 1443-1447
[265] Urban, M., A. Musyanovych, and K. Landfester, *Fluorescent Superparamagnetic Polylactide Nanoparticles by Combination of Miniemulsion and Emulsion/Solvent*

Evaporation Techniques. Macromolecular Chemistry and Physics **2009**, *210(11)*, 961-970

[266] Liu, P., *Facile preparation of monodispersed core/shell zinc oxide@polystyrene (ZnO@PS) nanoparticles via soapless seeded microemulsion polymerization.* Colloids and Surfaces a-Physicochemical and Engineering Aspects **2006**, *291(1-3)*, 155-161

[267] Tang, E. and S. Dong, *Preparation of styrene polymer/ZnO nanocomposite latex via miniemulsion polymerization and its antibacterial property.* Colloid & Polymer Science **2009**, *287(9)*, 1025-1032

[268] Agrawal, M., et al., *Polystyrene−ZnO Composite Particles with Controlled Morphology.* Chemistry of Materials **2007**, *19(7)*, 1845-1852

[269] Singh, A.K., V. Viswanath, and V.C. Janu, *Synthesis, effect of capping agents, structural, optical and photoluminescence properties of ZnO nanoparticles.* Journal of Luminescence **2009**, *129(8)*, 874-878

[270] Czarnecki, J. and J. Sestak, *Practical thermogravimetry.* Journal of Thermal Analysis and Calorimetry **2000**, *60(3)*, 759-778

[271] Rezapour, M. and N. Talebian, *Comparison of structural, optical properties and photocatalytic activity of ZnO with different morphologies: Effect of synthesis methods and reaction media.* Materials Chemistry and Physics **2011**, *129(1-2)*, 249-255

[272] Sakthivel, S., et al., *Solar photocatalytic degradation of azo dye: Comparison of photocatalytic efficiency of ZnO and TiO2.* Solar Energy Materials and Solar Cells **2003**, *77(1)*, 65-82

[273] Panyam, J. and V. Labhasetwar, *Biodegradable nanoparticles for drug and gene delivery to cells and tissue.* Advanced Drug Delivery Reviews **2003**, *55(3)*, 329-347

[274] Tracy, M.A., et al., *Factors affecting the degradation rate of poly(lactide-co-glycolide) microspheres in vivo and in vitro.* Biomaterials **1999**, *20(11)*, 1057-1062

[275] Cam, D., S.-h. Hyon, and Y. Ikada, *Degradation of high molecular weight poly(-lactide) in alkaline medium.* Biomaterials **1995**, *16(11)*, 833-843

[276] von Recum, H.A., et al., *Degradation of polydispersed poly(-lactic acid) to modulate lactic acid release.* Biomaterials **1995**, *16(6)*, 441-447

[277] Anna Musyanovych, J.S.-W.V.M.P.W.K.L., *Preparation of Biodegradable Polymer Nanoparticles by Miniemulsion Technique and Their Cell Interactions.* Macromolecular Bioscience **2008**, *8(2)*, 127-139

[278] Yasuda, N., et al., *Quantitative evaluation of photodegradation and racemization of poly(l-lactic acid) under UV-C irradiation.* Polymer Degradation and Stability **2010**, *95(7)*, 1238-1243

[279] Hong, R.Y., et al., *Synthesis, surface modification and photocatalytic property of ZnO nanoparticles.* Powder Technology **2009**, *189(3)*, 426-432

[280] Hagelueken, G., et al., *The crystal structure of SdsA1, an alkylsulfatase from Pseudomonas aeruginosa, defines a third class of sulfatases.* Proceedings of the National Academy of Sciences **2006**, *103(20)*, 7631-7636

[281] Xu, X., et al., *Biodegradable electrospun poly(l-lactide) fibers containing antibacterial silver nanoparticles.* European Polymer Journal **2006**, *42(9)*, 2081-2087

[282] Mora-Huertas, C.E., H. Fessi, and A. Elaissari, *Influence of process and formulation parameters on the formation of submicron particles by solvent displacement and emulsification-diffusion methods. Critical comparison.* Advances in Colloid and Interface Science **2011**, *163*, 90-122

[283] Agarwal A., W.T.L., Schurr M. J., Faith G. N., Czuprynski C. J., McAnulty J. F., Murphy C. J., Abbott N. L., *Surface modified with nanometer-thick silver-*

impregnated polymeric films that kill bacteria but support growth of mammamlian cells. Biomaterials **2010**, *31*, 680-690
[284] Korner, E., et al., *Formation and Distribution of Silver Nanoparticles in a Functional Plasma Polymer Matrix and Related Ag+ Release Properties.* Plasma Processes and Polymers **2010**, *7(7)*, 619-625
[285] Gonzalez-Benito, J. and G. Gonzalez-Gaitano, *Interfacial conformations and molecular structure of PMMA in PMMA/silica nanocomposites. Effect of high-energy ball milling.* Macromolecules **2008**, *41(13)*, 4777-4785
[286] Mulligan, R.F., A.A. Iliadis, and P. Kofinas, *Synthesis and characterization of ZnO nanostructures templated using diblock copolymers.* Journal of Applied Polymer Science **2003**, *89(4)*, 1058-1061
[287] Bockstaller, M.R., R.A. Mickiewicz, and E.L. Thomas, *Block Copolymer Nanocomposites: Perspectives for Tailored Functional Materials.* Advanced Materials **2005**, *17(11)*, 1331-1349
[288] Fu, Y.-S., et al., *Stable Aqueous Dispersion of ZnO Quantum Dots with Strong Blue Emission via Simple Solution Route.* Journal of the American Chemical Society **2007**, *129(51)*, 16029-16033
[289] Yang, K., D.H. Lin, and B.S. Xing, *Interactions of Humic Acid with Nanosized Inorganic Oxides.* Langmuir **2009**, *25(6)*, 3571-3576
[290] John, S., et al., *Hybrid Zinc Oxide Nanoparticles for Biophotonics.* Journal of Nanoscience and Nanotechnology **2010**, *10(3)*, 1707-1712
[291] Irimpan, L., et al., *Excitation wavelength dependent fluorescence behaviour of nano colloids of ZnO.* Journal of Physics D-Applied Physics **2007**, *40(18)*, 5670-5674
[292] Duque, L. and R. Förch, *Plasma Polymerization of Zinc Acetyl Acetonate for the Development of a Polymer-based Zinc Release System.* Plasma Processes and Polymers **2011**, *8(5)*, 444-451
[293] Tayel, A.A., et al., *Antibacterial Action of Zinc Oxide Nanoparticles Against Foodborne Pathogens.* Journal of Food Safety **2011**, *31(2)*, 211-218
[294] Seil, J.T. and T.J. Webster, *Reduced Staphylococcus aureus proliferation and biofilm formation on zinc oxide nanoparticle PVC composite surfaces.* Acta Biomater **2011**, *7(6)*, 2579-84
[295] Li, X.H., et al., *Antibacterial and Physical Properties of Poly(vinylchloride)-based Film Coated with ZnO Nanoparticles*

Food Science and Technology International **2010**, *16(3)*, 0225-8
[296] Li, X., et al., *Antimicrobial activities of ZnO powder-coated PVC film to inactivate food pathogens.* International Journal of Food Science & Technology **2009**, *44*, 2161-2168
[297] Sawai, J., et al., *Effect of particle size and heating temperature of ceramic powders on antibacterial activity of their slurries.* Journal of Chemical Engineering of Japan **1996**, *29(2)*, 251-256
[298] Yamamoto, O., et al., *Effect of lattice constant of zinc oxide on antibacterial characteristics.* Journal of Materials Science-Materials in Medicine **2004**, *15(8)*, 847-851
[299] Stoimenov, P.K., et al., *Metal oxide nanoparticles as bactericidal agents.* Langmuir **2002**, *18(17)*, 6679-6686
[300] Sawai J, I.H., Hashimoto A, Kokugan T, Shimizu M, J. Chem. Eng. Japan **1996**, *29(556)*

[301] Ruoslahti, E. and J.C. Reed, *Anchorage dependence, integrins, and apoptosis.* Cell **1994**, *77(4)*, 477-8
[302] Aulasevich, A., et al., *Optical Waveguide Spectroscopy for the Investigation of Protein-Functionalized Hydrogel Films.* Macromolecular Rapid Communications **2009**, *30(9-10)*, 872-877
[303] Hanley, C., et al., *Preferential killing of cancer cells and activated human T cells using ZnO nanoparticles.* Nanotechnology **2008**, *19(29)*, 295103
[304] Ostrovsky, S., et al., *Selective Cytotoxic Effect of ZnO Nanoparticles on Glioma Cells.* Nano Research **2009**, *2(11)*, 882-890
[305] Taccola, L., et al., *Zinc oxide nanoparticles as selective killers of proliferating cells.* Int J Nanomedicine **2011**, *6*, 1129-40
[306] Ben-Ze'ev, A., S.R. Farmer, and S. Penman, *Protein synthesis requires cell-surface contact while nuclear events respond to cell shape in anchorage-dependent fibroblasts.* Cell **1980**, *21(2)*, 365-72
[307] Frisch, S.M. and H. Francis, *Disruption of epithelial cell-matrix interactions induces apoptosis.* J Cell Biol **1994**, *124(4)*, 619-26
[308] Meredith, J.E., Jr. and M.A. Schwartz, *Integrins, adhesion and apoptosis.* Trends Cell Biol **1997**, *7(4)*, 146-50
[309] Richards, M.J., et al., *Nosocomial infections in combined medical-surgical intensive care units in the United States.* Infect Control Hosp Epidemiol **2000**, *21(8)*, 510-5
[310] Kilgore, M.L., et al., *The costs of nosocomial infections.* Med Care **2008**, *46(1)*, 101-4
[311] Kilgore, M. and S. Brossette, *Cost of bloodstream infections.* Am J Infect Control **2008**, *36(10)*, S172 e1-3

8. Acknowledgements

I would like to thank all the people who contributed to this work, especially my supervisor, my project leader and my collaboration partners. Second, I would like to express many thanks to my colleagues, friends and family for the constant support during the last three years.

9. Curriculum Vitae

Persönliche Daten

Name	Véronique Bernadette Schwartz
Geburtsdatum	23.10.1983
Geburtsort	Bernkastel-Kues

Ausbildung

11/2008-01/2012	**Promotion (Chemie)**, Max-Planck-Institut für Polymerforschung, Mainz Dissertationsschrift: "Design of nanoparticle systems with antimicrobial properties"
09/2008	**Dipl.-Chem.** , Max-Planck-Institut für Polymerforschung, Mainz Diplomarbeit: „Antikörperanbindung auf plasmapolymerisierte Maleinsäureanhydridfilme"
10/2003-09/2008	**Chemiestudium** , Johannes-Gutenberg-Universität Mainz
03/2003	**Abitur** Nikolaus-von-Kues Gymnasium, Bernkastel-Kues

Publikationen

Artikel

V. Schwartz, et al., *Antibacterial Properties of Zinc Oxide Nanoparticles Embedded in PNIPAAm Hydrogel Surface Layers*, eingereicht bei Advanced Functional Materials (Kapitel 5.4)

V. Schwartz et al., *Poly(2-methacryloyloxyethyl)dodecyldimethylammoniummethacrylat Nanoparticles by Combination of Miniemulsion and Solvent EvaporationTechniques*, in Vorbereitung (Kapitel 5.2.3)

Vorträge

Design of Polymer Nanoparticles with Antimicrobial properties, IMPRS Evaluierung, Mainz (31.05.2010)

Polymer Nanoparticles with Antimicrobial properties, Embek 1, 7th Framework Programme, 2-6th Ordinary Meetings, Exeter (UK, 13.09.2009), Mainz (28.01.2010), Paguera (Spanien, 28.06.2010), Köln (17.01.2011), Mainz (19.06.2011)

Poster

V. Schwartz et al., *Design of antimicrobial nanocapsules for improved antimicrobial material properties*, 12th Pacific Polymer Conference, Cairns, Australia (Dezember 2009)

V. Schwartz et al., *Antibacterial Properties of Zinc Oxide Nanoparticles Embedded in PNIPAAm Hydrogel Surface Layers Poster presentation*, 10th International Conference of Materials Chemistry, Manchester, UK (Juli 2011)

Posterbeitrag

Photocrosslinakble hydrogel layer systems for biosensing and biomedical applications, Makromoleculares Kolloquium, Freiburg (Februar 2012)